

MODELING AND CONTROLLING OF HYBRID ENERGY SYSTEMS WITH HYDROGEN STORAGE

**A Thesis Submitted to the Graduate School of Engineering and
Sciences of İzmir Institute of Technology in Partial Fulfilment of the
Requirements for the Degree of
MASTER OF SCIENCE
in Energy Engineering**

**by
Osmancan Denizli**

**July 2023
İZMİR**

We approve the thesis of **Osmancan Denizli**

Examining Committee Members:

Prof. Dr. Serhan ÖZDEMİR

Mechanical Engineering, İzmir Institute of Technology

Prof. Dr. Engin KARATEPE

Solar Energy Institute, Ege University

Asst. Prof. Dr. Başar ÇAĞLAR

Energy Systems Engineering, İzmir Institute of Technology

13 July 2023

Asst. Prof. Dr. Başar ÇAĞLAR

Supervisor, Energy Systems Engineering,
İzmir Institute of Technology

Dr. Müfit ALTIN

Co-Supervisor, Siemens GAMESA

Prof. Dr. Gülden Gökçen AKKURT

Head of the Department of Energy
Systems Engineering

Prof. Dr. Mehtap EANES

Dean of the Graduate School
of Engineering and Sciences

ACKNOWLEDGEMENTS

First and foremost, I would like to extend my heartfelt gratitude to my co-advisor Assist. Prof. Müfit ALTIN, for their valuable guidance, support, and insightful feedback throughout the research process. Your expertise and dedication have been instrumental in shaping the direction of this thesis.

I am also immensely grateful to my advisor, Asst. Prof. Dr. Başar ÇAĞLAR for their unwavering support, encouragement, and mentorship. Furthermore, I would like to acknowledge my former advisor, Assoc. Prof. Dr. Ferhat BINGÖL, for their contributions to my academic journey. Your initial guidance and direction were pivotal in laying the foundation for this research, and I appreciate the knowledge and skills I gained under your mentorship.

This thesis is supported by the Scientific and Technological Research Council of Turkey (TÜBİTAK; Project No: 120N498) as a part of the ERA-NET Smart Energy Projects. I would also like to express my sincere appreciation to those who accepted me as a member of this project. Your collaboration and shared expertise have provided a stimulating and enriching research environment, allowing me to explore new ideas and expand my knowledge.

I am also grateful to my co-workers for their support, insightful discussions, and camaraderie. Your collective efforts have fostered a collaborative atmosphere, and I am thankful for the opportunity to learn from and work alongside such talented individuals.

I extend my deepest gratitude to my family for their unwavering support, love, and encouragement throughout this thesis journey. Your belief in me and understanding of the demands of my work have been instrumental in keeping me motivated and focused. Last but not least, I would like to acknowledge my dear cat Tommy, your adorable antics and unconditional love brought joy and solace, reminding me to take breaks and appreciate the little moments.

ABSTRACT

MODELING AND CONTROLLING OF HYBRID ENERGY SYSTEMS WITH HYDROGEN STORAGE

Hybrid renewable energy systems are gaining more attention for the problems like Global Warming and high CO₂ emissions. Another topic that increases its popularity is hydrogen. Because it is a very good alternative fuel. In this work, every component of a basic Hybrid Renewable Energy System (HRES) will be modeled and short-time simulations will be made for any transient response of individual components. MATLAB Simulink is used for every model and simulation. HRES includes a wind turbine, PV array, battery energy storage, and electrolyzer. The system is also grid-connected. Additionally, different control strategies are investigated, obtained, and created. Maximum Power Point Tracking (MPPT) algorithms for Wind Energy Conversion System (WECS) and PV array were conducted. A control algorithm that combines the battery and the PV array was made and necessary circuits were designed. An overall model for different sizes and operations is created. One-day-long simulations were made for 11 different cases. The user can alter the overall model for different turbines, PV modules, and battery sizes. The total amount of hydrogen produced, energy generation, and consumption were observed for every case.

ÖZET

HİDROJEN DEPOLAMA DAHİL HİBRİT ENERJİ SİSTEMİNİN KONTROLÜ VE MODELLENMESİ

Küresel ısınma, karbondiyoksit emisyonlarındaki hızlı artışlar sebebiyle hibrit yenilenebilir enerji sistemleri gün geçtikçe daha fazla dikkat çekmektedir. Ek olarak, hidrojen iyi bir alternatif yakıt olması sebebiyle popüler bir konu haline gelmiştir. Bu çalışmada, basit bir hibrit yenilenebilir enerji sisteminin her bileşeni modellenmiş ve süreksiz bölgeleri gözlemleyebilmek için kısa süreli simülasyonlar yapılmıştır. Bütün simülasyon ve modeller için MATLAB Simulink kullanılmıştır. Hibrit Yenilenebilir Enerji Sistemi, PV dizilerden, rüzgar türbininden, batarya depolama sisteminden ve bir elektrolizörden oluşmaktadır. Sistem ayrıca şebekeye bağlıdır. Ek olarak, farklı kontrol stratejileri incelenmiş, yaratılmış ve elde edilmiştir. Rüzgar ve güneş enerjisi için 'Perturb and Observe' algoritması Maksimum Güç Noktası kontrolü için kullanılmıştır. Batarya ve PV panelleri birleştiren bir kontrol algoritması geliştirilmiş ve gerekli devre tasarımları yapılmıştır. Şebekeye bağlı, rüzgar türbini, PV seri, batarya depolama ve elektrolizör içeren bir bütün bir sistem tasarlanmıştır. Bir gün süreli simülasyonlar yapılmış ve 11 farklı senaryo incelenmiştir. Toplam hidrojen üretimi, enerji tüketim ve üretimi her senaryo için gözlenmiştir.

TABLE OF CONTENTS

LIST OF FIGURES	viii
LIST OF TABLES	xiii
CHAPTER 1 INTRODUCTION	1
1.1. Growing Importance of Wind Energy	2
1.2. Growing Importance of Solar Energy	4
1.3. Need for Energy Storage	6
1.4. Growing Importance of Hydrogen	8
1.5. Hybrid Renewable Energy Systems with Hydrogen Storage	9
CHAPTER 2 MODELLING COMPONENTS.....	10
2.1. Wind Turbine Model	10
2.1.1. Introduction	10
2.1.2. Simulink Model of Wind Turbine.....	14
2.1.3. System Components	16
2.1.4 Results	23
2.2. Solar Photovoltaic Model.....	26
2.2.1. Introduction	26
2.2.2. Simulink Model of Solar PV Array	28
2.2.3. System Components	30
2.3.4 Results	33
2.3 Battery Pack	35
2.3.1. Introduction	35
2.3.2. Simulink Model for Battery Pack.....	36
2.3.3. System Components	37
2.3.4. Results	39
2.4. Electrolyzer Model.....	41

2.4.1. Introduction	41
2.4.2. MathWorks Electrolyzer Model	43
2.4.3. System Components	45
2.4.4. Results	49
CHAPTER 3 CONTROL STRATEGIES	51
3.1. Introduction	51
3.2. Wind Turbine MPPT Control	51
3.2.1. Introduction	51
3.2.2. Perturb and Observe Control of Wind Turbine Energy Conversion.....	59
3.2.3. Simulink Model of P&O Algorithm for WECS	60
3.3. Solar PV Array MPPT Control.....	61
3.2.1. Introduction	61
3.2.2. Perturb and Observe Control for Solar PV MPPT	65
3.2.3. Simulink Model for P&O Algorithm for PV Array	66
3.4. Charge and Discharge Control between Solar PV Array and Battery Pack.....	67
3.3.1. Proposed Flow Chart and Circuit Scheme.....	67
3.3.2. Control System in Simulink	69
3.3.3. Results	69
3.5. Electrolyzer Power Control.....	71
CHAPTER 4 OVERALL SYSTEM	72
4.1. System Configuration.....	72
4.2. Overall System Simulink Model.....	72
4.3. Subsystems.....	73
4.3.1. Wind Turbine	73
4.3.2. PV Array	74
4.3.3. Battery Energy Storage.....	76
4.3.4. Electrolyzer.....	78

4.3.5. Control Block	79
4.3.6. Measurement	80
4.4. Results	82
CHAPTER 5 CONCLUSIONS	97
REFERENCES	99
APPENDIX I – MATLAB code of P&O Algorithm	109
APPENDIX II – MATLAB code for Electrolyzer Power Control	110
APPENDIX III – Simulation Results of Case IV and Case V	111



LIST OF FIGURES

<u>Figure</u>	<u>Page</u>
Figure 1.1 New and projected new capacity, capacity gaps to meet Net Zero[10].....	3
Figure 1.2 Global capacity and annual additions of solar PV [16].....	5
Figure 1.3 Annual Solar PV Market scenarios [17].....	5
Figure 1.4 Energy storage technologies.....	6
Figure 1.5 Hydrogen demand by sectors [25].....	8
Figure 2.1 Wind Energy Conversion System and power stages.	11
Figure 2.2: Different schematics of WECS; (a) constant speed with multiple-stage geared SCIG, (b) limited speed with multiple-stage geared WRIG, (c) variable speed with multiple-stage geared DFIG, (d) variable speed with multiple-stage geared SCIG and full-scale converter, (e) variable speed with multiple stages geared PMSG and full-scale converter, (f) variable speed with multiple-stage geared PMSG and full-scale converter. (g) direct-drive variable speed with PMSG and full-scale converter.....	13
Figure 2.3 Overall system schematics.	14
Figure 2.4 Overall WECS in Simulink	15
Figure 2.5 Power characteristics of the wind turbine.	16
Figure 2.6 PMSG model and voltage-current measurement blocks of Simulink	17
Figure 2.7 Three Phase voltage and current measurements and universal bridge model.	17
Figure 2.8 Boost converter.....	18
Figure 2.9 PO MPPT control and PWM generation blocks.....	19
Figure 2.10 Inverter and three-phase voltage and current measurement block	19
Figure 2.11 Unfiltered waveforms of (a) voltage and (b) current.....	20
Figure 2.12 Per-unit calculations blocks.....	21
Figure 2.13: Measurement scopes for (a) turbine’s rotational speed and electromagnetic torque, (b) machine side AC and DC and voltage measurements, (c) Grid side filtered AC voltage and current measurements, (d) grid side unfiltered AC voltage and currents.	22
Figure 2.14 (a) rotational speed in per units, (b) electromagnetic torque in Nm.....	23
Figure 2.15 Machine side voltages in V and currents in A; (a) voltage after the generator, (b) current after the generator, (c) voltage after the rectifier, (d) current after	

the rectifier, (e) voltage after the boost converter, (f) current after the boost converter for both overall and closer look.....	24
Figure 2.16 Grid side voltage and currents: overall (a) voltages, (b) currents; closer look to (c) voltages, (d) currents after 10 seconds; waveforms of (e) voltage, (f) current	25
Figure 2.17 PV cell model [43].....	26
Figure 2.18: Single diode model in ideal (a) and non-ideal (b) conditions [43].....	26
Figure 2.19 System Scheme for Solar PV	28
Figure 2.20 Changing Irradiations values (W/m^2) with respect to time.	28
Figure 2.21 Overall PV system in Simulink	29
Figure 2.22 I-V and Power Curves for the selected module for different irradiation values.	30
Figure 2.23 DC-DC Boost Converter Block Diagram.....	31
Figure 2.24 MPPT and PWM generation blocks	32
Figure 2.25 Scopes for both voltages and currents (a) and powers.	32
Figure 2.26 (a) Irradiation W/m^2 , (b) PV voltage, (c) PV current, (d) Load voltage, (e) Load current.....	33
Figure 2.27 (a) Ideal power from the power curve, (b) measured power.	34
Figure 2.28 Comparison between different battery technologies [50].	35
Figure 2.29 Main Structure of Li-ion battery and main processes in it [51].	36
Figure 2.30: System Scheme for Battery and Charging & Discharging of the Battery. .	37
Figure 2.31 Overall Battery System in Simulink including charge and discharge circuits.	37
Figure 2.32 (a) Battery Pack, (b) Subsystem for battery pack.....	38
Figure 2.33 Charge or Discharge decision blocks.	38
Figure 2.34 Charge and discharge circuits.....	39
Figure 2.35 (a) SOC of battery pack (%), (b) Voltage of battery (V), (c) Current of battery (A).....	40
Figure 2.36 Schematics for PEM Electrolyzer [59].....	42
Figure 2.37 Equivalent Electrical Model of Single Cell PEM Electrolyzer [60]	42
Figure 2.38 MathWorks PEM Electrolysis System	44
Figure 2.39 Electrical Supply Subsystem	45
Figure 2.40 Anode fluid channel subsystem.....	45
Figure 2.41 Cathode Gas Channel Subsystem.....	46

Figure 2.42 Dehumidifier Subsystem	46
Figure 2.43 Heat exchanger subsystem.	47
Figure 2.44 Hydrogen output subsystem.	47
Figure 2.45 Recirculation subsystem.	48
Figure 2.46 Separator tank subsystem.	48
Figure 2.47 Water tank subsystem.	49
Figure 2.48 (a) Measurement block, (b) Subsystem of measurement block.	49
Figure 2.49 (a) Hydrogen production (g/s), (b) Stack voltage (V), (c) Power both electrical and heat (kW), (d) Stack Temperature (°C)	50
Figure 2.50 (a) mass flow rates of water and hydrogen, (b) total amount of hydrogen production and total energy consumed.	50
Figure 4.1 Operating Regions of Wind Power System [71]	52
Figure 4.2 Several different MPPT Algorithms for Wind Energy Conversion Systems [69].	53
Figure 4.3 Block Diagram for TSR control [73].	54
Figure 4.4 Relation between Power Coefficient C_p (a) and turbine power (b) with respect to TSR [73].	55
Figure 4.5 Block diagram for OT control [73].	55
Figure 4.6 Relation between mechanical torque (a) and turbine power (b) with respect to generator speed [69].	56
Figure 4.7 Block diagram for PSF method [73].	56
Figure 4.8 ORB schematic [69].	57
Figure 4.9 INC algorithm [69].	57
Figure 4.10 MPP Process regarding generator speed vs. Power [73].	58
Figure 4.11 Used P&O algorithm in the thesis.	59
Figure 4.12 Inside of the MPPT block's subsystem.	60
Figure 4.13 Different MPPT methods for Solar PV.	64
Figure 4.14 Circuit schematics.	67
Figure 4.15 Proposed flow chart.	68
Figure 4.16 Proposed system for PV & Battery Control.	69
Figure 4.17 (a) Irradiances (b) V_{pv} , (c) SOC of battery, (d) Charge state, (e) Discharge state, (f) PV supplies the load state.	70
Figure 5.1 Proposed configuration of the system.	72

Figure 5.2 Power Curves of wind turbines; (a) Ryse E5, (b) Vestas V47, (c) VestasV87	73
Figure 5.3 (a) Subsystem, (b) inside of the subsystem.	74
Figure 5.4 User Interface for Wind Energy Subsystem.	74
Figure 5.5 (a) Overall PV Solar system, (b) inside of the subsystem.	75
Figure 5.6 User Interface for PV Array Subsystem.	75
Figure 5.7 (a) BES subsystem, (b) inside of the subsystem.	76
Figure 5.8 User Interface of BESS	77
Figure 5.9 (a) electrolyzer subsystem and (b) inside of the subsystem.	78
Figure 5.10 (a) Control subsystem, (b) inside of the subsystem.....	79
Figure 5.11 User interface of Control Subsystem.....	80
Figure 5.12 (a) measurement scopes, (b) subsystem for electrolyzer measurements.	81
Figure 5.13 (a) Wind speed and (b) GHI	82
Figure 5.14 Input powers for Case-I.....	83
Figure 5.15 Input and output powers for Case 1-a.	84
Figure 5.16 Electrolyzer Measurements for Case I-a.	84
Figure 5.17 Battery measurements for Case I-a.	85
Figure 5.18 Input and Output Powers for Case I-b.....	85
Figure 5.19 Electrolyzer Measurements for Case I-b.	86
Figure 5.20 Battery Measurements for Case I-b.....	86
Figure 5.21 Input and Output Powers for Case I-c.	87
Figure 5.22 Battery Measurements Case I-c.....	87
Figure 5.23 Input powers for Case II.....	88
Figure 5.24 Input and output powers for Case II-a.	89
Figure 5.25 Electrolyzer Measurements for Case II-a.....	89
Figure 5.26 Battery measurements for Case II-a.	90
Figure 5.27 Input and Output Powers for Case II-b.	90
Figure 5.28 Electrolyzer Measurements for Case II-b.....	91
Figure 5.29 Battery Measurements for Case II-b.	91
Figure 5.30 Input and Output Powers for Case II-c.....	92
Figure 5.31 Battery Measurements for Case II-c.....	92
Figure 5.32 Input powers for Case III.....	93
Figure 5.33 Input and output powers for Case III-a.	93
Figure 5.34 Electrolyzer Measurements for Case III-a.....	94

Figure 5.35 Battery measurements for Case III-a.....	94
Figure 5.36 Input and Output Powers for Case III-b.....	95
Figure 5.37 Electrolyzer Measurements for Case III-b.....	95
Figure 5.38 Battery Measurements for Case III-b.....	96
Figure 5.39 Input and Output Powers for Case III-c.....	96
Figure a.1: Input powers for Case IV.....	111
Figure a.2: Input and output powers for Case IV.....	112
Figure a.3: Electrolyzer Measurements for Case IV.....	112
Figure a.4: Battery measurements for Case IV.....	113



LIST OF TABLES

<u>Table</u>	<u>Page</u>
Table 1.1 Various research on Hydrogen generation	9
Table 2.1 Parameters of wind turbine.	16
Table 2.2 Components and their values in Boost converter.....	18
Table 2.3: Module Parameters	30
Table 2.4: Boost Converter components and values of them.....	31
Table 3.1: Function conditions and actions.....	68
Table 4.1: Different cases investigated.	82



CHAPTER 1

INTRODUCTION

Renewable energy sources including solar, wind, hydro, geothermal, and biomass create very little or no greenhouse emissions. Renewable energy is essential for combating climate change and lowering global carbon dioxide (CO₂) emissions because it reduces reliance on fossil fuels, which are the main cause of greenhouse gas emissions. The International Panel on Climate Change (IPCC) underlines the urgency of making the switch to renewable energy in order to keep global warming at a safe level and avoid catastrophic climatic impact (Edenhofer et al. 2012).

Renewable energy sources have fewer negative environmental effects than the exploitation of fossil fuels. For instance, when used, wind and solar energy do not pollute the air or the water. They contribute to reduced water use, better air quality, and ecosystem protection. Contrarily, the exploitation, and burning of fossil fuels have several adverse effects, such as air pollution, water contamination, deforestation, and habitat destruction.

Diversifying the energy mix with renewable energy lessens reliance on limited fossil fuel supplies that are prone to price swings and geopolitical concerns. Utilizing domestic renewable energy sources, nations may increase their energy security and lessen their susceptibility to disruptions in the energy supply and price volatility brought on by the markets for fossil fuels (Olz and Kirchner 2007; Cox, Beshilas, and Hotchkiss, n.d.). However, this transition will not be soon but will be promising (Foss 2022; Johansson 2013).

Other advantages of having renewables are economic growth and job creation. The market for renewable energy has significant business prospects. The local economy is boosted, jobs are created, and innovation is encouraged through investments in renewable energy initiatives. According to IRENA's 2022 report, there is 12.6 worldwide employment in renewable energy. The same report expects 38.2 worldwide employment in 2030 (International Renewable Energy Agency and Abu Dhabi and International Labour Organization Geneva, n.d.).

1.1. Growing Importance of Wind Energy

Wind energy is an environmentally sustainable energy source. By replacing fossil fuel-based electricity generation, wind energy is a good solution for reducing air pollution. Wind is an abundant resource that is accessible everywhere and is suitable for all climates. Utilizing wind power lessens the reliance on limited fossil fuel supplies by utilizing this resource and diversifying the energy mix. Due to its long-term sustainability and environmental friendliness, wind power supports sustainable development. Wind farms can range in size from modest installations to significant utility-scale operations, making it a very scalable energy source. It may be incorporated into already-established power networks, providing flexibility in electricity generation, and assisting in the integration of other renewable energy sources (Jose Zayas 2014). It can be used in a variety of contexts to promote equitable growth and lower energy poverty. In comparison to fossil fuel power plants, the operating costs of a wind turbine are comparatively inexpensive once it is established. Over time, this results in stable energy prices. Wind power enhances energy independence and security, contributing to a diversified energy mix and reducing vulnerability to geopolitical tensions and fuel price fluctuations (Naveen Sharma n.d.). Additionally, technology breakthroughs in turbine design, components, and grid integration are driven by the wind energy industry, which also pushes cost reductions, cost reductions, and increases in power output and efficiency, making wind energy more competitive and available (Wind Energy Technologies Office 2023).

According to Global Wind Energy Council's 2022 report, the wind energy sector is growing rapidly. However, the acceleration of the growth should also increase to meet Net Zero scenarios. Figure 1.1 shows the new and projected new installation capacities, annual and cumulated wind capacity gaps to meet net zero by 2050 scenarios.

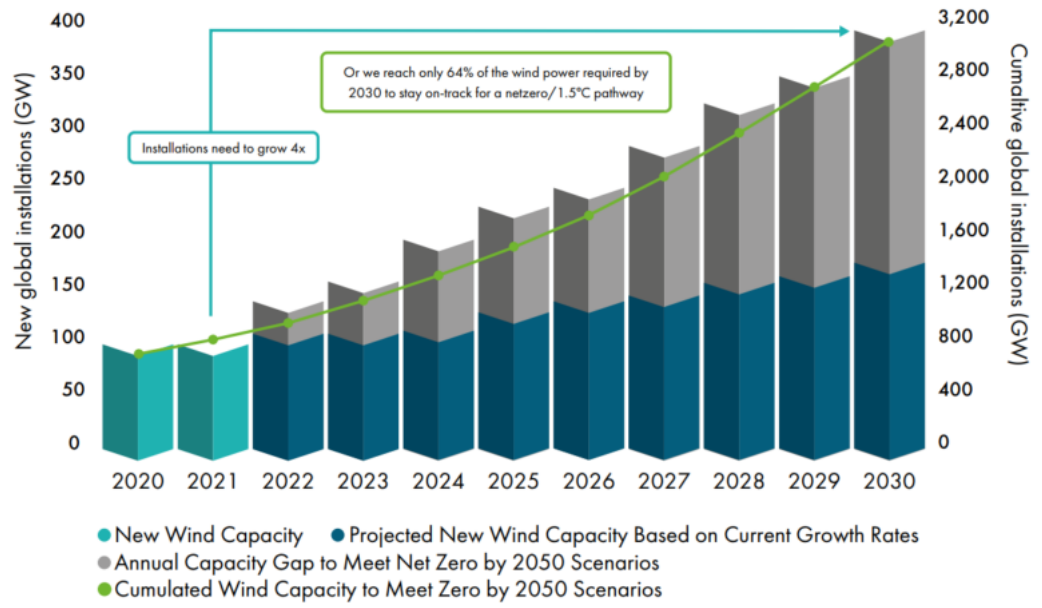


Figure 1.1. New and projected new capacity, capacity gaps to meet Net Zero (GWEC, n.d.).

1.2. Growing Importance of Solar Energy

Photovoltaic (PV) Solar energy is the process of converting light from the sun into electricity using solar panels or modules made of solar cells. Solar cells absorb photons from sunlight and release electrons, producing an electric current. They are frequently made of semiconductor materials like silicon. Solar panels or modules with several solar cells connected can be assembled into larger arrays or systems to produce more electricity. Several advantages of solar PV energy systems can differ from the advantages of wind energy mentioned before.

Due to the consistent availability of sunlight during the day, solar energy displays high dependability. While the amount of solar energy produced varies throughout the day and with the seasons, it is largely predictable and can be accurately forecasted. Because of predictability, grid stability and management are supported by better energy planning and integration into the grid (Zsiborács et al. 2022; Cros et al. 2020). Solar energy has the benefit of being simple to install at various scales, from small-scale solar farms to individual homes. Solar panels can be integrated into buildings, installed on rooftops, or in open spaces. This allows for distributed generation. This decentralized strategy relieves pressure on centralized power grids by empowering people and communities to produce their electricity (International Energy Agency (IEA) 2019). Solar energy systems can be easily expanded or changed as needed because they are highly scalable. In order to increase capacity or meet rising energy demands, extra solar panels can be added. From small residential installations to substantial utility-scale solar projects, this scalability enables incremental growth and flexible deployment in a variety of applications. Solar panels can be integrated into urban environments more seamlessly than wind turbines. They can be installed on rooftops, facades, and other urban structures, utilizing underutilized spaces for energy production (Akrofi and Okitasari 2022). Solar power reduces energy losses that take place during long-distance transmission by producing electricity nearer the location of consumption. Resources are saved and expensive infrastructure upgrades are not as necessary thanks to this efficiency. Compared to wind turbines, solar installations typically have a less noticeable visual presence. Solar panels are more aesthetically pleasing in urban and residential settings because they can be discretely integrated into structures or created to blend with the surroundings (Sánchez-Pantoja, Vidal, and Pastor 2018).

A report (Renewables 2022 – Global Status Report) from REN21 showed solar PV’s global capacities and annual additions between 2011 and 2021 (REN21 Renewables Now 2022). It can be seen in Figure 1.2. Additionally, Solar Power Europe predicted the solar PV market in Europe by giving numbers for 2026 (SolarPower Europe 2022) which can be seen in Figure 1.3. In both figures, an increasing trend can be seen.

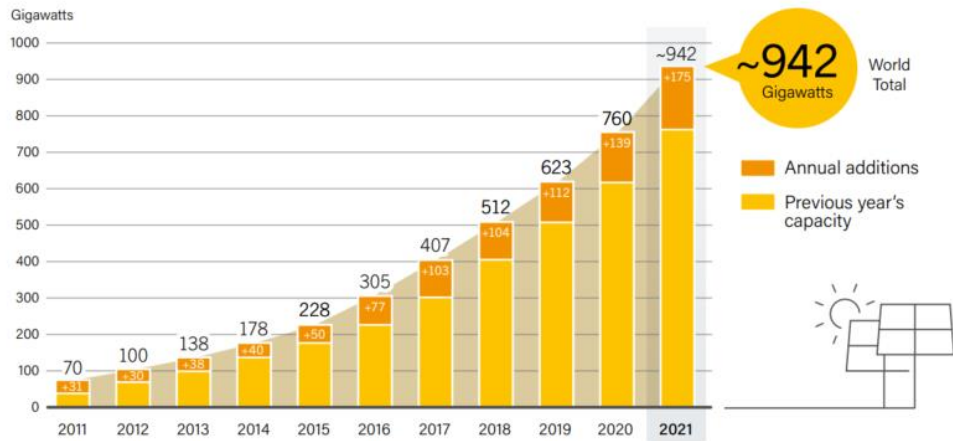


Figure 1.2. Global capacity and annual additions of solar PV (REN21 Renewables Now 2022).

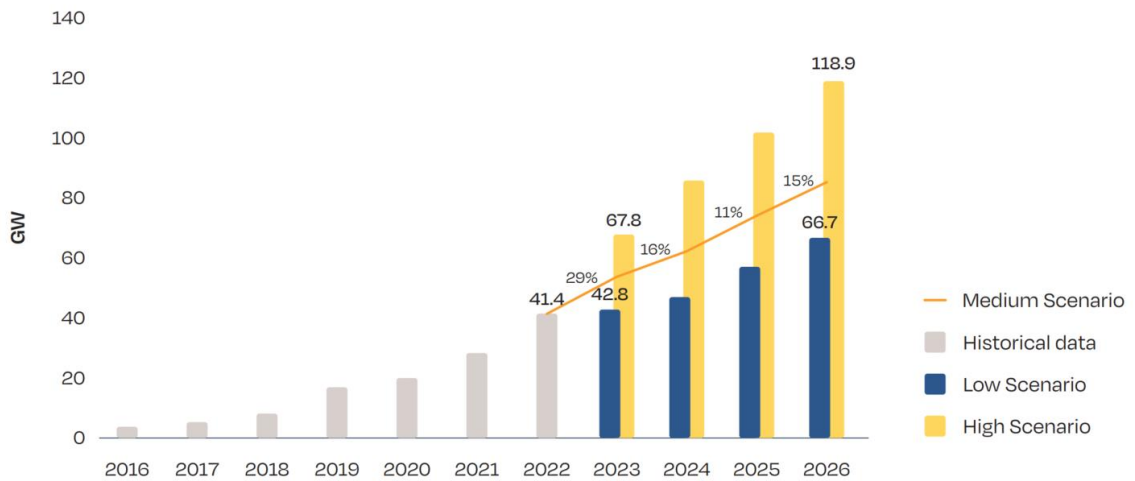


Figure 1.3. Annual solar PV market scenarios (SolarPower Europe 2022).

1.3. Need for Energy Storage

The intermittent nature of energy sources like wind and solar provides an issue. Energy storage and forecasting are highlighted in this scenario. This encourages the development of energy storage system technologies. Energy storage applications are necessary for off-grid energy system applications. There is also an increase in energy storage applications in on-grid applications.

Energy storage applications can essentially be divided into mechanical, electrical, thermal, and chemical categories. Compressed air energy storage (CAES) pumped hydro energy storage (PHES), and flywheel-based energy storage (FESS) are all examples of mechanical energy storage devices. Electrical energy storage systems include supercapacitors (or ultracapacitors) and superconducting magnetic energy storage systems (SMES). Systems for storing energy electrochemically include batteries and fuel cells. Figure 1.4 shows the categorization of energy storage technologies.

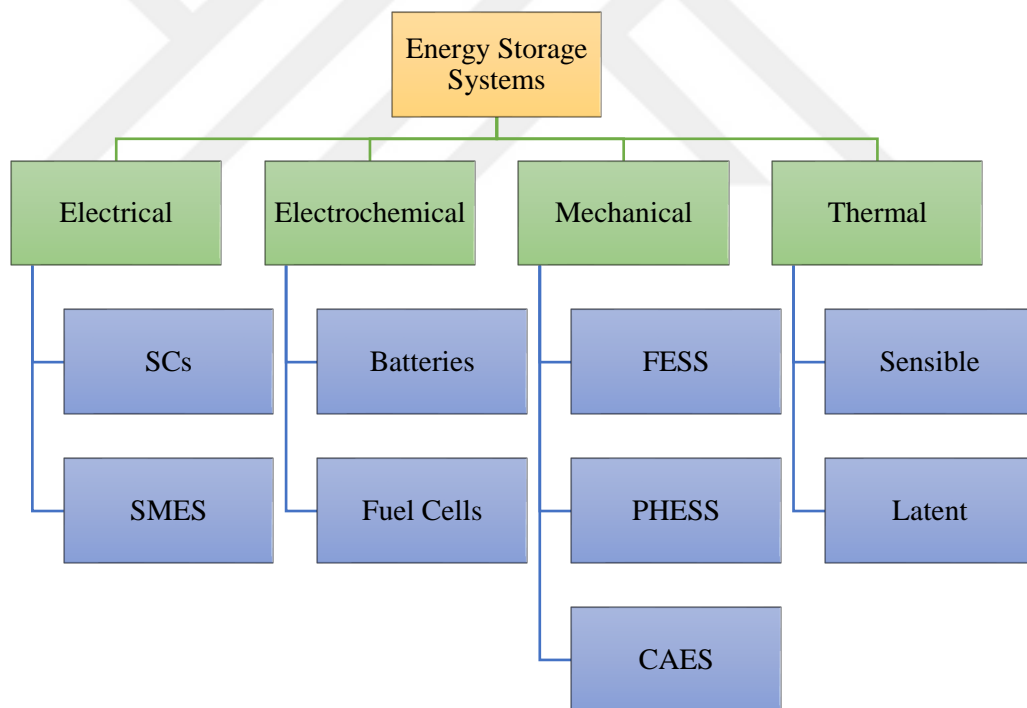


Figure 1.4. Energy storage technologies.

The controllable and cost-effective compressed air energy storage system permits the more effective utilization of intermittent renewable energy sources. Air is compressed when energy is produced in excess by delivering it through compressors into mines, caves, or containers. In times of need, compressed air is converted into energy by doing the reverse action (Krupke et al. 2017). Energy is stored in water's potential energy form

using pumped hydroelectric energy storage. It uses a system with two connected reservoirs, one of which is at a lower elevation than the other. Water is pumped from the lower reservoir to the higher one during the period of energy surplus. In contrast, at times of high demand, water is discharged from the higher reservoir to power a reversible turbine. It is one of the most economical methods for storing high amounts of electrical energy. Costs and proper geographic conditions, however, are important considerations (Rehman, Al-Hadhrami, and Alam 2015). A flywheel energy storage system uses kinetic energy to store energy. To balance this power flow, the storage device trades power with an external network. When there is little wind, some of the energy that was previously stored in the flywheel is then released to the grid (Díaz-González et al. 2013).

Like regular capacitors, supercapacitors (also known as electrochemical capacitors or ultracapacitors) store energy in an electrical field. Electrodes, a separator, and an electrolyte are the three primary components of SCs. Charges build up at the conductor-electrolyte interface. This results in a double layer, of which one is produced by a charged electrode and the other by ions (Simon et al. 2019). Superconducting Magnetic Energy Storage uses DC to create a magnetic field on the coil. Energy is stored in a magnetic field. Energy is lost because of the resistance that the wire's substance causes. The use of a superconducting wire can lower this resistance to extremely low levels. The loss of energy that needs to be stored is avoided in this way. The substance must be maintained at low temperatures in order to be superconductive (Evans, Strezov, and Evans 2012).

Systems for mechanical energy storage have substantial initial costs. Additionally, research on supercapacitors and superconducting magnetic energy storage systems is ongoing, and little is known about their applicability in business and industry. However, given their variety, batteries can be regarded as the best alternative.

Batteries are crucial to the development of sustainable energy storage. Low self-discharge, a long-life cycle, and high charge or discharge efficiency are all essential characteristics of a battery (Baker 2008). A fuel cell transforms the chemical energy of fuels directly into electrical energy. Additionally, fuel cells provide several benefits, including great effectiveness, minimal influence on the environment, and silence (Rezk et al. 2019).

1.4. Growing Importance of Hydrogen

According to International Energy Agency's (IEA) 2021 Global Hydrogen Review, many governments released hydrogen strategies, and many more announced publicly that working on strategies. Also, many companies are paying attention to hydrogen business opportunities. Next to that, hydrogen demand has increased. Figure 1.5 shows the hydrogen demand of different sectors ("Global Hydrogen Review 2021" 2021). In addition, Turkey also released the Prior Areas for Turkish Hydrogen Strategy report in 2021. It investigates the sectoral areas and expects an accelerated increase in hydrogen applications (Saygın, Emre, and Sanlı 2021).

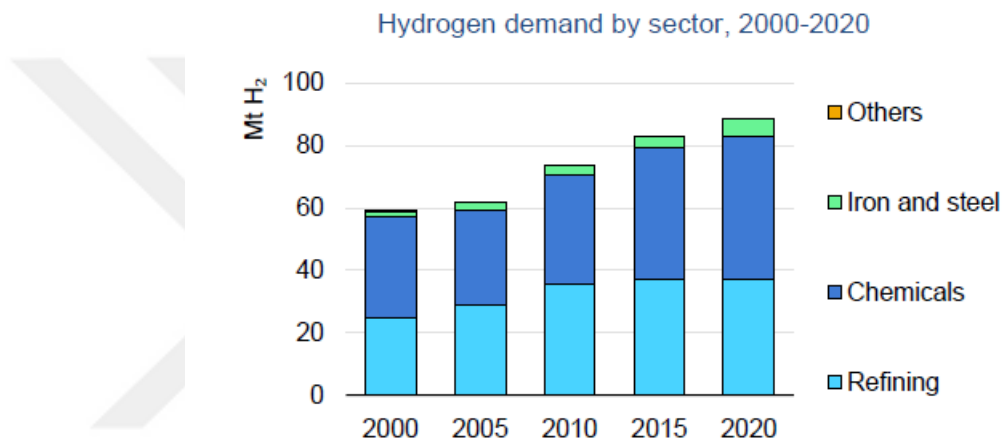


Figure 1.5. Hydrogen demand by sectors ("Global Hydrogen Review 2021" 2021).

1.5. Hybrid Renewable Energy Systems with Hydrogen Storage

Using variable renewable energy sources is an assessable option for a sustainable future (Leidy Tatiana Contreras Montoya, Santiago Lain, Mohamad Issa, Adrian Ilinca 2021). Combining them as a Hybrid Energy System (HES) is also an alternative and has an increasing interest. However, this leads to new technological, and non-technical challenges which include economic, technical, social, and environmental factors (Taskin Jamal 2021). In order to solve these kinds of challenges a good approach for modelling is essential. HES are congregated with different generations (Photovoltaic, wind, etc.), storage (Battery, fuel cells, etc.), and consumption (micro-grid, grid-connected, etc.)(G. Konstantinou 2021). Table 1.1 shows similar research projects with their aims for the research based on a work similar to Babei et al. (Babaei, Ting, and Carriveau 2022).

Table 1.1 Various research on hydrogen generation

Ref.	Hybrid System*	Research Topic**
(Abdin, Webbn, and Gray 2018)	WT & PV and combinations	Techno-economic analysis & determination of COE
(Luta and Raji 2018)	WT & PV & FC & ELC	Breakeven point & COE & electricity generation
(Qolipour, Mostafaeipour, and Tousi 2017)	WT & PV & ELC	Techno-economic feasibility
(Samy, Barakat, and Ramadan 2019)	PV & FC & ELC	LCOE & LPSP & ABC & PSO
(Ma et al. 2022)	WT&PV&Diesel&Battery&ELC	Techno-feasibility
(Nasser et al. 2022b)	WT & PV & ELC	Techno-economic with different climatic conditions
(Basu et al. 2021)	WT & PV & ELC	LCOE analysis on both hybrid and standalone energy generation
(Macedo and Peyerl 2022)	WT & PV & ELC & FC	Prospects and economic feasibility
(Nasser et al. 2022a)	WT & PV & ELC	Energy, exergy, economic, enviro-economic analysis

*WT: Wind Turbine, PV: Photovoltaic, FC: Fuel Cell, ELC: Electrolyzer

**COE: Cost of Energy, LCOE: Levelized Cost of Energy, LPSP: Loss of Power Supply Probability, ABC: Artificial Bee Colony, PSO: Particle Swarm Optimization

In this thesis, a HES including solar photovoltaics, wind as generation; battery as storage; an electrolyzer, and grid connection as consumption will be modeled and controlled in MATLAB Simulink.

CHAPTER 2

MODELLING COMPONENTS

2.1. Wind Turbine Model

2.1.1. Introduction

A wind turbine works by harnessing the kinetic energy from the wind and converting it into electrical energy. The wind turbine consists of a tower that supports a rotor with two or three blades. The blades rotate because of the wind's interaction with them. The wind energy will be captured by the spinning blades. To enhance their ability to capture energy from flowing air, the blades' design and angle have been carefully considered. The rotational speed is increased by transferring the blades' spinning action through a gearbox or direct drive system. The generator requires a high-speed rotation, which the gearbox or direct drive system connects the blades' low-speed rotation to. The generator is connected to the drive train's high-speed shaft which produces electricity. Wind turbines have control systems that keep track of the wind's direction, speed, and other factors to maximize energy capture, guarantee safe operation, and safeguard the turbine from severe weather, these systems continuously adjust the blade pitch, rotor speed, and yaw direction. Output mechanical power can be expressed by Equation-2.1.

$$P_m = \frac{1}{2} \rho A v^3 C_p(\lambda, \beta) \quad (2.1)$$

Where v is the velocity of wind, ρ is the air density, A is the swept area of rotor blades, and $C_p(\lambda, \beta)$ is the power coefficient of the wind turbine which is a function of blade pitch angle (β), and tip-speed ratio (λ). The power coefficient is a non-linear function that can be approximated in several ways.

The tip-speed ratio can be expressed as

$$\lambda = \frac{R\omega_m}{v} \quad (2.2)$$

Where R is blade radius, ω_m is the angular speed of the rotor turbine.

There are several losses due to aerodynamics, generator, and converters. Most of the losses are caused by Betz Limit which states only 59.25% of wind's kinetic energy can be converted to mechanical power. Figure 2.1 shows the power stages of a wind energy conversion system (Mahela and Shaik 2016).

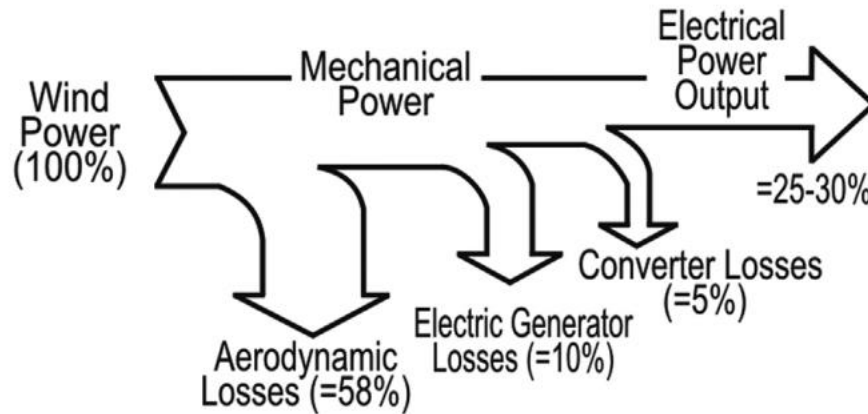


Figure 2.1. Wind Energy Conversion System and power stages.

There are several schematics for different Wind Energy Conversion systems which can be seen in Figure 2.2.

- a. The multiple-stage gearbox and SCIG, which are directly connected to the grid through a transformer, have been used with the constant speed WECS. Due to its simplicity, dependability, and low cost, this concept was adopted by numerous Danish wind turbine manufacturers during the 1980s and 1990s. The need for a reactive power source to create the magnetic field, however, is a drawback of this WECS. Then, during the 1980s, a capacitor bank was expanded for reactive power compensation. A soft starter is additionally frequently used to lower the inrush currents during startup.
- b. The limited variable speed WECS consists of a multiple-stage gearbox and a wound rotor induction generator (WRIG). The rotor windings in this WECS are coupled to a variable resistor that can be changed by the electronic control system. The rotor windings' increased resistance causes the WRIG's slip to increase. But a large slip indicates a high-power extraction rate by the rotor, which results in a low generator efficiency.
- c. Variable Speed WECS includes a DFIG, a multiple-stage gearbox, and a partial-scale power converter. While the stator of the DFIG is connected to the grid directly, the rotor is connected to the grid via a back-to-back converter. A crowbar

circuit, a rapidly short-circuiting circuit for power supply protection, is added to the rotor-side converter,

- d. Variable speed WECS with SCIG includes SCIG which has benefits like straightforward structure, minimal cost, great reliability, and full-scale converter. While the grid-side converter can manage the DC bus voltage and the reactive power transmitted to the grid, the generator-side converter can be used to adjust the generator speed. The high cost and losses of the full-scale converter in comparison to the constant speed WECS with SCIG are the drawbacks of this design.
- e. Variable speed WECS with Synchronous Generator (SG) includes a full-scale power converter, and a multiple-stage geared SG. When compared to a direct-drive system, the use of a multistage gearbox can minimize the size and weight of the generator, which also lessens the difficulties of its design and production. Permanent magnet synchronous generators (PMSGs) and electrically excited synchronous generators (EESGs) can both be used in this system, but PMSG is preferred because it offers benefits including high efficiency. However, because permanent magnet materials are more expensive than those used in EESG, SCIG, and DFIG, the cost of the PMSG is higher.
- f. Direct-drive variable speed WECS includes EESG and a full-scale converter. The field system is supplied with a DC excitation, and the EESG is constructed with a rotor transporting it. To enable the gearless method, the generator must be built with many poles. As a result, compared to multiple-stage geared generators, these low-speed generators have a substantially larger volume and weight. For the exciting windings, which raise the need for system maintenance, the EESG needs slip rings and brushes. In addition, power losses from the field winding will reduce system efficiency.

g. Direct-drive WECS with PMSG is a promising system because unlike the EESG, where external stimulation and slip rings are required, the efficiency and reliability are higher. Additionally, because high-performance permanent magnets are used, the PMSG is lighter and smaller than the EESG. Due to the removal of the gearbox and independent excitation system, this system also has the benefit of being quieter (Cheng and Zhu 2014).

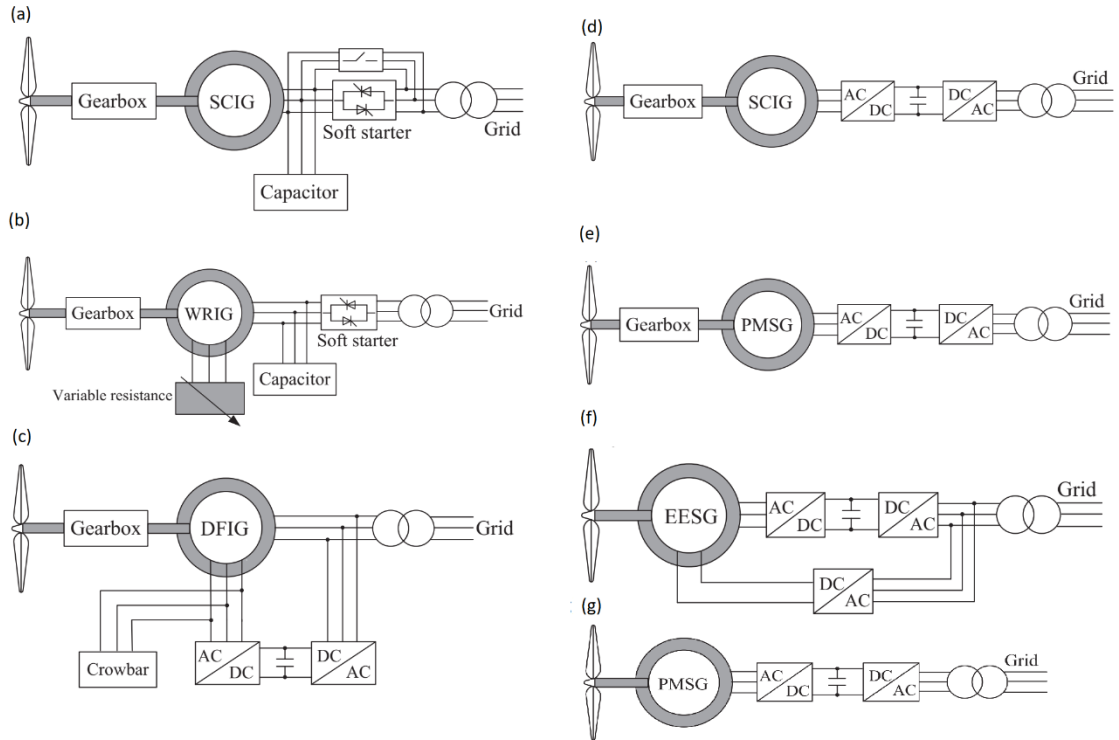


Figure 2.2. Different schematics of WECS; (a) constant speed with multiple-stage geared SCIG, (b) limited speed with multiple-stage geared WRIG, (c) variable speed with multiple-stage geared DFIG, (d) variable speed with multiple-stage geared SCIG and full-scale converter, (e) variable speed with multiple stages geared PMSG and full-scale converter, (f) variable speed with multiple-stage geared PMSG and full-scale converter. (g) direct-drive variable speed with PMSG and full-scale converter.

In this thesis, direct-drive variable speed with the PMSG model of a wind turbine will be used because of promising developments.

2.1.2. Simulink Model of Wind Turbine

Figure 2.3 shows the overall schematics for the wind energy conversion system. The system consists of the wind turbine, PMSG, universal bridge, boost converter, MPPT and PWM generation blocks, inverter, filter, per-unit conversion blocks, and measurement blocks. Figure 2.4 shows the overall Simulink model of the WECS.

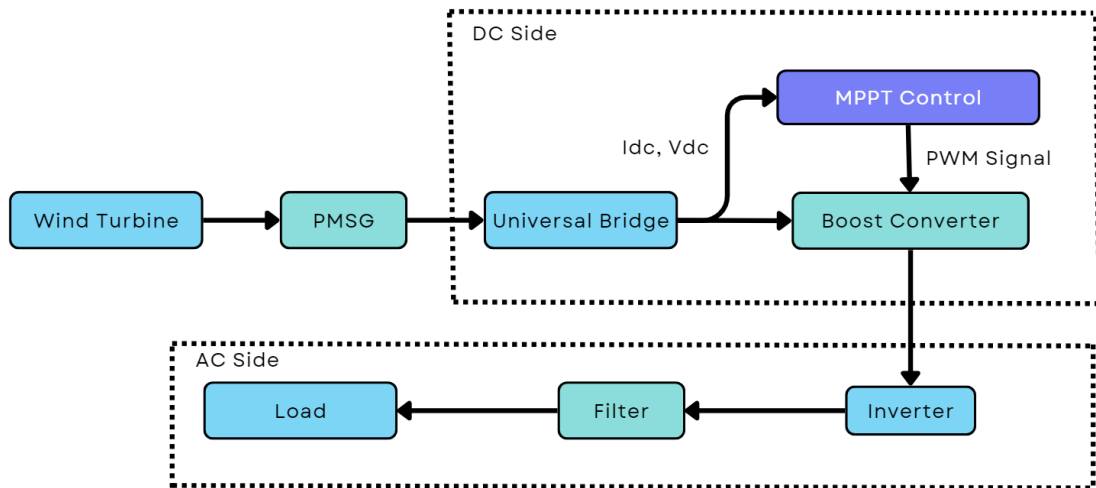


Figure 2.3. Overall system schematics.

Fixed step solver with 2×10^{-6} step size and ode3 (Bogacki-Shampine) solver type is used. A total of 30 seconds of simulation was made. Wind speed is taken constant at 12 m/s simulation and pitch angle stayed constant at 0° .

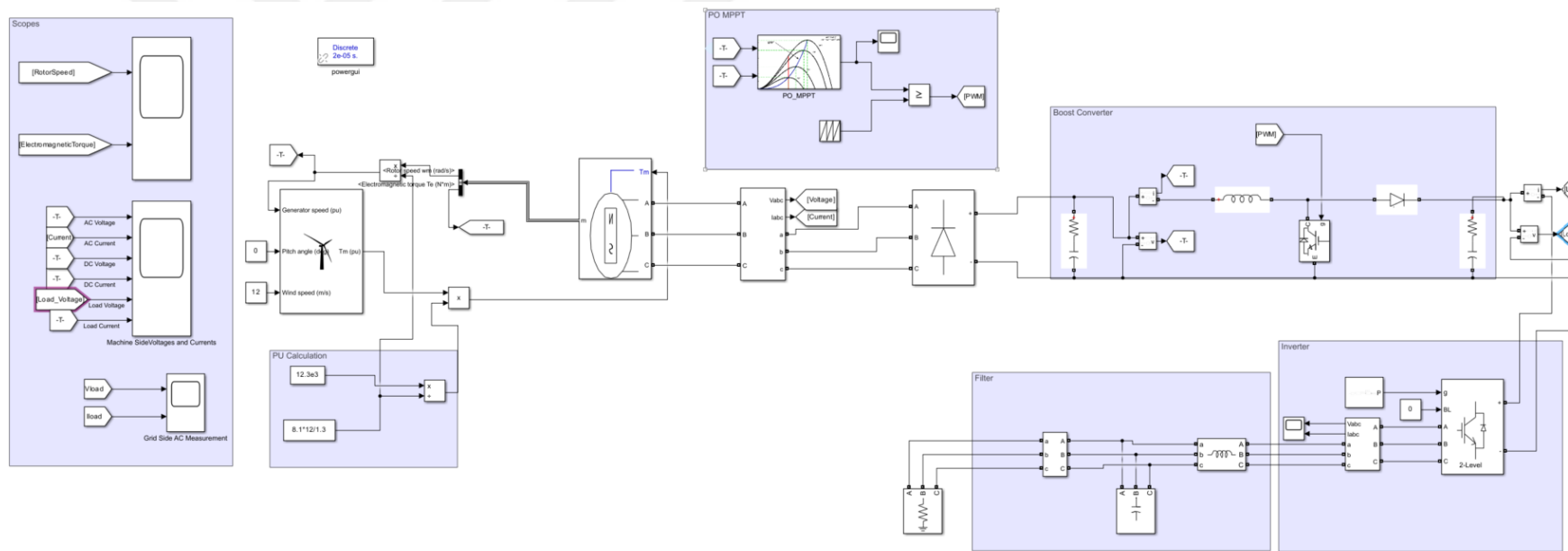


Figure 2.4. Overall WECS in Simulink

2.1.3. System Components

2.1.3.1. Wind Turbine

Simulink model of wind turbine which represents the pitch wind turbine model, is used. The model takes the wind speed in m/s, pitch angle, and generator speed per unit as input. Output is the per unit torque applied to the generator. Table 2.1 shows the parameters of selected wind turbines and

Table 2.1 Parameters of the wind turbine.

Nominal mechanical output power (W)	12300
The base power of the electrical generator (VA)	13667
Base wind speed (m/s)	12
Maximum power at base wind speed (pu. of nominal power)	0.85
Base rotational speed (pu. Of base generator speed)	1.2

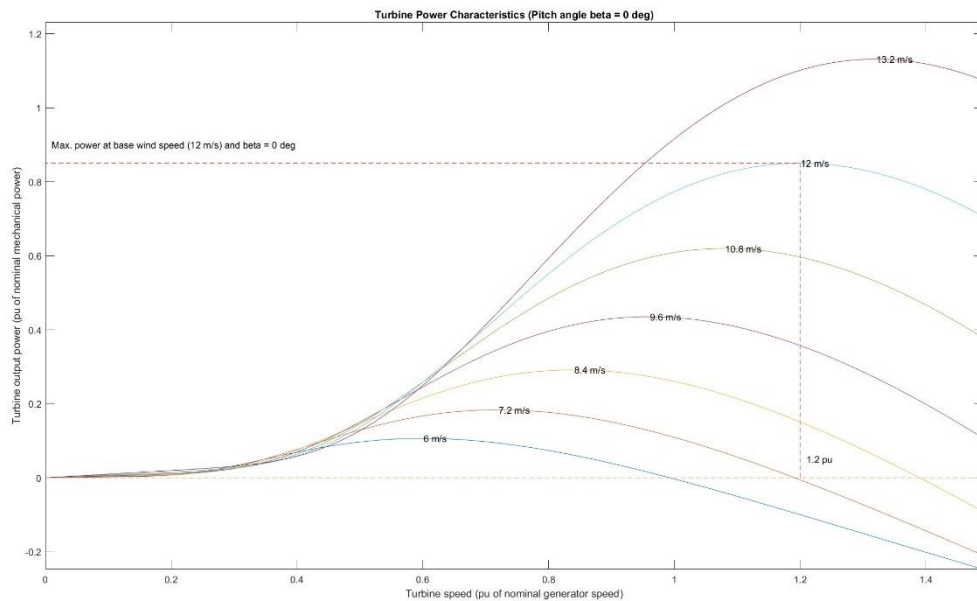


Figure 2.5. Power characteristics of the wind turbine.

2.1.3.2. Permanent Magnet Synchronous Generator

A Simulink model of PMSG, which represents a three-phase or five-phase permanent synchronous machine, is used. Number of phases selected as 3. Sinusoidal back EMF waveform and salient-pole rotor type are chosen. It takes wind turbine torque as mechanical input. Figure 2.6 shows the PMSG model of Simulink and the following block represents 3-phase current and voltage measurements to see the power side characteristics of voltage and current waveforms.

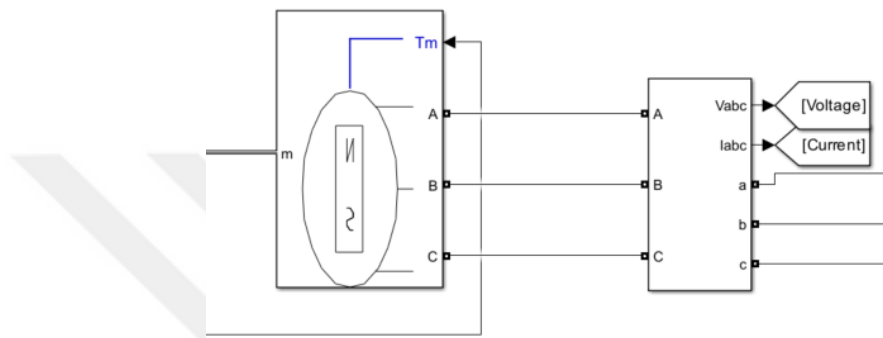


Figure 2.6. PMSG model and voltage-current measurement blocks of Simulink

2.1.3.3. Universal Bridge

In order to perform the full-scale converter topology mentioned in 2.1.1 AC voltage of the generator should be converted to DC. Universal bridge block of Simulink which has 3 bridge arms and has snubber resistance of $R_s = 2 \times 10^5$ is used. Figure 2.7 shows the block diagram.

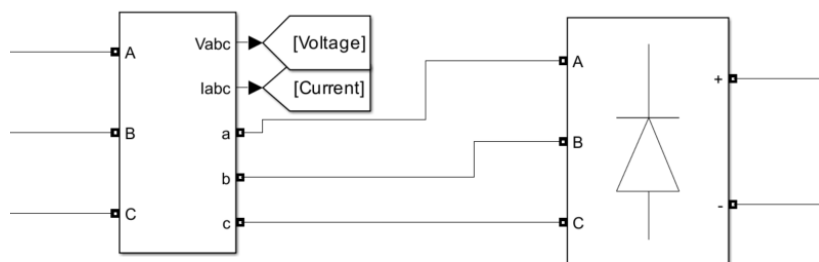


Figure 2.7. Three-Phase voltage and current measurements and universal bridge model.

2.1.3.4. Boost Converter

In order to control the system at its maximum power point a DC-DC converter is needed. Figure 2.8 shows the block diagram for the Boost DC-DC converter. Gates signal of the IGBT block is the PWM signal from MPPT and PWM blocks.

Table 2.2. Components and their values in Boost converter.

Component	Value	
Inductor	4.5573×10^{-5} H	
Capacitor	6.6094×10^{-4} F	
IGBT Diode	Internal Resistance	$1 \times 10^{-3} \Omega$
	Snubber Resistance	$1 \times 10^5 \Omega$

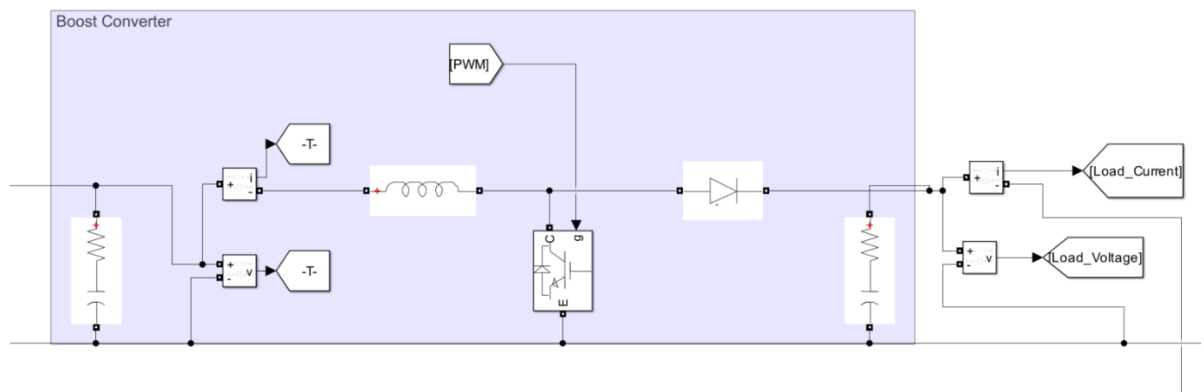


Figure 2.8. Boost converter.

2.1.3.5. Maximum Power Point Tracking and Pulse Width Modulation Generation

Perturb and Observe MPPT block is used for MPPT control. This block determines a duty cycle by taking DC side voltage and current as input. Afterward becomes a PWM signal with the help of a repeating sequence. Details of this algorithm will be given in Chapter 3. Figure 2.9 shows PO MPPT control and PWM generation blocks.

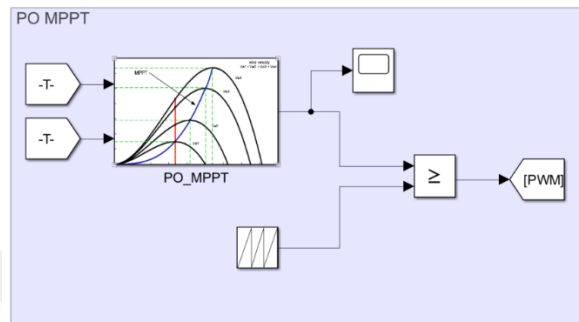


Figure 2.9. PO MPPT control and PWM generation blocks.

2.1.3.6. Inverter

In order to convert the signal DC to AC a 2-level converter block of Simulink is used. The model type is selected as switching diodes. The gate signal of the converter block comes from a 2-level PWM generator which has 2000Hz switching frequency and uses a three-phase bridge (6 pulses) generator type. All firing pulses can be disabled by applying a signal value of 1 to the BL input. It is beneficial to have such a signal in case of any fault on the grid side. Figure 2.10 shows the inverter, pulse generation block, and three-phase voltage and current measurement block to see the unfiltered voltage and current waveforms.

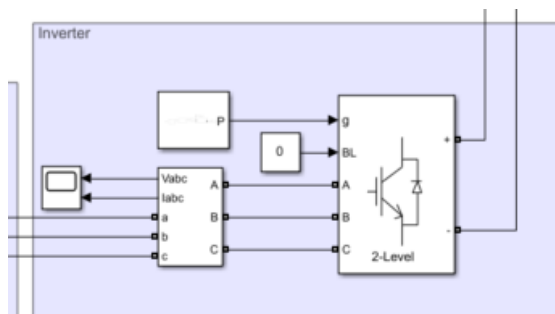


Figure 2.10. Inverter and three-phase voltage and current measurement block.

2.1.3.7. Filter

Figure 2.11 shows unfiltered waveforms of voltage and current from the inverter. It can be seen that voltage waveform has a lot of distortion. In order to filter it an inductor and a parallel capacitor bank are used.

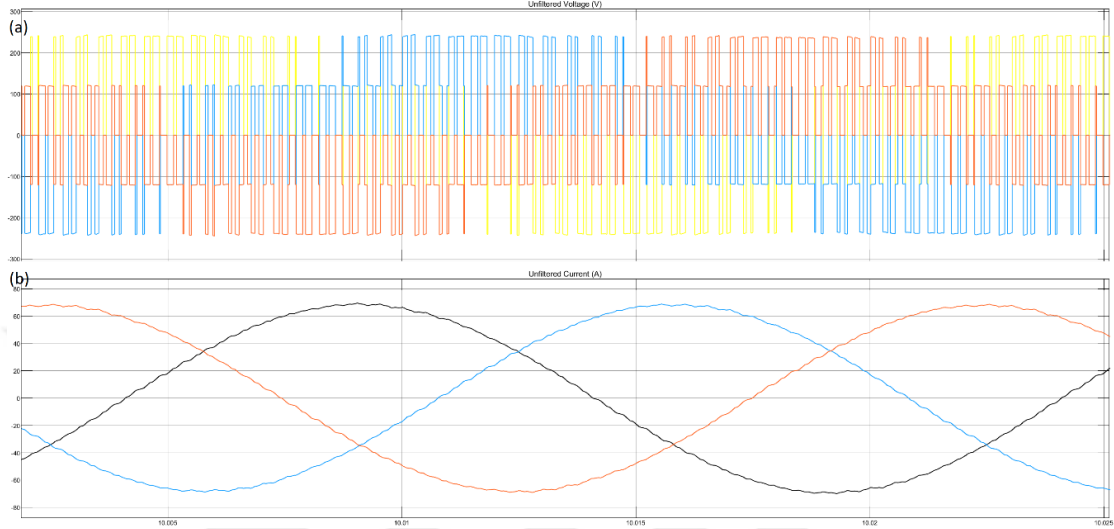


Figure 2.11. Unfiltered waveforms of (a) voltage and (b) current.

Following calculations for the capacitor bank were made,

$$V_{\text{RMS,unfiltered}} = \frac{V_{\text{p-p,unfiltered}}}{2\sqrt{2}} = \frac{400}{2\sqrt{2}} = 141.421\text{V}$$

$$I_{\text{rms,unfiltered}} = \frac{I_{\text{p-p,unfiltered}}}{2\sqrt{2}} = \frac{80}{2\sqrt{2}} = 28.285\text{A}$$

Where $V_{\text{rms,unfiltered}}$, $I_{\text{p-p,unfiltered}}$ are the peak-to-peak voltage and current (Fig 2.11) and $V_{\text{rms,unfiltered}}$, $I_{\text{rms,unfiltered}}$ are the RMS voltage and current values. The apparent power of the inverter can be calculated as

$$S = \sqrt{3}V_{\text{rms}}I_{\text{rms}} = (141.421) \times (28.285) = 6928\text{VA} \cong 7\text{kVA}$$

The reactive power of the capacitor bank is chosen as 10% of the rated power. So that,

$$Q_c = 0.1S = 0.1 \times 7000 = 700\text{Var}$$

$$C = \frac{0.1S}{V^2 2\pi f} = \frac{0.1 \times 7000}{141.421^2 \times 2\pi \times 50} = 111.4\mu\text{F} \cong 120\mu\text{F}$$

Where the frequency, f , is equal to 50Hz. Filtered wave forms will be presented in the results of this section.

2.1.3.8. Per Unit Conversion

The wind turbine gives torque as output and takes the rotational speed as input in per-units. In order to calculate the real values, a simple per-unit calculation blocks which can be seen in Figure 2.12

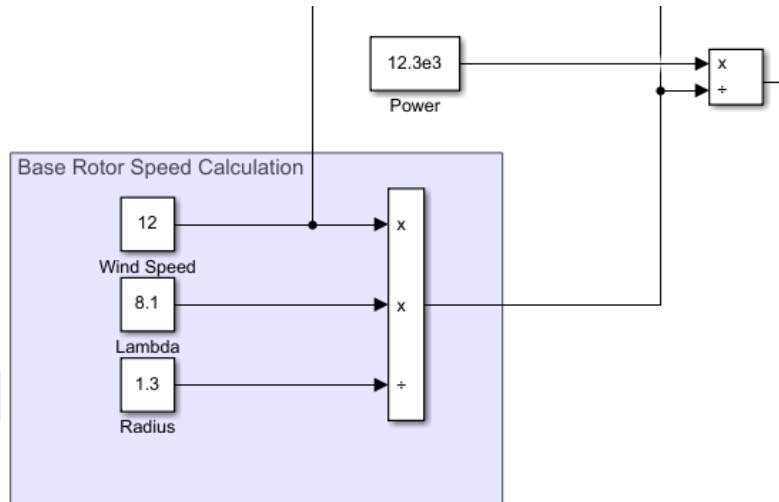


Figure 2.12. Per-unit calculations blocks

Based torque and rotational speed can be calculated as follows,

$$\tau_{\text{base}} = \frac{P}{\omega_{\text{base}}} \quad \& \quad \omega_{\text{base}} = \frac{v \lambda}{r}$$

where P is power, ω is the base rotor speed, v is wind speed, r is Radius, λ tip speed ratio.

For this turbine radius is taken as 1.3 and the tip speed ratio is taken as 8.1 (Cheng and Zhu 2014)

2.1.3.9. Measurement Blocks

Rotor speed, electromagnetic torque, both DC and AC voltages & currents of the machine side, and both filtered and unfiltered voltages and currents of the grid side are measured.

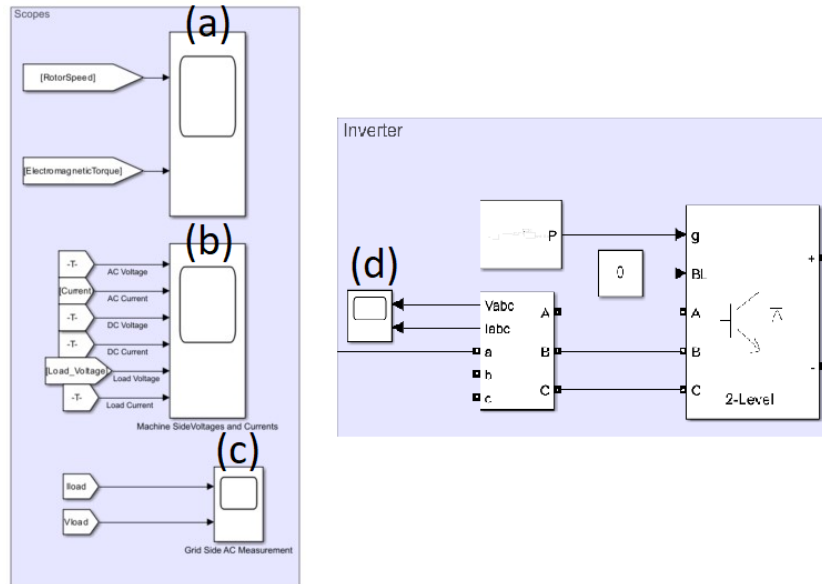


Figure 2.13. Measurement scopes for (a) turbine's rotational speed and electromagnetic torque, (b) machine side AC and DC and voltage measurements, (c) Grid side filtered AC voltage and current measurements, (d) grid side unfiltered AC voltage and currents.

2.1.4. Results

30 seconds of the simulation were made. Figure 2.14 shows the rotational speed per unit and electromagnetic torque in Nm. Electromagnetic torque is negative because the permanent magnet synchronous machine works as a generator. Figure 2.15 shows all current and voltage measurements on the machine side. Voltages are decreased due to a decrease in rotor speed, in contrast, currents seem to be increasing due to an increase in electromagnetic torque. After the rectifier, voltage and current values follow the same pattern on the AC side. Figure 2.16 shows the grid-side voltages and currents. Distortions in the waveforms (see Figure 2.11) are eliminated after the filter.

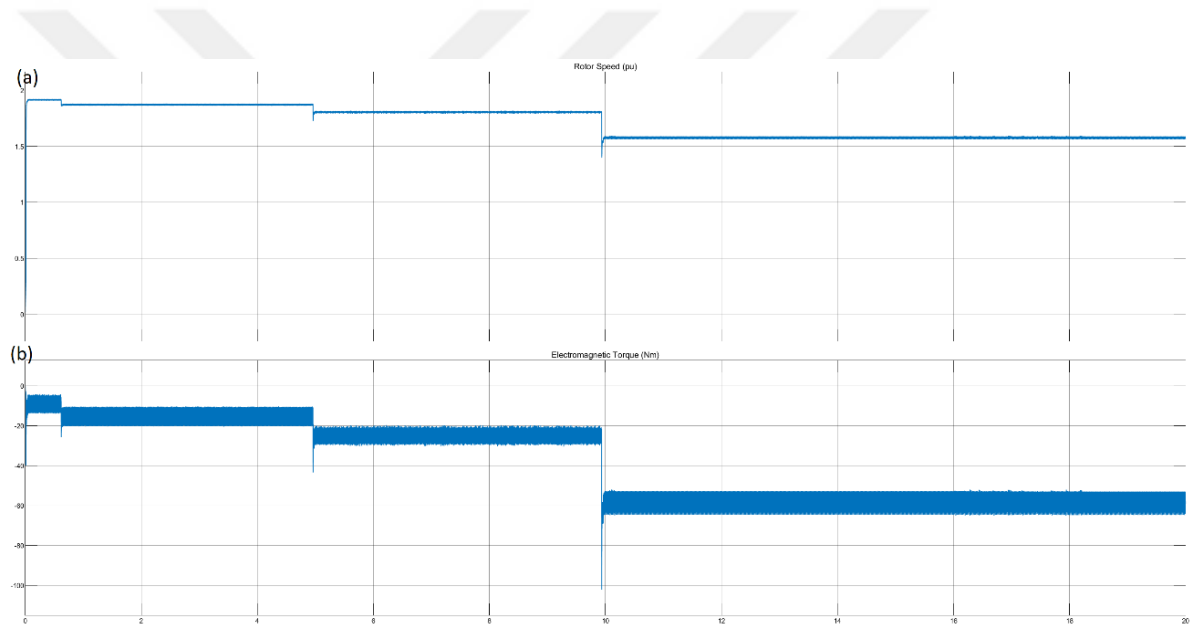


Figure 2.14. (a) Rotational speed in per units, (b) electromagnetic torque in Nm

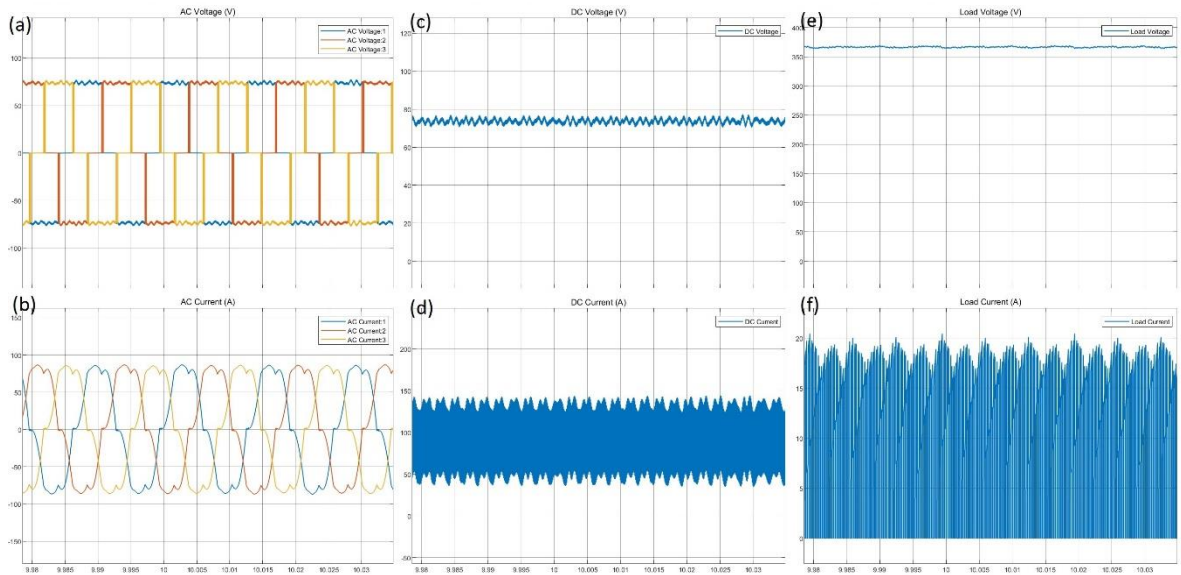
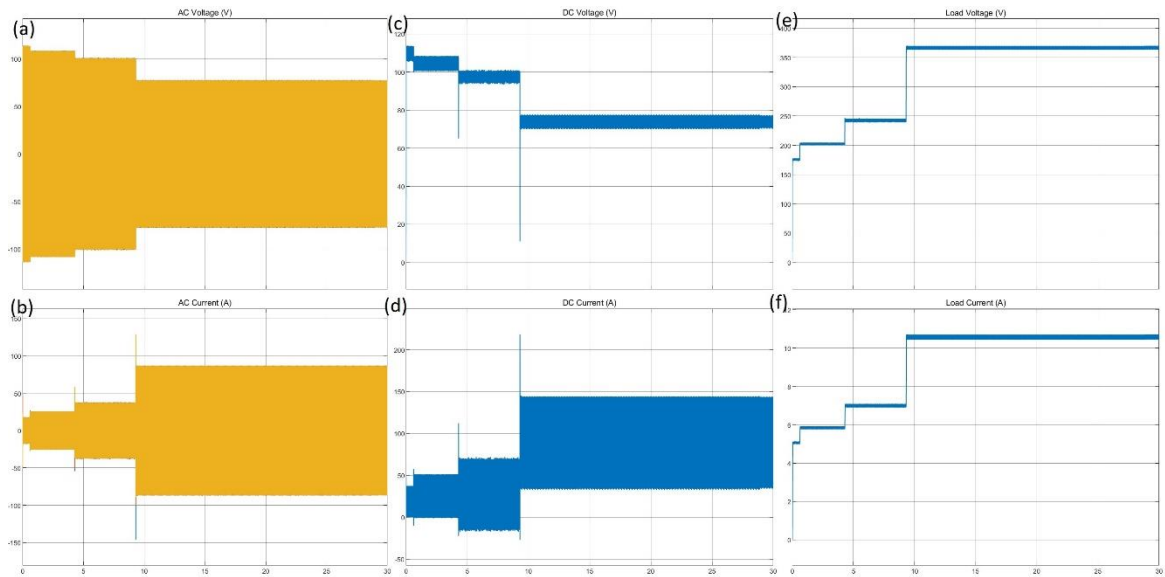


Figure 2.15. Machine side voltages in V and currents in A; (a) voltage after the generator, (b) current after the generator, (c) voltage after the rectifier, (d) current after the rectifier, (e) voltage after the boost converter, (f) current after the boost converter for both overall and closer look.

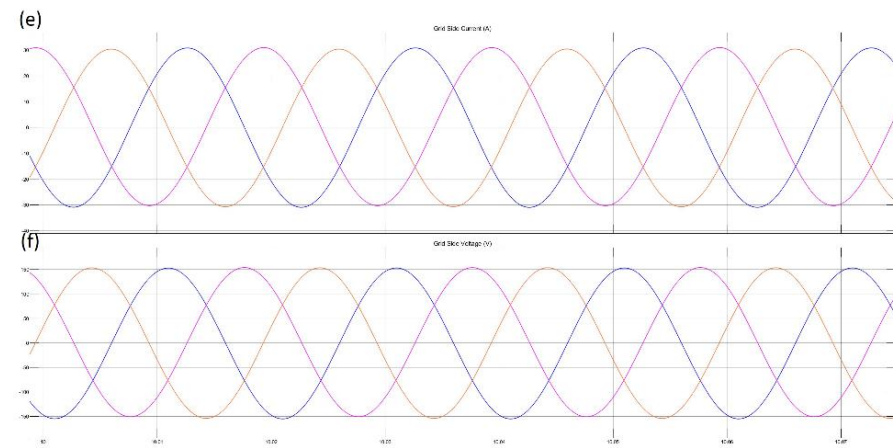
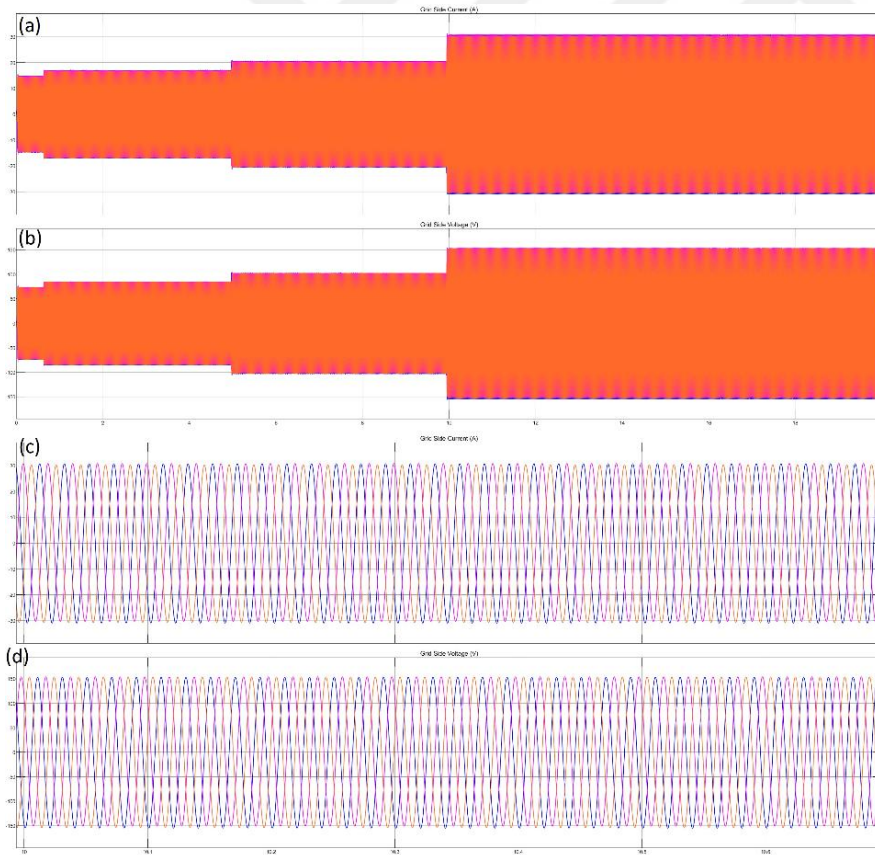


Figure 2.16. Grid side voltage and currents:
 overall (a) voltages, (b) currents;
 closer look to (c) voltages, (d) currents after 10 seconds;
 waveforms of (e) voltage, (f) current

2.2. Solar Photovoltaic Model

2.2.1. Introduction

A solar cell is an electrical device that transforms sunlight directly into energy. Light shining on a solar cell generates both a current and a voltage, which is used to create electricity. This procedure necessitates the use of a material in which light absorption increases an electron to a higher energy state, followed by the passage of this higher energy electron from the solar cell into an external circuit. After dissipating its energy in the external circuit, the electron returns to the solar cell (Christiana Honsberg and Stuart Bowden n.d.). After electric field formation and separation of charges, current flow begins which results in the generation of electricity. Figure 2.17 shows the solar cell mechanism (Kar, Banerjee, and Chanda 2021).

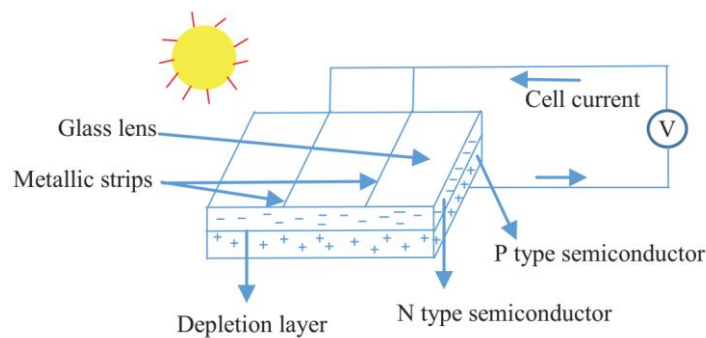


Figure 2.17. PV cell model (Kar, Banerjee, and Chanda 2021).

Mostly circuit modeling is used for PV models. Figure 2.18 shows the single-diode circuit modeling of PV cells in both ideal and non-ideal conditions (Kar, Banerjee, and Chanda 2021; Nasirudeen et al. 2021). Two diode models also can be used for the PV cell model (Hoarca 2021).

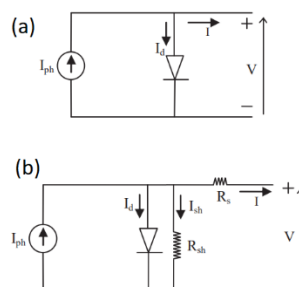


Figure 2.18. Single diode model in ideal (a) and non-ideal (b) conditions (Kar, Banerjee, and Chanda 2021).

The following sets of equations are used to model PV cells (Kar, Banerjee, and Chanda 2021). Equation 2.3 represents the reverse saturation current I_o .

$$I_o = \left(\frac{T}{T_n}\right)^3 I_{rs} e^{\left(\frac{1}{T_n} - \frac{1}{T}\right)qE_{go}/nK} \quad (2.3)$$

Where T is the ambient temperature, T_n is the reference temperature, I_{rs} is the reference saturation current, E_{go} is the band gap (1.1eV), q is the charge of the electron (1.602×10^{-19} C), K is the Boltzmann constant 1.3806×10^{-23} J/K, and the n is the ideality factor of the photodiode. Photocurrent (I_{ph}) and shunt current (I_{sh}), can be written in Equation 2.4 and Equation 2.5, respectively.

$$I_{ph} = \frac{G}{1000} (I_{sc} + k_i(T - T_n)) \quad (2.4)$$

Where G is the solar insolation (W/m^2) and k_i is the short-circuit current's temperature coefficient. Reverse saturation current can be derived from Equation 2.5.

$$I_{rs} = \frac{I_{sc}}{e^{nN_sKT} - 1} \quad (2.5)$$

Where V_{oc} is the open circuit voltage, N_s is the number of cells connected in series.

By combining the equations that are given, the output PV current can be expressed in Equation 2.6.

$$I = I_{ph} - \left(e^{\frac{(I_{rs} + V)q}{nKT N_s}} - 1 \right) I_o - I_{sh} \quad (2.6)$$

In this study, the Simulink model for PV array is used and necessary system components for Maximum Power Tracking (MPPT) are added.

2.2.2. Simulink Model of Solar PV Array

A Simulink model of the PV array was used for this part of the thesis. The reason behind it is not only it is a very well-established model but also many different commercial modules can be selected through the PV array block. Figure 2.19 shows an overall scheme for the solar PV part, and Figure 2.21 shows the Simulink model according to it. The system consists of a PV array, repeating sequence for irradiation, Boost converter, MPPT function block, PWM generator, measurement blocks and a load. Details about components will be addressed in 2.2.3.

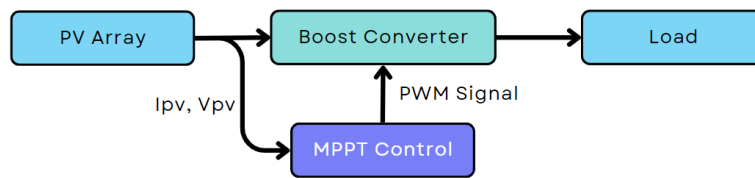


Figure 2.19. System scheme for solar PV.

Fixed step solver with 5×10^{-6} s fixed-step size is used. Solver was chosen as ode23t (mod. stiff/trapezoidal) because the system consists of components from Simulink Simscape Electrical models (MathWorks n.d.). A total of 10 seconds of simulation was made with changing irradiancies at a constant temperature of 25°C. Figure 2.20 shows the changing irradiancies (W/m^2) during the simulation with respect to time.

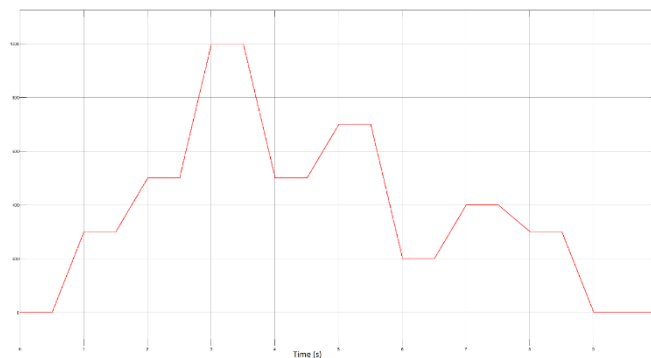


Figure 2.20. Changing irradiancies values (W/m^2) with respect to time.

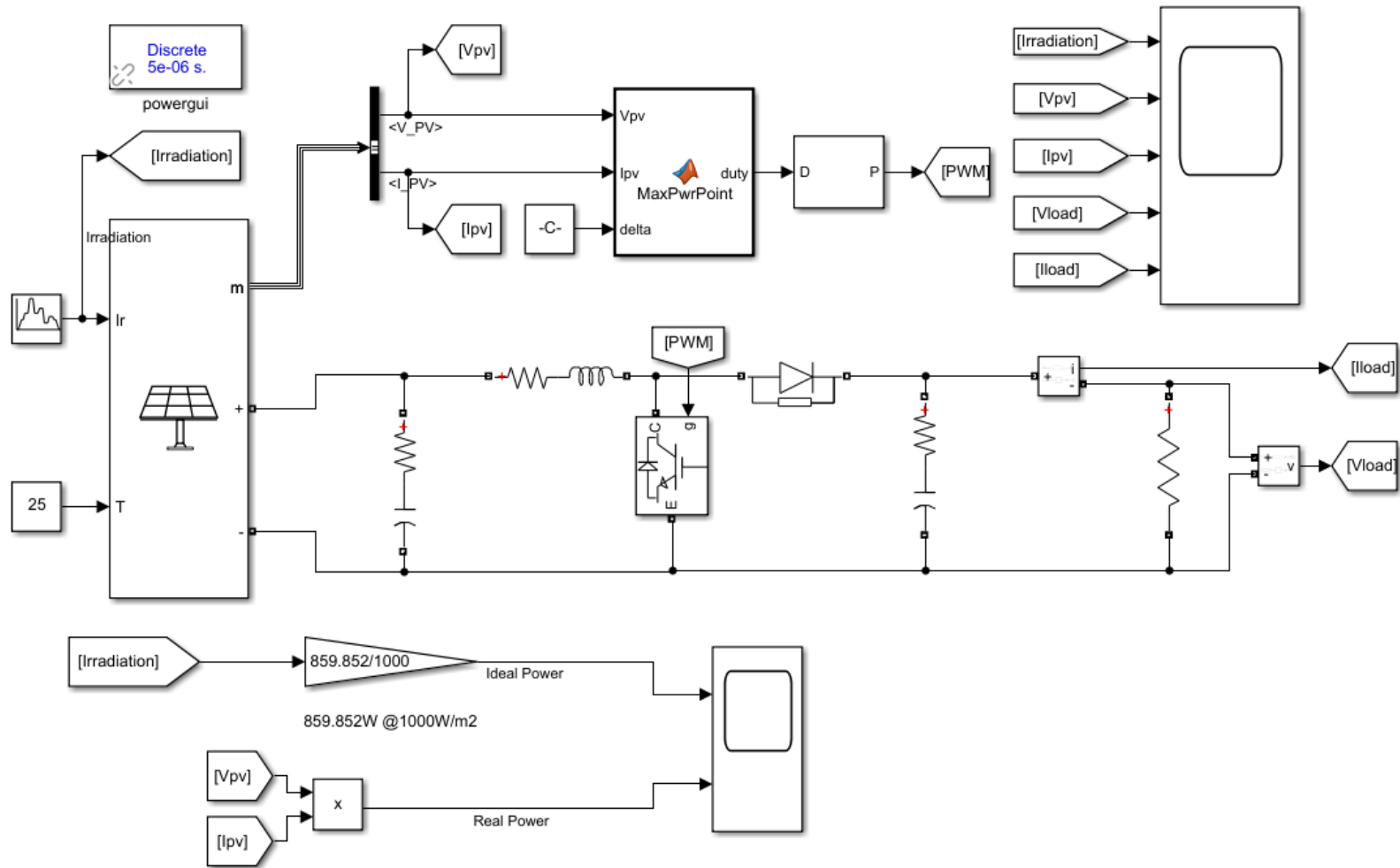


Figure 2.21. Overall PV system in Simulink

2.2.3. System Components

2.2.3.1. PV Array

Simulink PV Array block is used. It allows for the selection of different commercial PV panels and array details (parallel strings and series-connected modules per string) can be altered. For this simulation, 2 parallel and 2 series-connected modules per string are used. STR215 model of Solartech Renewables is used. Table 2.3 shows PV module parameters and Figure 2.22 shows the I-V curves for that panel for different irradiation values.

Table 2.3 Module parameters

Maximum Power (W)	214.9
# of cells per module	60
Open-circuit voltage, V_{oc} (V)	36
Short-circuit current, I_{sc} (A)	7.73
Maximum Power Point Voltage, V_{mp} (V)	28.7
Maximum Power Point Current, I_{mp} (A)	7.49
Temperature coefficient for voltage (%/°C)	-0.41
Temperature coefficient for current (%/°C)	-0.05

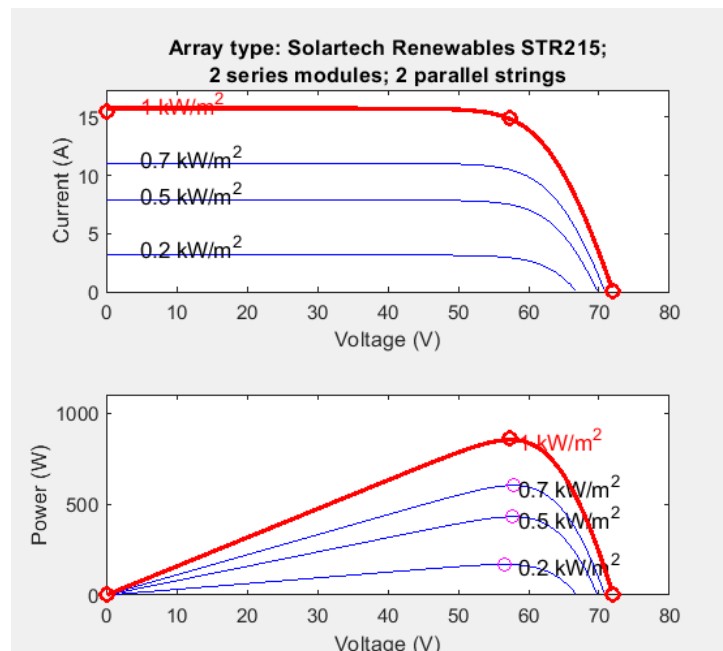


Figure 2.22. I-V and power curves for the selected module for different irradiation values.

2.2.3.2. Boost Converter

In order to control the PV array at Maximum Power Point, a Boost DC-DC converter was used. Figure 2.23 shows the Simulink block diagram for the Boost converter and Table 2.4 shows values of circuit elements. Pulse Width Modulation (PWM) signal was obtained from a MATLAB function block for Maximum Power Point Tracking which uses Perturb and Observe algorithm. MATLAB function block basically returns a duty cycle. After that, the PWM generation block is used to drive the Boost converter's switch. Details about this algorithm will be given in Chapter IV. Ripples in current and voltage differ because of varying duty cycles over time.

Table 2.4 Boost Converter components and values of them.

Component		Value
	Inductor	$4.5573 \times 10^{-5} \text{ H}$
	Capacitor	$6.6094 \times 10^{-4} \text{ F}$
IGBT Diode	Internal Resistance	$1 \times 10^{-3} \Omega$
	Snubber Resistance	$1 \times 10^5 \Omega$

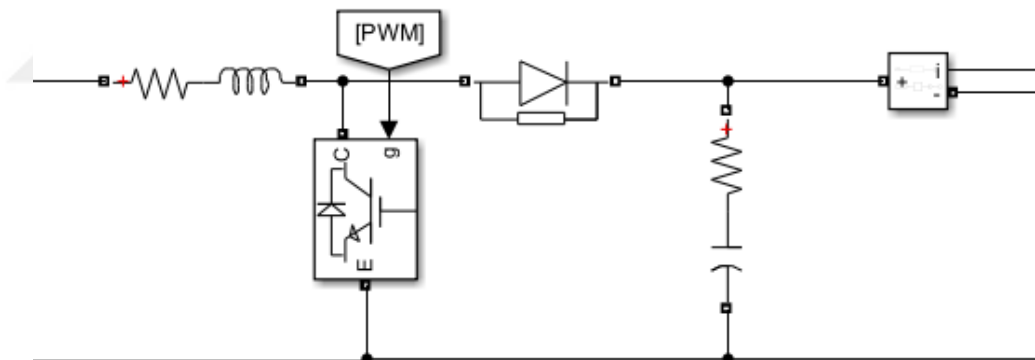


Figure 2.23. DC-DC Boost Converter block diagram.

2.2.3.3. Maximum Power Point Tracking and Pulse Width Modulation Generation

A MATLAB function block is used for Perturb and Observe MPPT algorithm. V_{pv} and I_{pv} are continuously measured from PV panels measurement port and function calculates power and changes duty cycle by seeking a point the derivative of the power

becomes nearly zero $\frac{dP}{dV} \approx 0$ (Local Maximum Point) on the power curve. After deciding the duty cycle, Simulink's PWM generator block for DC-DC converters is used. The switching frequency of the PWM block is 5kHz and the sample time is 5×10^{-6} s. Figure 2.24 shows the overall block diagram.

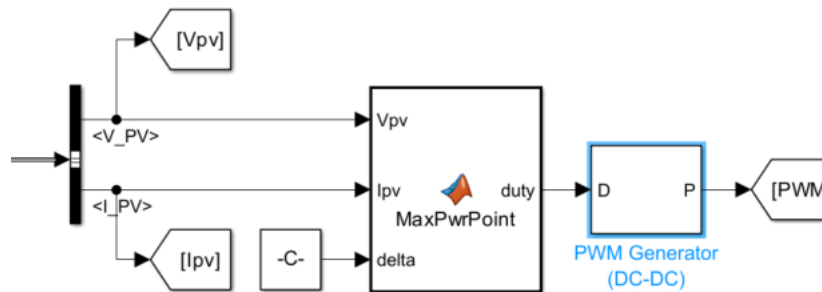


Figure 2.24. MPPT and PWM generation blocks.

2.2.3.4. Measurement Blocks

Current and voltages on both the PV side and load side are measured. In addition, changing irradiation values can be seen in the same scope. Power measurements are also made in different scopes. The panel gives 859.852W of power at its maximum power point of $1000\text{W}/\text{m}^2$ radiation. In order to see if the system is able to follow the maximum power point at different irradiation, one input of the same scope shows the maximum power point for different irradiation values. Figure 2.25 shows the measurement scopes.

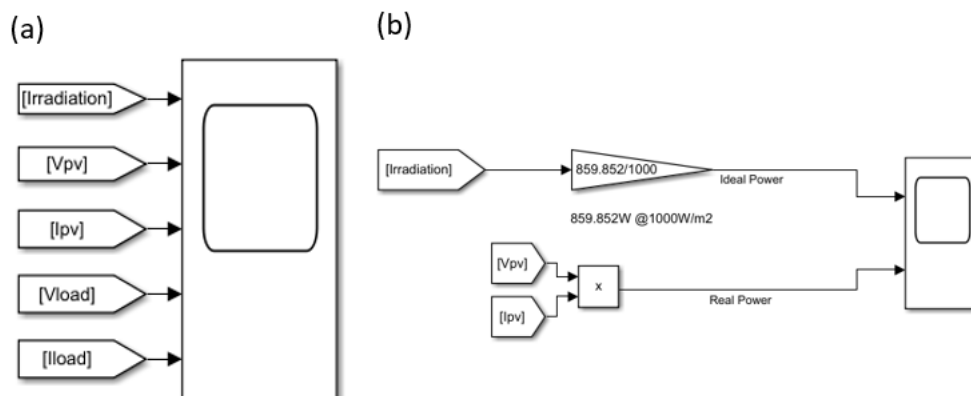


Figure 2.25. Scopes for both (a) voltages and currents and (b) powers.

2.3.4 Results

10 seconds of the simulation were made. Figure 2.26 shows voltage and current waveforms for both the PV side and load side. There are some ripples for both measurements due to the boost converter. Figure 2.27 shows the power measurements; the PV array follows ideal power which shows MPPT for this model works.

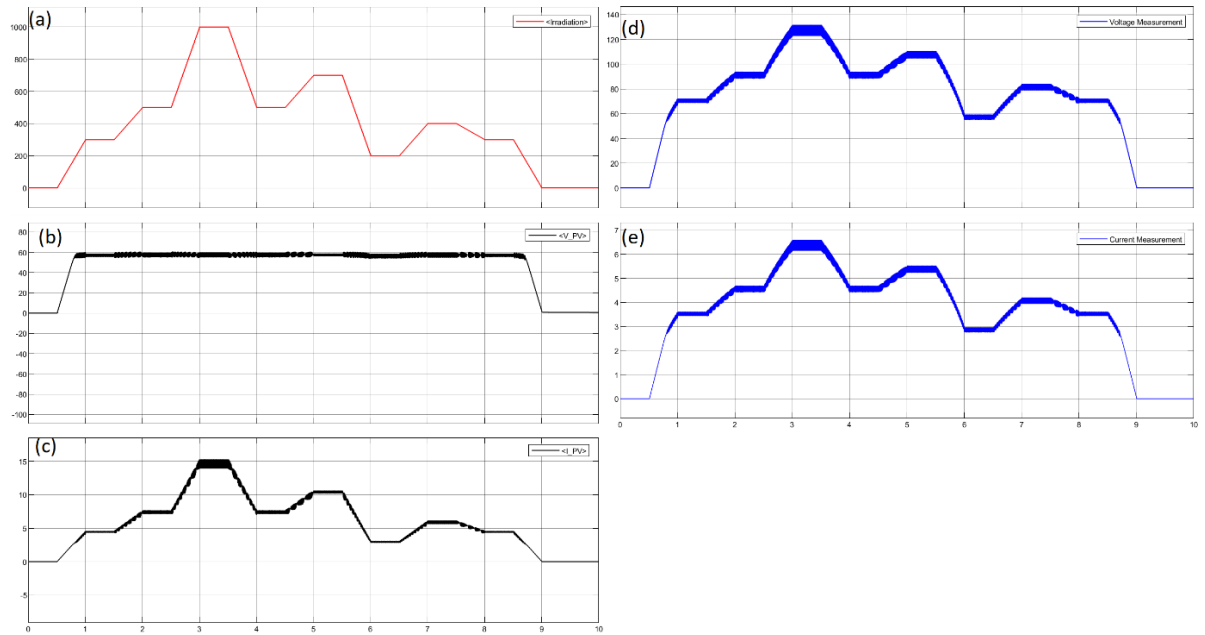


Figure 2.26. (a) Irradiation W/m², (b) PV voltage, (c) PV current, (d) Load voltage, (e) Load current

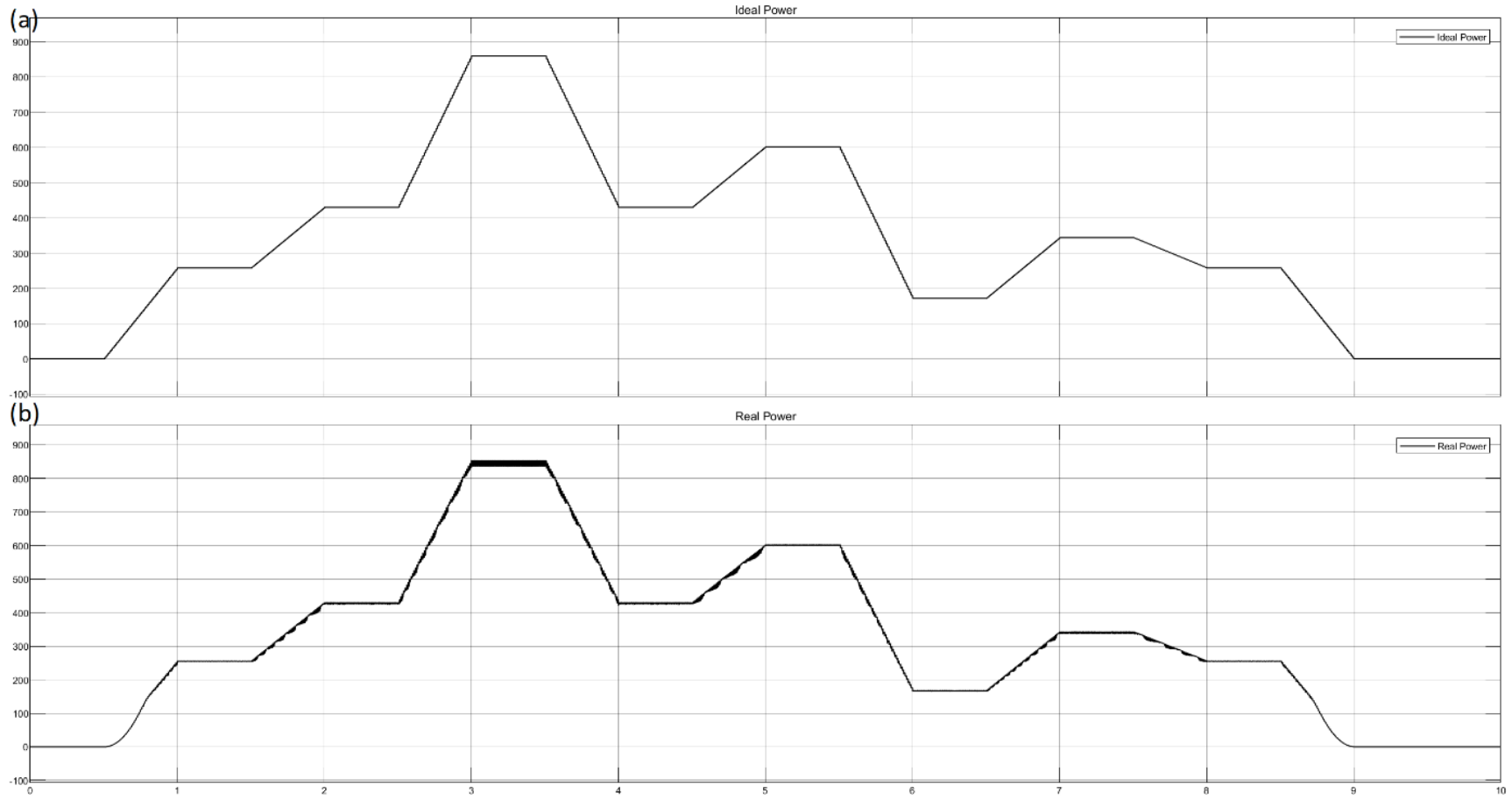


Figure 2.27. (a) Ideal power from the power curve, (b) measured power.

2.3 Battery Pack

2.3.1. Introduction

The battery offers chemical energy storage that can be delivered as portable electrical energy with a high conversion efficiency and no gaseous emissions. Additionally, it is preferable to convert alternative energy sources into direct current (DC) electrical energy that is suitable for storing as chemical energy in batteries (Goodenough and Kim 2010).

Although there are different energy storage systems and other battery technologies, Lithium batteries are the leading option for effectively storing (HCI Energy 2023). Li-ion batteries almost cover 90% of the global market (Lottie Limb 2022). Longer lifespan and greater higher power and energy densities are the main advantages of Li-ion batteries compared to Lead acid batteries (Diouf and Pode 2015). Figure 2.28 shows the volumetric and gravimetric energy density comparison between different battery technologies.

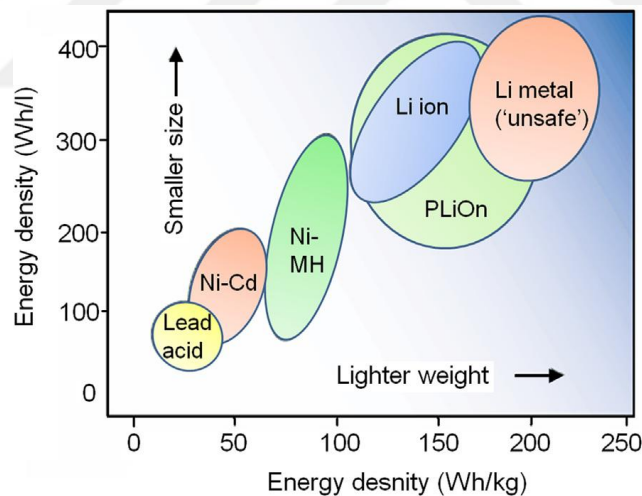


Figure 2.28. Comparison between different battery technologies (Diouf and Pode 2015).

Lithium-ion (Li-ion) batteries are used in many applications. They consist of an anode, cathode, electrolyte, separator, and current collectors: The negative electrode, or anode, is typically made of graphite and serves as a reservoir for lithium ions during charging; the positive electrode, or cathode, receives lithium ions during discharge; it is typically made of metal oxides, conductive medium, or electrolyte, which enables lithium ions' movements; porous material placed between the anode and cathode, or separator, which prevents direct contact or short circuits while allowing the flow of lithium ions

(Miranda, Costa, and Lanceros-Mendez 2015). Figure 2.29 shows the main structure of the Li-ion battery and the extraction and insertion processes of ions.

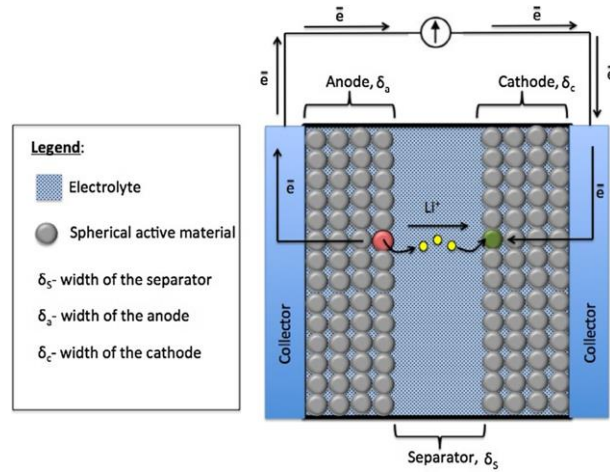


Figure 2.29. Main structure of Li-ion battery and main processes in it (Miranda, Costa, and Lanceros-Mendez 2015).

There are several battery models in the literature based on the application. Generally, batteries can be modeled as electrical circuits including resistors and capacitors which represent different features of the batteries (Castano et al. 2015; Chen and Rincón-Mora 2006). Mousavi and Nikdel reviewed various models in their paper for different needs of applications (Mousavi G. and Nikdel 2014).

In this study, Simulink's Generic Battery block is used for simulations.

2.3.2. Simulink Model for Battery Pack

Simulink's Generic Battery block is used for this model. This model is very easy to use regarding easiness of selection of the battery's type (Lead-acid, Lithium-ion, Nickel-Cadmium, Nickel-Metal-Hydride) and giving its parameters (Nominal voltage, rated capacity, response time of the battery). It also allows us to give an initial state of charge. Additionally, simulation of aging and temperature effects can be possible with this model. Figure 2.30 shows an overall scheme for the battery and charging & discharging of the battery. The system consists of a battery pack, charge or discharge decision blocks, and charging & discharging circuits. Figure 2.31 shows the Simulink system for battery and charge-discharge circuits.

Fixed step solver with 1×10^{-3} s fixed-step size is used. Solver was chosen as ode23t (mod. stiff/trapezoidal) because the system consists of components from Simulink

Simscape Electrical models (MathWorks n.d.). A total of 500 seconds of simulation was made.

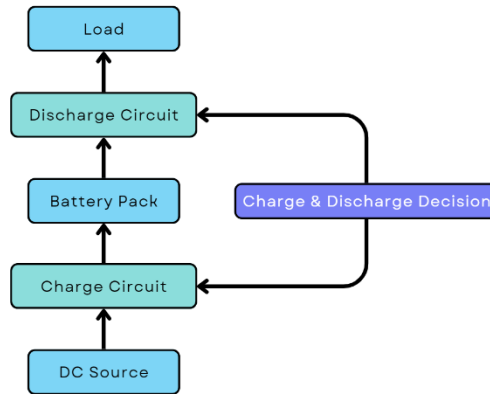


Figure 2.30. System scheme for battery and charging & discharging of the Battery.

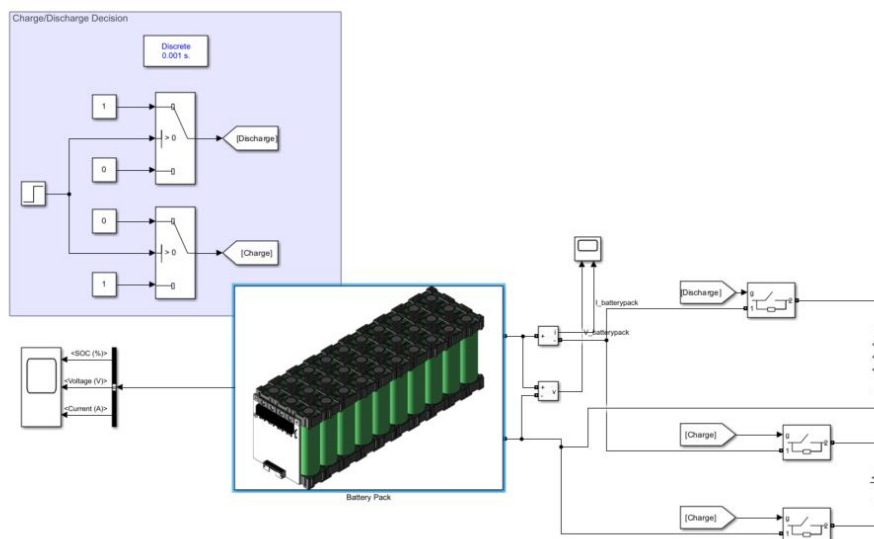


Figure 2.31. Overall battery system in Simulink including charge and discharge circuits.

2.3.3. System Components

2.3.3.1. Battery Pack

The battery pack consists of 3 parallel and 3 series total of 9 batteries. For each battery, the nominal voltage is chosen as 12V, and the rated capacity is 30Ah. The resulting capacity of the battery pack can be calculated as follows:

Voltage of the storage system \times Capacity of the storage system = $36V \times 90Ah = 3.24kWh$

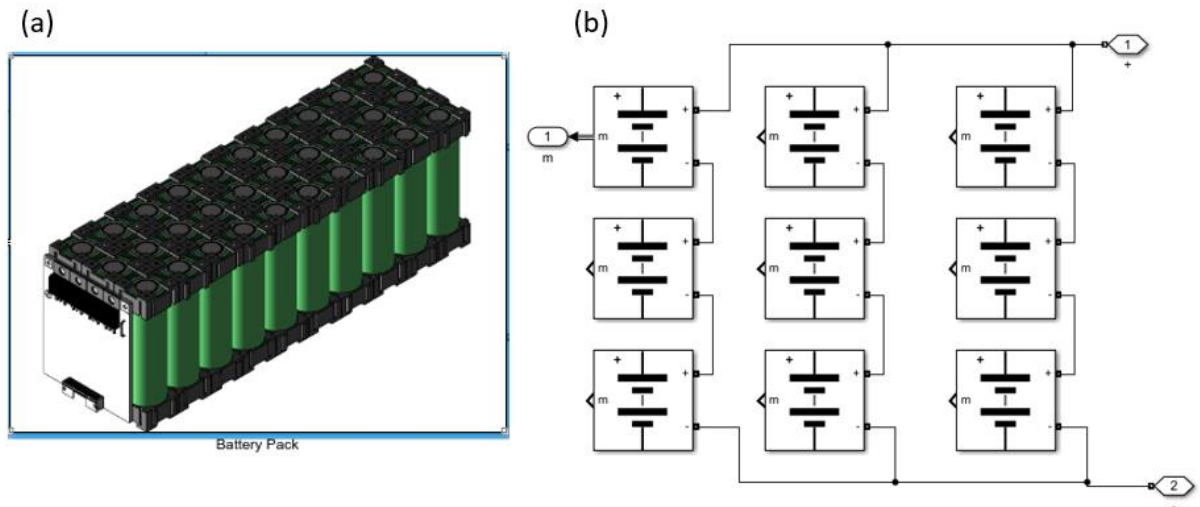


Figure 2.32. (a) Battery Pack, (b) Subsystem for battery pack

2.3.3.2. Charge & Discharge Decision

The decision for charging or discharging is made on time dependency. It uses a step function that values changes between 0 and 1 for a given step time. It can be altered by applying any kind of function which decides the gate signals of ideal switches. Figure 2.33 shows the decision block for charge or discharge states.

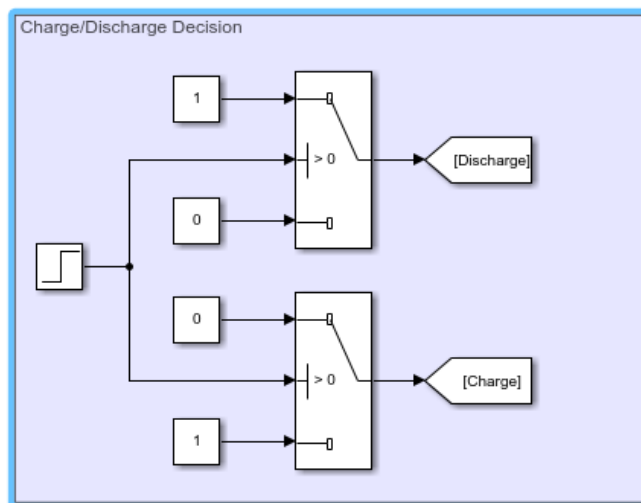


Figure 2.33. Charge or discharge decision blocks.

2.3.3.3. Charge & Discharge Circuits

Charge or discharge circuits are consisting of a voltage source with $V = 50V$ and a pure resistive load with $R = 1 \Omega$, respectively. Figure 2.34 shows charge and discharge circuits.

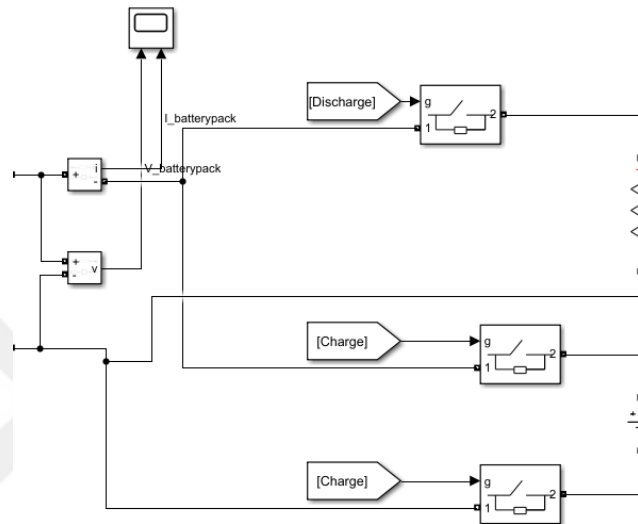


Figure 2.34. Charge and discharge circuits.

2.3.4. Results

A total of 500 seconds of simulation was made. The initial SOC of the battery pack is 100%. Simulation is initialized for the system that allows it to discharge for 250 seconds and afterward charge for 250 seconds. Figure 2.35 shows resulted graphs for SOC, voltage, and current. It can be seen that based on the charge or discharge decision, the system works correctly.

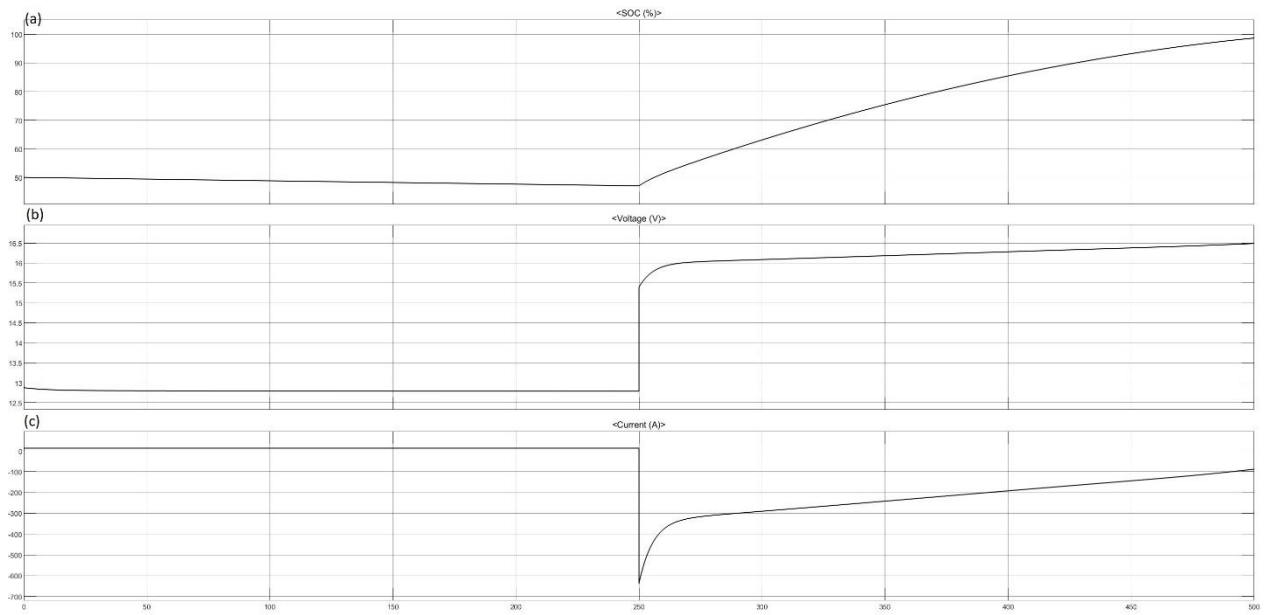


Figure 2.35. (a) SOC of battery pack (%), (b) Voltage of battery (V), (c) Current of battery (A)

2.4. Electrolyzer Model

2.4.1. Introduction

An electrolyzer produces gases that can be utilized for a variety of purposes, such as fuel cells, industrial processes, or energy storage, by splitting water or other electrolytes into their component components or ions using electrical energy. It consists of an electrolyte solution and two electrodes—an anode and a cathode—immersed in the electrolyte.

There are several types of electrolyzers: Alkaline Water Electrolyzer (AWE), Alkaline Anion Exchange Membrane (AEM) Electrolyzer, Proton Exchange Membrane (PEM) Electrolyzer, High-Temperature Steam Electrolyzer (HTSE), Solid Oxide Electrolyzer (SOE). AWE consists of two electrodes, a diaphragm, and a liquid electrolyte solution while The PEM Electrolyzer consists of electrodes and electrolytes (mostly platinum, iridium, and ruthenium). The PEM employs a solid polymer membrane electrolyte, whereas the AWE uses a corrosive liquid electrolyte. AEM Electrolyzer is a combination of PEM and AEM electrolyzers which also combines the advantages of both. HTSE uses heat as the replacement of electrical energy for decomposing the water molecule. SOE operates at high temperatures to achieve efficient ionic conductivity through the solid oxide electrolyte (Benghanem et al. 2023; Faye, Szpunar, and Eduok 2022; Nikolaidis and Poullikkas 2017). There are several ways to model electrolyzers; thermal models, electrochemical models, equivalent circuit models, and mass transfer models (Majumdar et al. 2023).

In this thesis, a PEM electrolyzer is used in HRES. Figure 2.36 shows the schematic for the PEM electrolyzer and Figure 2.37 shows an equivalent circuit model for the PEM electrolyzer (Atlam and Kolhe 2011; Sood et al. 2020).

Eq 2.7 and Eq 2.8 can be used for the I – V characterization of PEM.

$$V(T, p) = e_{rev}(T, p) - e_{rev}(T, p)e^{-\frac{5I}{0.02}} + IR_i(T, p) \quad (2.7)$$

$$I(T, p) = \begin{cases} 0, & V \leq e_{rev}(T, p) \\ \frac{1}{R_i(T, p)}(V - e_{rev}(T, p)) & V \geq e_{rev}(T, p) \end{cases} \quad (2.8)$$

where $e_{rev}(T, p)$ is the reverse voltage which is a function of temperature (T) and pressure (p). I is the input current R_i is initial PEM cell resistance.

In this thesis, the MathWorks PEM Electrolysis system is used for simulations.

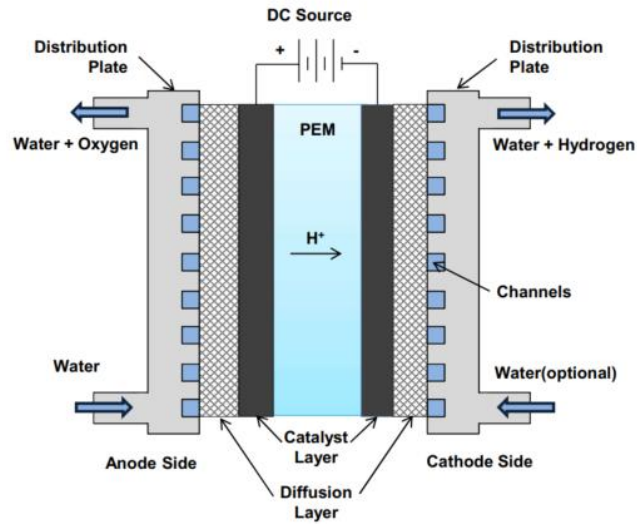


Figure 2.36. Schematics for PEM electrolyzer (Atlam and Kolhe 2011).

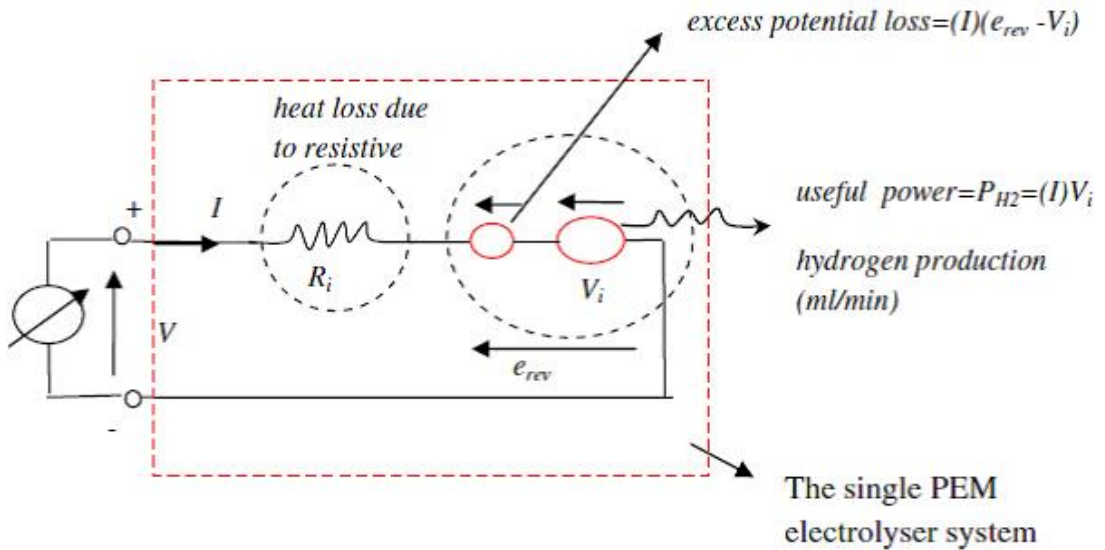


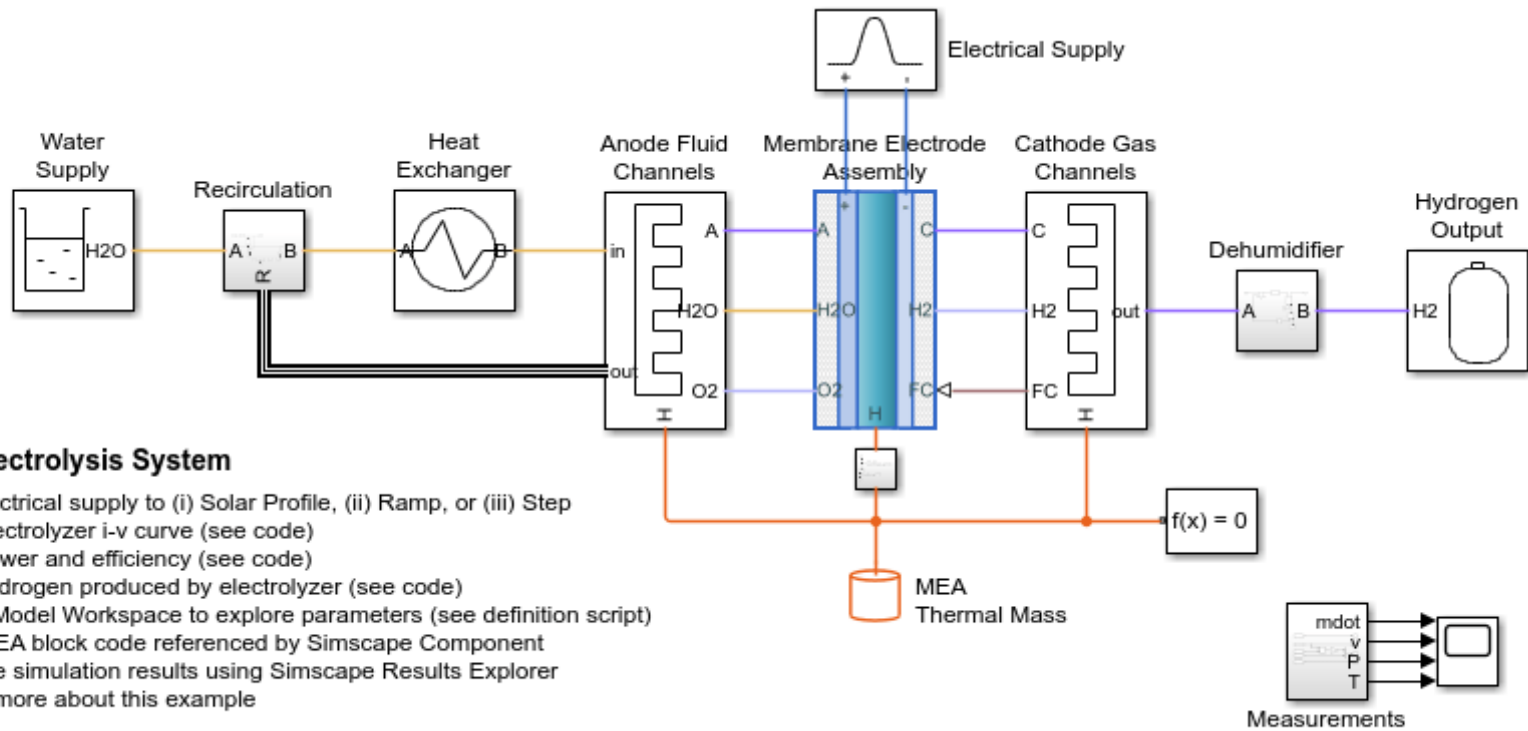
Figure 2.37. Equivalent electrical model of single cell PEM Electrolyzer (Sood et al. 2020).

2.4.2. MathWorks Electrolyzer Model

MathWorks Electrolyzer Model is used for this part. This is a very good model that enables different power sources and also all parameters of the model can be altered through a m.file. Also, it measures stack temperatures, and hydrogen flow rate during the simulation. Additionally, it allows plot efficiency, I-V curves, and hydrogen production. The model consists of an electrical supply, anode fluid channels, cathode gas channels, a dehumidifier, a heat exchanger, a hydrogen output system, a recirculation system, a separator tank, and a water supply. Figure 2.38 shows the overall system.

A thermal liquid network that simulates the water supply, an anode moist air network that simulates the flow of oxygen, and a cathode moist air network that simulates the flow of hydrogen are all connected to the custom block that represents the membrane electrode assembly (MEA).

A global solver configuration is used for the overall model. A total of 86400 seconds of simulation (representing one day) was made.



PEM Electrolysis System

1. Set electrical supply to (i) Solar Profile, (ii) Ramp, or (iii) Step
2. Plot electrolyzer i-v curve (see code)
3. Plot power and efficiency (see code)
4. Plot hydrogen produced by electrolyzer (see code)
5. Open Model Workspace to explore parameters (see definition script)
6. See MEA block code referenced by Simscape Component
7. Explore simulation results using Simscape Results Explorer
8. Learn more about this example

Copyright 2021-2022 The MathWorks, Inc.

Figure 2.38. MathWorks PEM Electrolysis System

2.4.3. System Components

2.4.3.1. Electrical Supply

The electrical supply for this model can be set to solar profile, ramp, and step. Also, it can be altered from the embedded m.file. Figure 2.39 shows the electrical subsystem.

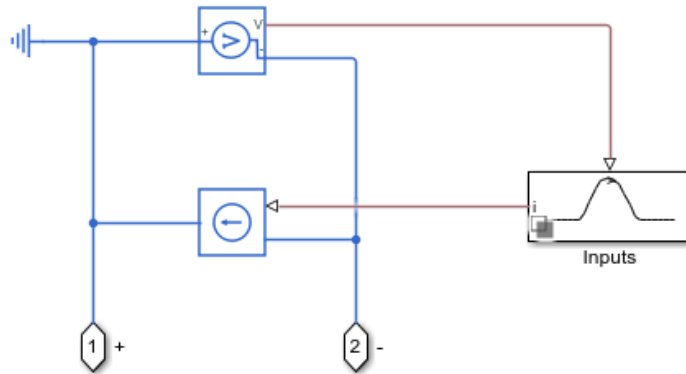


Figure 2.39. Electrical supply subsystem

2.4.3.2. Anode Fluid Channels

The excess water flow carries away the oxygen produced at the anode, and the anode moist air network models it separately. Figure 2.40 shows the anode fluid channel subsystem.

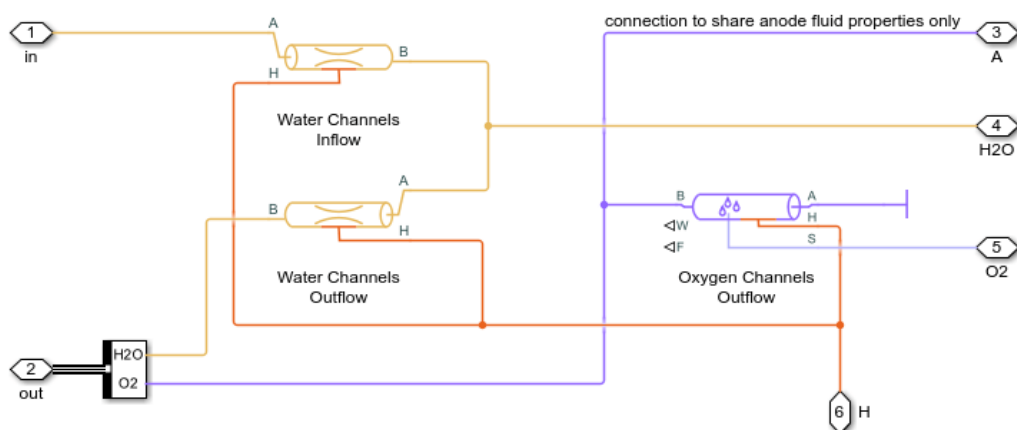


Figure 2.40. Anode fluid channel subsystem.

2.4.3.3. Cathode Gas Channels

The cathode moist air network models the hydrogen created at the cathode side as well as any water that has been transferred across the MEA. Figure 2.41 shows the cathode gas channel subsystem.

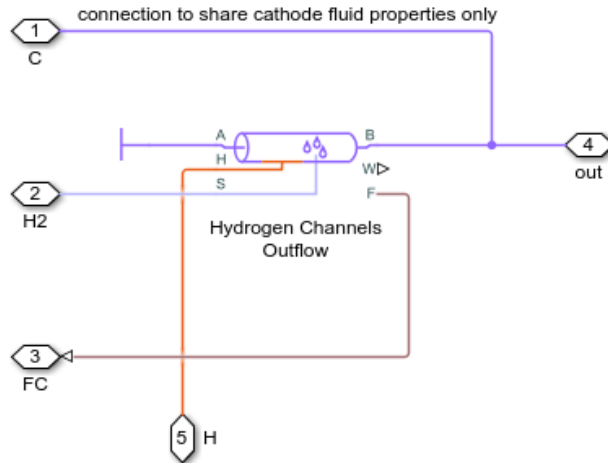


Figure 2.41. Cathode Gas Channel Subsystem

2.4.3.4. Dehumidifier

Unwanted water vapor from the hydrogen is eliminated by the dehumidifier. Figure 2.42 shows the dehumidifier subsystem.

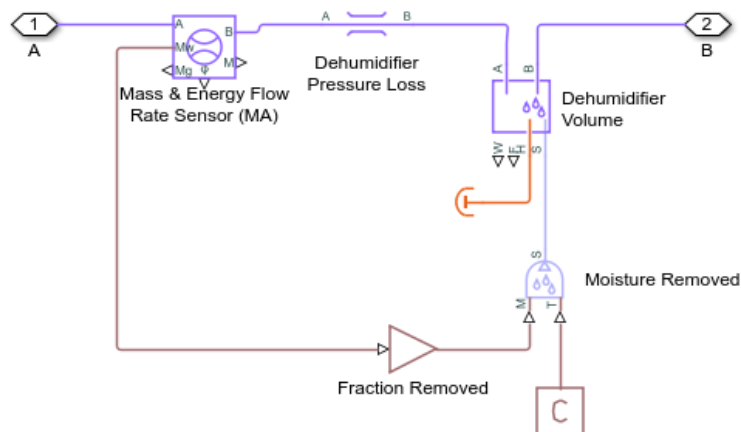


Figure 2.42. Dehumidifier subsystem

2.4.3.5. Heat Exchanger

Excess water is used for carrying away heat dissipation and is rejected by the heat exchanger. Figure 2.43 shows the heat exchanger subsystem.

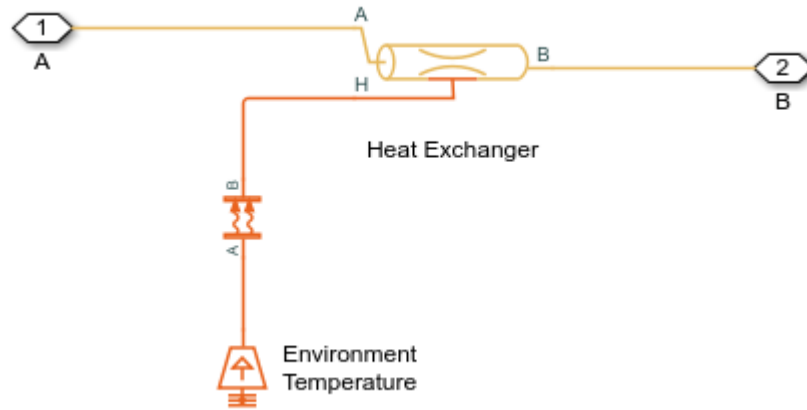


Figure 2.43. Heat exchanger subsystem.

2.4.3.6. Hydrogen Output

The hydrogen output subsystem measures the mass flow rate of the hydrogen under defined parameters. Figure 2.44 shows the hydrogen output subsystem.

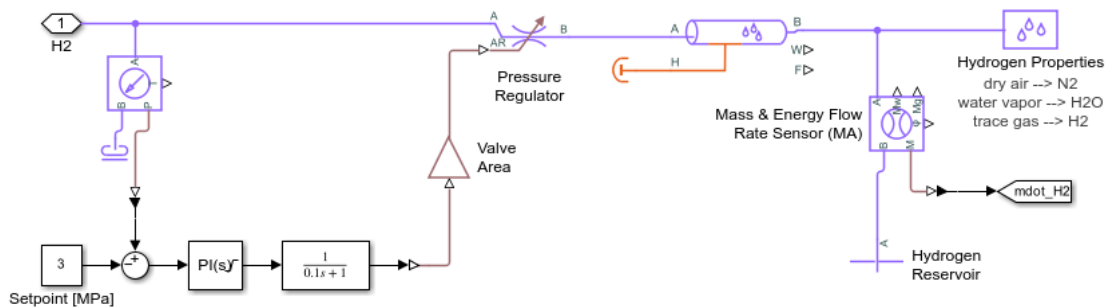


Figure 2.44. Hydrogen output subsystem.

2.4.3.7. Recirculation

The recirculating water of the electrolyzer is controlled to keep the temperature at 80 degrees Celsius. Figure 2.45 shows the recirculation subsystem.

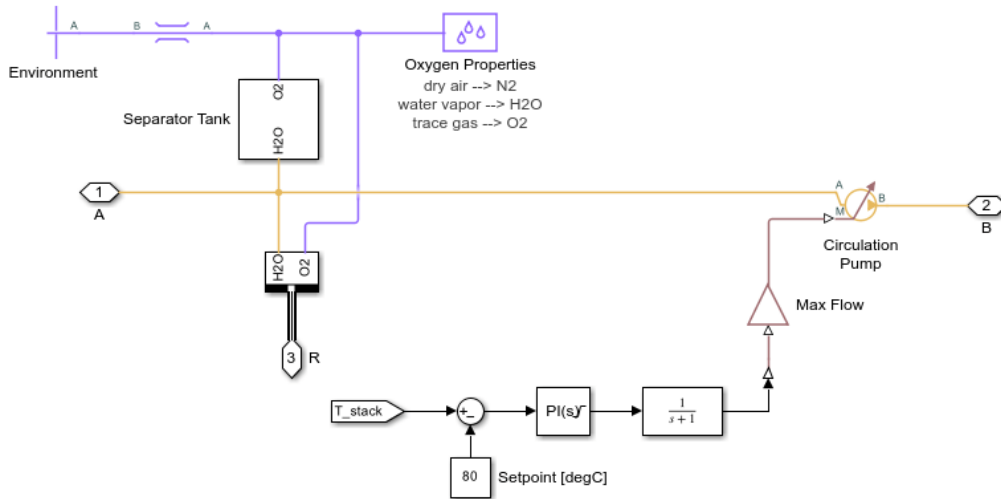


Figure 2.45. Recirculation subsystem.

2.4.3.8. Separator Tank

Before the oxygen is vented, the water and oxygen balance in the return flow is modeled in the separator tank. Figure 2.46 shows the separator tank subsystem.

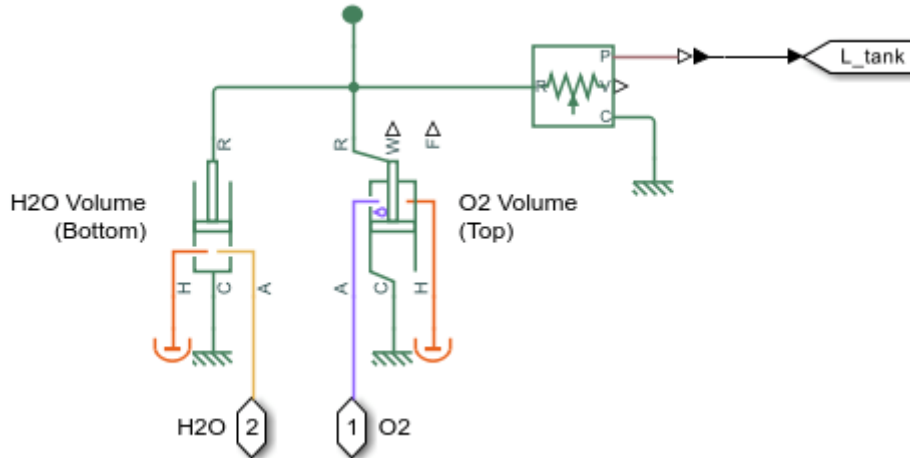


Figure 2.46. Separator tank subsystem.

2.4.3.9. Water Supply

The system is refilled with new water by the supply pump. Figure 2.47 shows the water tank subsystem.

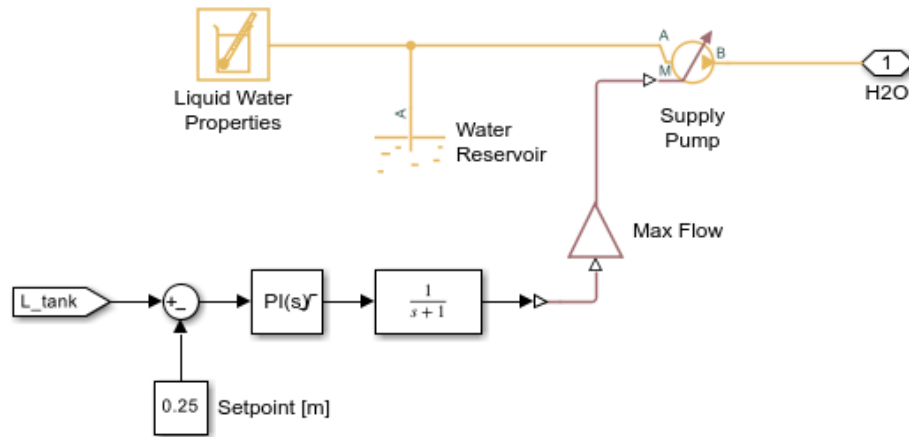


Figure 2.47. Water tank subsystem.

2.4.3.10. Measurement Block

This model measures the hydrogen flow rate in kg/s, stack voltage in V, stack current in A, power of the stack power (both electrical and heat) in kW, and stack temperature in °C. Figure 2.48 shows the block diagram for measurements and the subsystem beneath it.

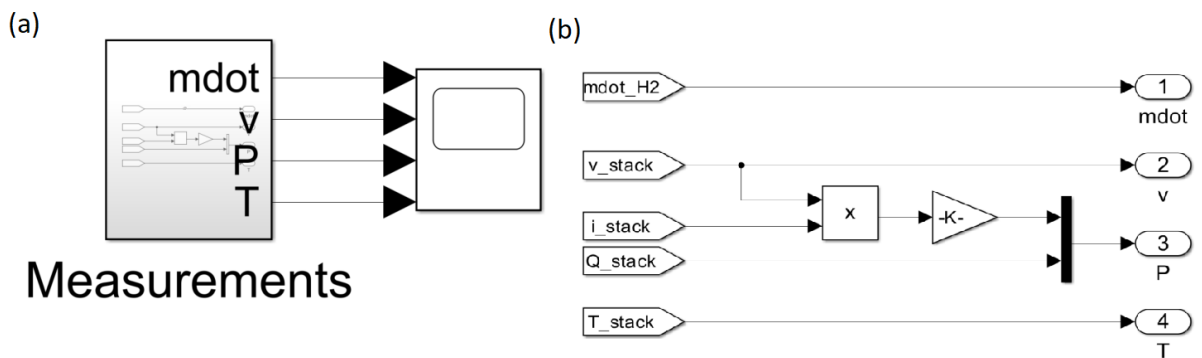


Figure 2.48. (a) Measurement block, (b) Subsystem of measurement block.

2.4.4. Results

86400 seconds of simulation which represents one day was made. Electrical supply is selected as the step function which starts to give constant power at hour 1. Figure 2.36 shows the results of the simulation. It can be seen that hydrogen production, powers, stack voltage and currents, and temperature stay constant after the step function is applied.

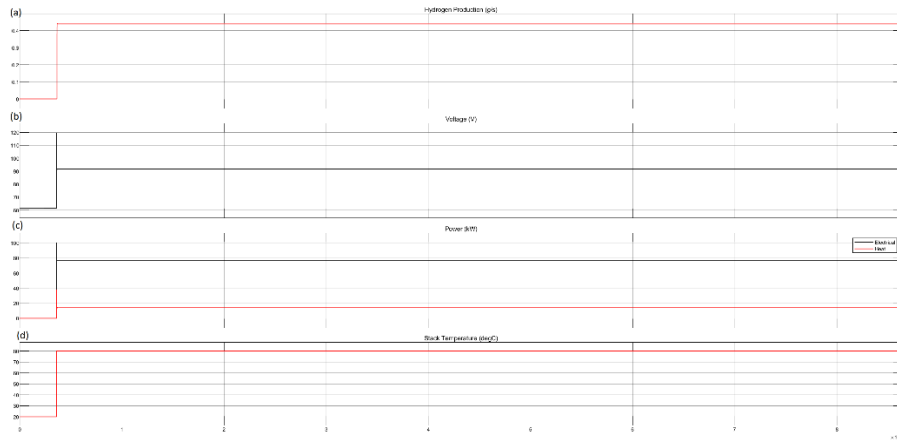


Figure 2.49. (a) Hydrogen production (g/s), (b) Stack voltage (V), (c) Power both electrical and heat (kW), (d) Stack temperature (°C)

The model also allows plotting total hydrogen production and total energy consumption. Additionally, Mass flow rates of water consumed, transported in Membrane Electrode Assembly, and hydrogen production can be plotted through the model.

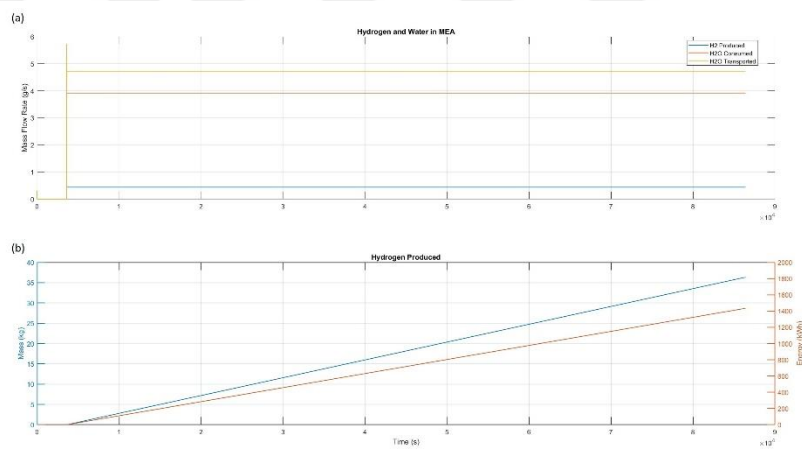


Figure 2.50. (a) mass flow rates of water and hydrogen, (b) total amount of hydrogen production and total energy consumed.

CHAPTER 3

CONTROL STRATEGIES

3.1. Introduction

Different control algorithms can be used for controlling the HES. In this work, Maximum Power Point Tracking (MPPT) is proposed to use for both wind and solar parts. There are many MPPT methods; conventional ones are Perturb and Observe (P&O), incremental conductance (INC), constant voltage, etc. There are also soft computing methods including fuzzy logic, artificial neural networks, swarm optimization, etc. (Baba, Liu, and Chen 2020). MPPT methods also differ in terms of the application area; mostly for PV (Ali and Mohamed 2022; Bendib, Belmili, and Krim 2015a; Kota and Bhukya 2017; S. Ahmed et al. 2022), but also for wind energy systems (Kumar and Chatterjee 2016; Apata and Oyedokun 2020a).

3.2. Wind Turbine MPPT Control

3.2.1. Introduction

Wind turbines need control over wind speed since it is the key parameter that gives the limitation of the turbine. In addition to that, the electrical load on the generator must be corrected for any given instantaneous moment to increase efficiency. Several early methods such as the anemometer method which relies on a pre-determined look-up table for wind turbines, and the calculation method which relies on calculation based on electrical parameters at the generator's output were suggested (Moor and Beukes 2004).

A safe power generation for the turbine and the generator, the turbine should be operated in certain wind speed values; cut-in wind speed ($V_{\text{cut-in}}$) and cut-out wind speed ($V_{\text{cut-off}}$). Figure 3.1 shows an ideal power curve of a wind turbine (Mousa, Youssef, and Mohamed 2021). As it can be seen in Figure 3.1 there are basically 4 regions that can a turbine operate.

- In Region-1 and Region-4, wind turbines should be stopped to prevent any damage.

- In Region-2, Maximum Power Point Tracking (MPPT) is useful for providing maximum energy.
- In Region-3, the Pitch controller comes in handy to decrease the total stress on the turbine.

In summary, there are several control strategies over these regions: Producing the maximum power while protecting the integrity of the overall system, a safe operation, power quality regarding the grid connection, avoiding any over-loading ensuring minimal damage (Apata and Oyedokun 2020b).

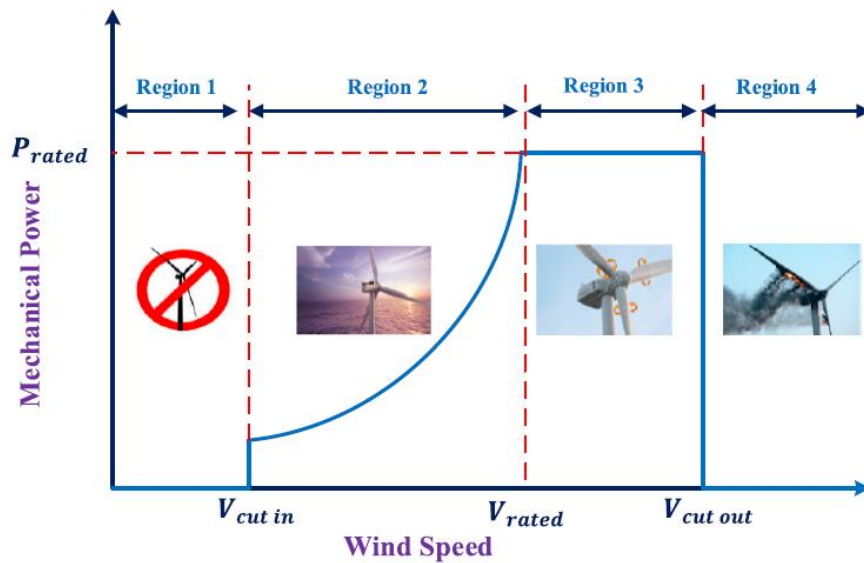


Figure 3.1. Operating regions of wind power system (Mousa, Youssef, and Mohamed 2019)

As part of this project, Region-3, which is more focused on Maximum Power Point Tracking will be based on. There are several MPPT algorithms for wind energy conversion systems. Figure 3.2 shows a classification.

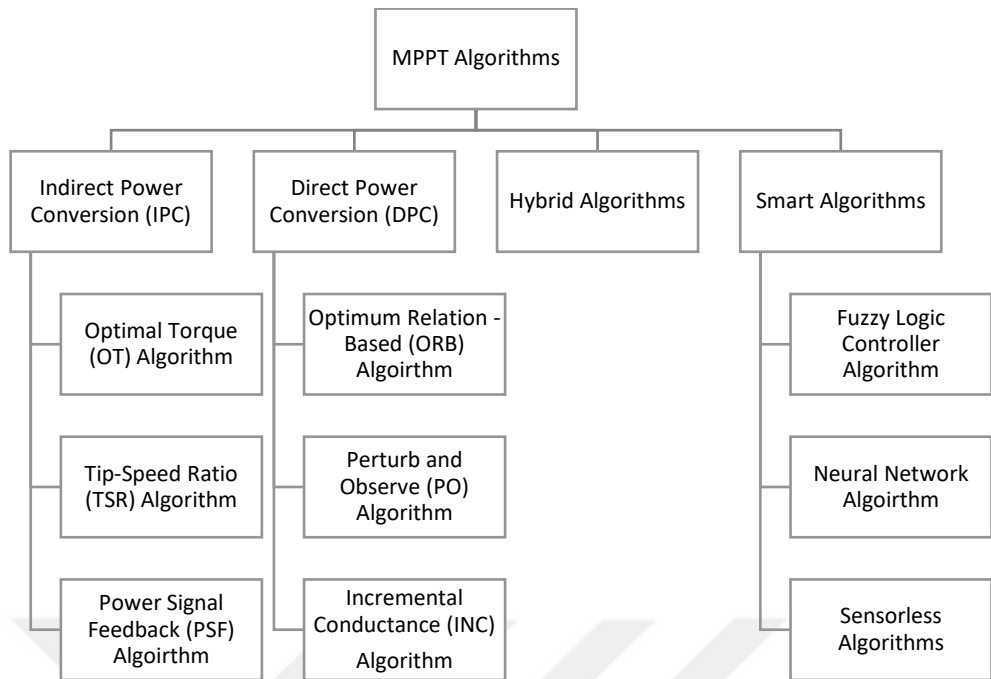


Figure 3.2. Several different MPPT algorithms for Wind Energy Conversion Systems (Mousa, Youssef, and Mohamed 2021).

3.2.1.1. Indirect Power Conversion Algorithms

In order to understand Tip Speed Ratio Algorithm, Tip-Speed Ratio must be further reviewed; Eq-1 shows the equation for Tip-Speed Ratio (λ);

$$\lambda = \frac{R\omega_m}{v_w} \quad (3.1)$$

where R is the radius of the turbine, ω_m is the shaft speed and v_w is the wind speed.

To use this method, an optimal shaft speed which gives an optimal tip-speed ratio must be provided (Nasiri, Milimonfared, and Fathi 2014). So that,

$$\omega_{m_ref} = \frac{\lambda_{opt}}{R} v_w$$

A block diagram for the TSP control algorithm can be seen in Figure 3.3. A Proportional Integral (PI) controller can be used for the controller block (Nasiri, Milimonfared, and Fathi 2014). The relation between the power coefficient and turbine with respect to TSR can be seen in Figure 3.3.

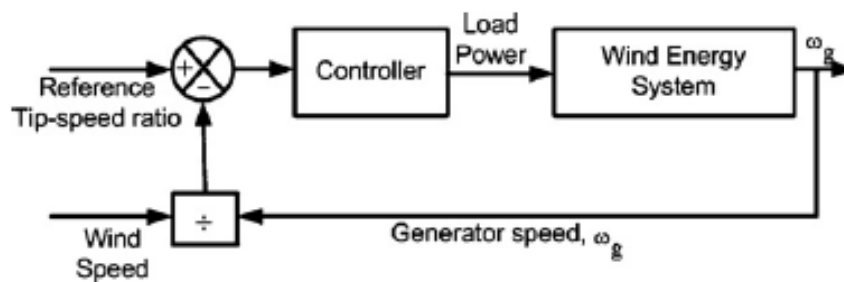


Figure 3.3. Block diagram for TSR control (Abdullah et al. 2012).

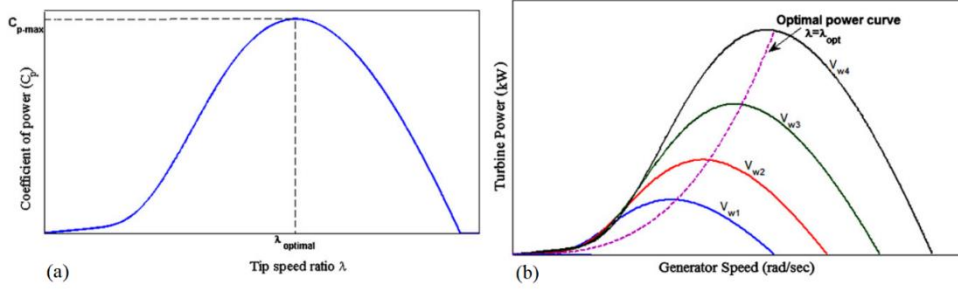


Figure 3.4. Relation between power coefficient C_p (a), and turbine power (b) with respect to TSR (Abdullah et al. 2012).

The optimal Torque Algorithm has a basis that assigns an optimal torque value for PMSG. Recalling the equations for wind turbine torque and tip speed ratio (Eq 3.2);

$$T_{tur} = \frac{1}{2} \rho A \frac{C_p(\lambda, \beta)}{\lambda} v_m^2 \quad (3.2)$$

where T_{tur} is the torque of the turbine ρ is the air density, A is the swept area of the blades, C_p is the power coefficient which depends on tip-speed ratio (λ) and pitch angle (β), and wind speed (v_m). The following equation for optimal torque value can be derived from Eq-1 and Eq-2 (Nasiri, Milimonfared, and Fathi 2014);

$$T_{m_{ref}} = k_{opt} \omega_m^2$$

Where,

$$k_{opt} = \frac{1}{2} \rho \pi R^5 \left(\frac{C_{p_max}}{\lambda_{opt}^3} \right)$$

A block diagram for OT control can be seen in Figure 3.5. Mechanical torque vs. generator speed and power vs. generator speed characteristics can be seen in Figure 3.6.

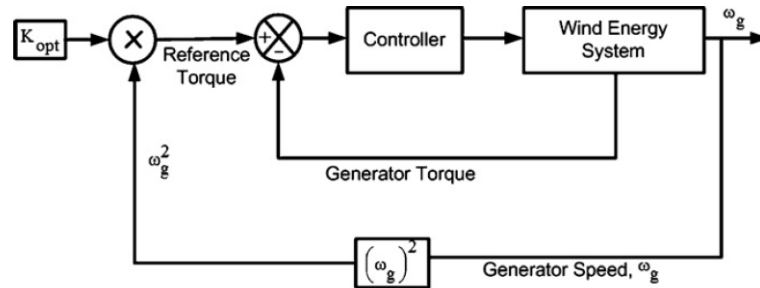


Figure 3.5. Block diagram for OT control (Abdullah et al. 2012).

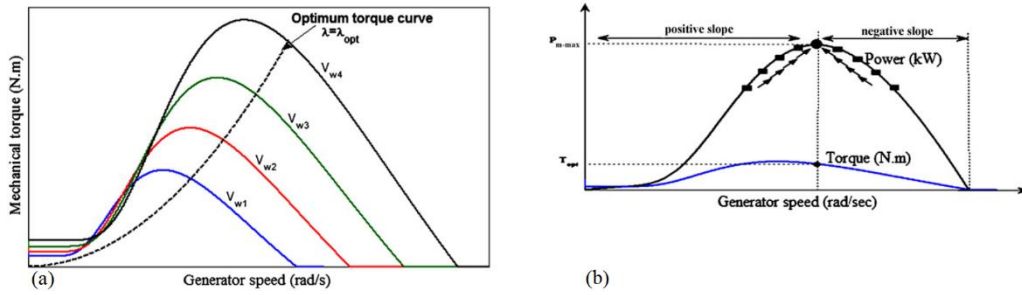


Figure 3.6. Relation between mechanical torque (a) and turbine power (b) with respect to generator speed (Mousa, Youssef, and Mohamed 2021).

The same topology with optimal torque is suitable for the Power Signal Feedback algorithm (Novaes Menezes, Araújo, and Bouchonneau da Silva 2018). However, this control needs a look-up table that relies on experimental results (Abdullah et al. 2012). Figure 3.7 shows the block diagram for the PSF control method.

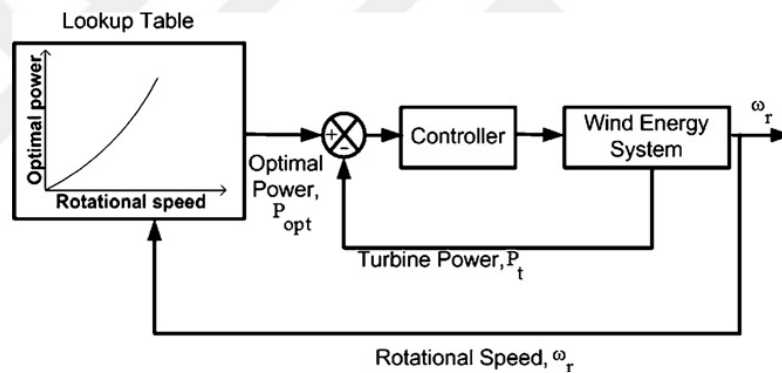


Figure 3.7. Block diagram for PSF method (Abdullah et al. 2012).

3.2.1.2. Direct Power Conversion Algorithms

Pre-acquired relations such as power vs. electromagnetic torque, rotor speed, etc. are the main basis of the Optimum Relation Based algorithm. Nevertheless, its requirement for memory space for these such relationships is the main disadvantage of this algorithm (Mousa, Youssef, and Mohamed 2021). Schematics for ORB are seen in Figure 3.8.

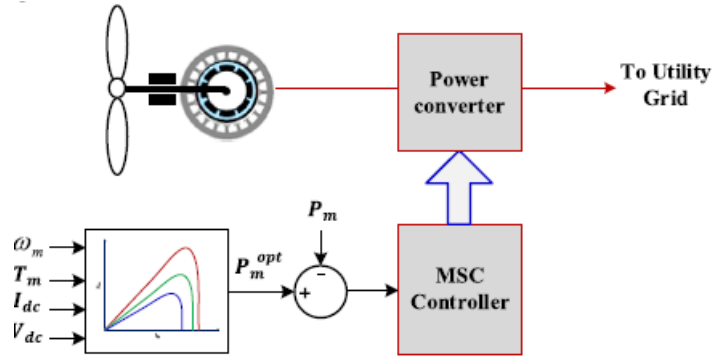


Figure 3.8. ORB schematic (Mousa, Youssef, and Mohamed 2021).

Commonly used as the PV MPPT algorithm, this control algorithm calculates output power regarding power slope and varies perturbation step sizes which are similar to Perturb and Observe algorithm. INC algorithm calculates the incremental conductance ($\frac{dI}{dV}$) and finds the maximum point. Also, it checks DC-link voltage and requires a DC-DC conversion stage (Wei Cheng 2013). However, high-resolution current and voltage measurements are needed. Figure 3.9 shows the INC algorithm.

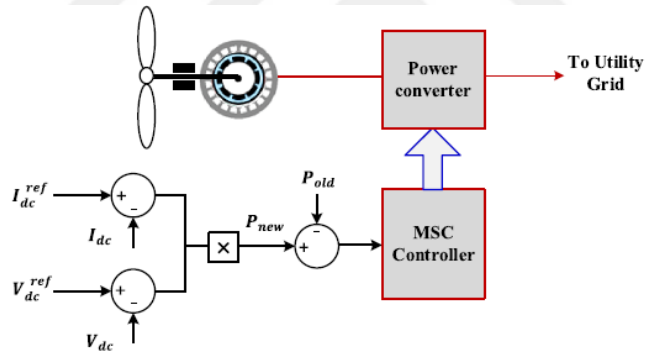


Figure 3.9. INC algorithm (Mousa, Youssef, and Mohamed 2021).

The P&O algorithm mathematically searches for local maximum (or optimum) points. This method adjusts a small amount of a parameter (called perturbation); rotor speed by observing the mechanical power, inverter input voltage by observing the generator's output power, and can also control parameter of converters namely duty cycle by observing input current and voltage (S. Ahmed et al. 2022; Mousa, Youssef, and Mohamed 2021; Abdullah et al. 2012). Figure 3.10 shows the process of MPP by using output power and torque characteristics.

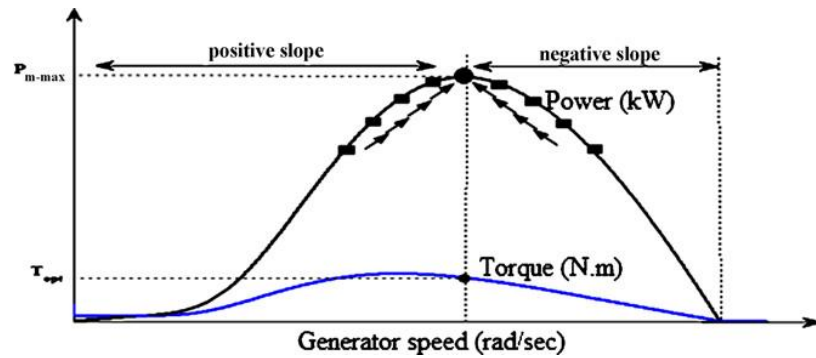


Figure 3.10. MPP process regarding generator speed vs. power (Abdullah et al. 2012).

The characteristic curve of the wind turbine is not needed for this algorithm which makes it simple, independent, and also flexible. However, there are some flaws in this algorithm. Firstly, areas where wind conditions are changing rapidly cause this algorithm to lose its track of MPP. Additionally, step-size selection can also cause some problems; a decrease in efficiency but a fast response by choosing a larger step size, slow convergence speed but an increase in efficiency (Abdullah et al. 2012; Mousa, Youssef, and Mohamed 2021).

3.2.1.3. Smart & Hybrid Algorithms

Different MPPT algorithms can be combined to overcome individual algorithms flow to enhance overall efficiency. For example, INC can be merged with a conventional P&O algorithm in order to accomplish a fast-changing wind speed flow of the PO algorithm (Abdullah et al. 2012; Mousa, Youssef, and Mohamed 2021).

There are several Smart MPPT algorithms associated with Artificial Intelligence (AI), fuzzy logic, and neural networks. The following examples can be given,

- 1- MPPT Algorithms with Fuzzy Logic Controller by designation of membership functions, surface errors.
- 2- MPPT Algorithms with Neural Networks by using input, output, and hidden layers.
- 3- Multivariable P&O MPPT algorithm for current optimization for all generators in wind farms by observing individual effects on other generators to increase overall efficiency.

3.2.2. Perturb and Observe Control of Wind Turbine Energy Conversion

A mathematical optimization method called perturbation and observation (P&O), also known as the hill-climb searching (HCS) method, is used to look for the local optimum point of a given function. To find the ideal operating point that will maximize the energy extracted, it is frequently used in wind energy systems. The foundation of this approach is the small-step perturbation of a control variable, followed by observation of the changes in the target function until the slope is zero. The P&O method is independent, straightforward, and adaptable because it doesn't call for prior knowledge of the characteristic curve of a wind turbine. When applied to large and medium inertia wind turbines, still, it does not reach the maximum power points during rapid wind variations (Abdullah et al. 2012).

There are several perturbations that can be made in this algorithm. Perturbation of inverter input voltage (Wang and Chang 2004), duty cycle (Koutroulis and Kalaitzakis 2006; Soetedjo et al. 2011; Tiang and Ishak 2012), output current (Neammanee, Sirisumranukul, and Chatratana, n.d.), or directly input voltage (Kesraoui, Korichi, and Belkadi 2011) is possible. There are also some modified P&O algorithms algorithm that can be used (Mousa, Youssef, and Mohamed 2021). In this thesis, perturbation of DC power by measuring voltage and current is used since it is not required pre-knowledge of turbine power characteristics.

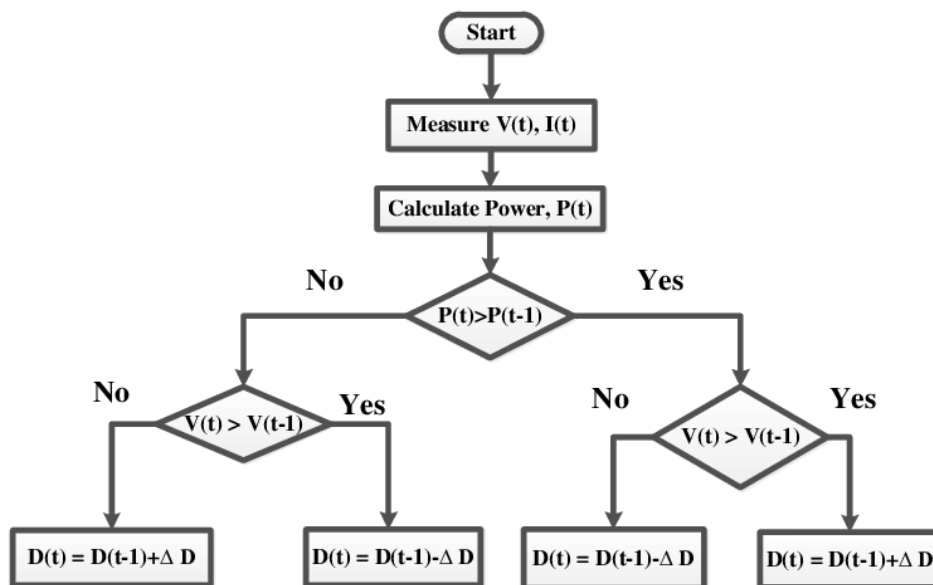


Figure 3.11. Used P&O algorithm in the thesis.

3.2.3. Simulink Model of P&O Algorithm for WECS

In the overall system of WECS, there is one MPPT block (see Figure 2.9). This block is a subsystem for P&O (or hill climbing) algorithm which takes voltage and current as input and gives a duty cycle as output. Figure 3.12 shows the inside of the subsystem.

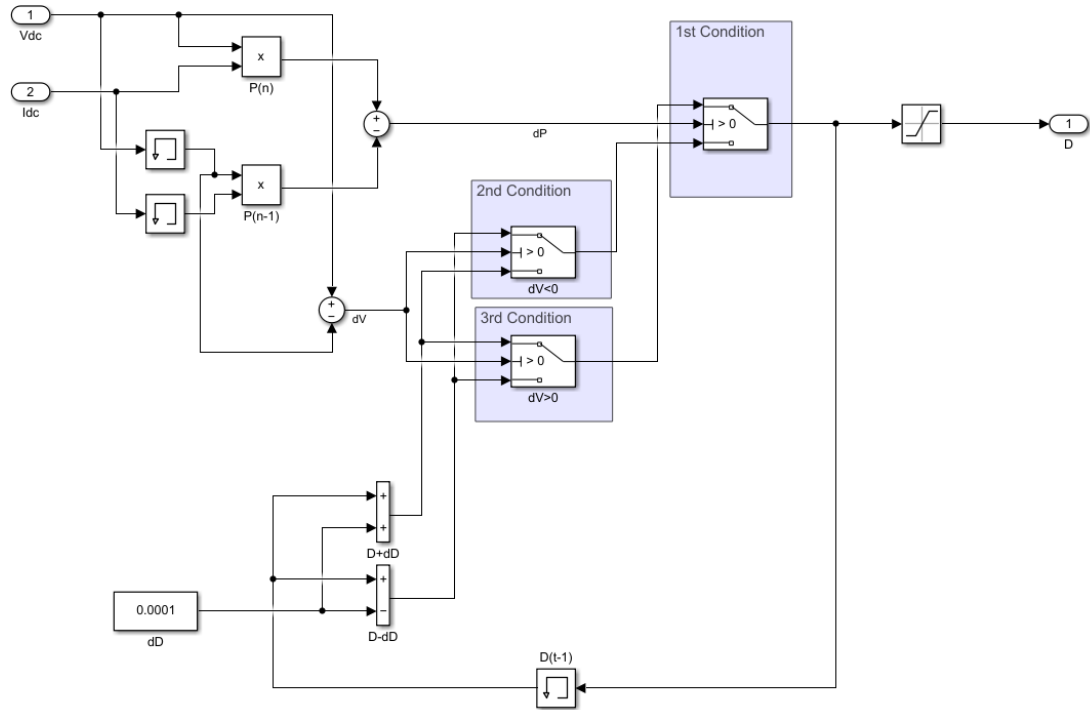


Figure 3.12. Inside of the MPPT block's subsystem

The subsystem basically calculates the power by using DC side voltage and current values and memorizes the previous values by Simulink's memory block. Then compares the current values with the previous one. If the previous value is higher than the next value, it checks for voltages. If the previous voltage value is lower than the next value, it decreases the duty cycle by ΔD , else it increases the duty cycle by ΔD . If the previous power is lower than the next power value, it again checks for voltages. If the previous voltage value is higher than the next value, it decreases the duty cycle by Δd , else it increases the duty cycle by ΔD (see Figure 3.11). ΔD is a pre-determined change in the duty cycle. The system also remembers the previous duty cycle in order to make a difference.

3.3. Solar PV Array MPPT Control

3.2.1. Introduction

There are multiple ways to MPPT control solar PV panels. But basically, it can be divided into Traditional Control Algorithms, Intelligent Control Algorithms, and MPPT under Partial Shading Conditions. Traditional control algorithms are subdivided into Parameter Selection Control and Direct Control. Intelligent control algorithms consist of Artificial Intelligence and Non-linear controlling. MPPT under partial shading conditions includes Array Reconfiguration, Modified Direct Control, and again Artificial Intelligent methods (Mao et al. 2020a). Figure 3.13 shows the classifications.

Constant Voltage, Open Voltage, Current, and Short Circuit Current Tracking are some ways of parameter selection control. The simplest parameter selection MPPT method, known as CVT, is predicated on the idea that the module voltage at MPP and the open circuit voltage have a linear relationship. Based on the value of the open circuit, this method controls the module terminal voltage. However, the method is unable to achieve perfect MPPT, especially when temperatures vary widely (Lasheen et al. 2017). The OVT method begins with the open circuit, reduces the module voltage in steps of varied voltage, and then tracks the varying voltage (Sonia Veerapen, Huiqing Wen, and Yang Du 2017). In contrast to CVT, which tracks a constant voltage, SCT operates on a similar concept to VCT. The output characteristics of the PV array show that the maximum power point current I_M of the PV array similarly fluctuates roughly linearly with the short circuit current when the short-circuit current of the PV array changes with the environment, primarily owing to irradiance (Sher et al. 2017). By varying the array current over an adequate range and analyzing the voltage at the peak power point, CS is able to immediately derive the I-V characteristic curve of the PV array. The primary drawback of the current scanning technique is the slow tracking speed when compared to other approaches (Noguchi, Togashi, and Nakamoto 2002).

Perturb and Observe (PO), Incremental Conductance (IC), Parasite Capacitance (PC), Power Feedback (PF), Photovoltaic Array Control (PAC), and Actual measurements (AM) are direct control methods. One of the most popular methods for applying MPPT in a PV system is P&O (or Hill Climbing Method). The basic idea behind P&O is to periodically modify the voltage or duty cycle of the terminal converted from a PV array

and then monitor the subsequent change in power direction to determine the subsequent control signal (Alik and Jusoh 2018). Another popular technique for MPPT control, IC compares the instantaneous conductance I/V with the slope conductance's negative value, $-dI/dV$, which becomes equal at the MPP (Motahhir et al. 2018). PC approach considers the stray inductance between the PV cells as well as the parasitic capacitance of the PN junctions in the cell (Wu et al., n.d.). PAC is an older technique that modifies the number of series and parallel connections between PV arrays in accordance with various loads, allowing the PV array to function at the MPP and satisfy various load needs (Salameh and Dagher 1990). By gathering the output voltage and current values of the PV array, PF determines the current output power using either hardware or software. According to the power difference between the current and the previous cycle, it modifies the output voltage value (Hua, Lin, and Shen 1998).

There are several intelligent AI algorithms; Fuzzy Logic Control (FLC), and Artificial Neural Network (ANN). A popular class of artificial intelligence algorithms known as FLC is built using a collection of fuzzy rules. Fuzzification, control rule evaluation, and defuzzification are the three processes of implementation. Integrating professional experience and knowledge into linguistic rules to govern the system is the main component of FLC. Additionally, FLC offers greater dynamic and steady-state performance since it can track the MPP fast and there is no volatility once it has been reached in steady settings. However, the main drawbacks of FLC are that its implementation is difficult and that irradiance change can lead to drift (Li et al. 2019). An innovative sort of information processing technology is the ANN. Input, hidden, and output layers make up the three layers of the most widely used neural network structure. In a PV system, numerous samples of input and output data are used to train network parameters like weights and deviations, resulting in the creation of a mathematical model of the system's unknown function (Hamdi, Ben Regaya, and Zaafouri 2019). There are also some intelligent non-linear control methods such as Sliding Mode Controller (SMC). In order to force the closed loop system to reach and stay on the intended sliding surface, SMC is proposed by utilizing the discontinuity of the control and depending on its high-frequency conversion. The PV system tracking speed can be greatly increased with this technique, but the dynamic and steady-state features of the system tracking will depend on the choice of the step size and modulation depth of the switching device (Pahari and Subudhi 2018).

MPPT under PSCs can be divided into three groups; Array Reconfiguration, AI, Modified Direct Control, and others. Array reconfigurations consist of control algorithms such as; Simple Series (SS), Series-Parallel (SP), Bridge Link (BL), and Total Cross Tied (TCT). SS is highly applicable, but the main disadvantages are low efficiency and high-power losses (Pongratananukul and Kasparis, n.d.). There are several advantages of different SP algorithms like high applicability, convergence, and compatibility. However, they have high randomness and complexity (Mao et al. 2020b). BL model uses irradiance as an acquired parameter. It is highly applicable and low cost. On the other hand, they are not widely used and complex (Belhachat and Larbes 2015). Several TCT models can have some advantages such as short processing time and reliability, but they are complex (Matam and Barry 2018). Particle Swarm Optimization (PSO), Artificial Bee Colony (ABC) algorithms, Salp Swarm Algorithm (SSA), Gray Wolf Optimization (GWO) (Mohamed et al. 2019), Genetic Algorithm (GA), and Differential Evolution (DE) (Tey et al. 2018) are part of AI methods of MPPT under PSCs. There are also Firework Algorithms (FWA) (Manickam et al. 2017) and $0.8U_{oc}$ (J. Ahmed and Salam 2015) for this type of control. Modified Direct control methods use different algorithms together. Some examples of them are PSO-P&O, FLC-P&O, and ANN-P&O.

Similar to WECS MPPT control, P&O is chosen for PV MPPT control for this thesis because it is widely used.

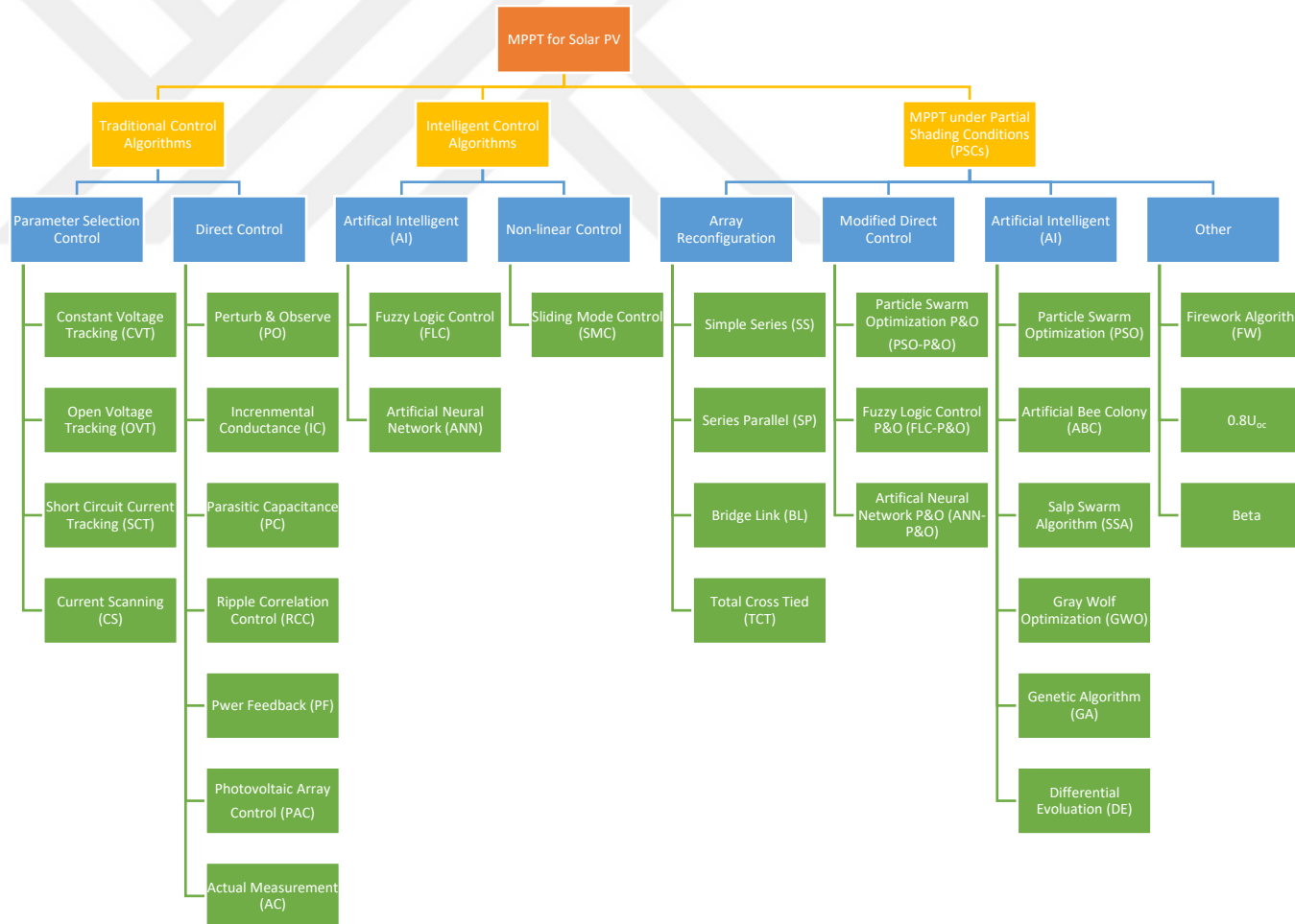


Figure 3.13. Different MPPT methods for solar PV.

3.2.2. Perturb and Observe Control for Solar PV MPPT

In order to determine the direction of change and provide it to the voltage reference V_{ref} , the P&O algorithm regularly perturbs the operational voltage point and measures the power variation. The operational point has shifted toward the MPP if the PV array's operating voltage V is perturbed in a particular direction and the power taken from the array grows as a result. As a result, the operating voltage must be perturbed further in the same direction. Otherwise, the operating point will have shifted away from the MPP if the power drawn from the PV array diminishes, in which case the direction of the operating voltage perturbation must be changed (Bendib, Belmili, and Krim 2015b).

Perturbation of PV array current (consequently array voltage) is achieved by perturbing the duty ratio of the power converter when it is connected to a DC-DC converter. An increase in the voltage results in a higher power when it is used to the left of the MPP and lower power when it is used to the right of the MPP (Mohanty et al. 2014). The following equations (Eq 3.1-3.2) show the mathematical relationships.

$$\text{If } \frac{dP}{dV} > 0; \quad V_{ref} = V_{ref} + dV \quad (3.1)$$

$$\text{If } \frac{dP}{dV} < 0; \quad V_{ref} = V_{ref} - dV \quad (3.2)$$

3.2.3. Simulink Model for P&O Algorithm for PV Array

The overall model of PV Array MPPT control for various irradiances (see Figure 2.21) includes an MPPT block (see Figure 2.24). This block is a MATLAB function (See Appendix-I) that takes PV voltage, PV current, and a pre-determined delta value as input and gives a duty cycle. The duty cycle will be transformed into PWM signal which drives the IGBT diode's gate signal of the boost converter.

Similar to the P&O algorithm for WECS, first it calculates power by $P_{pv} = V_{pv}I_{pv}$ and tries to determine the MPP point where the derivation of power becomes nearly zero ($\frac{dP}{dV} \approx 0$). If it is nearly zero and voltage derivation (dV) is negative it decreases the duty cycle by pre-determined delta, else it increases it by delta. Otherwise, it again checks dV value. If it is negative, it increases the duty cycle, else decreases. It also prevents the duty cycle from becoming too low or too high.

3.4. Charge and Discharge Control between Solar PV Array and Battery Pack

3.3.1. Proposed Flow Chart and Circuit Scheme

The working principle of this system is based on both the V_{pv} and SOC of the battery. It checks V_{pv} and State of the Charge (SOC) in every time step. PV array charges until the battery is full then if V_{pv} is still bigger than zero, the PV array starts to supply the load until V_{pv} becomes zero. After that, the battery starts to supply the load. Figure 3.15 shows the flowchart of the control algorithm. All system depends on switches and signals that drive the switches. Switch signals are decided by 3-different functions. Table 3.1 shows the defined functions for the signals. Switch groups and circuit schematics can be seen in Figure 3.14.

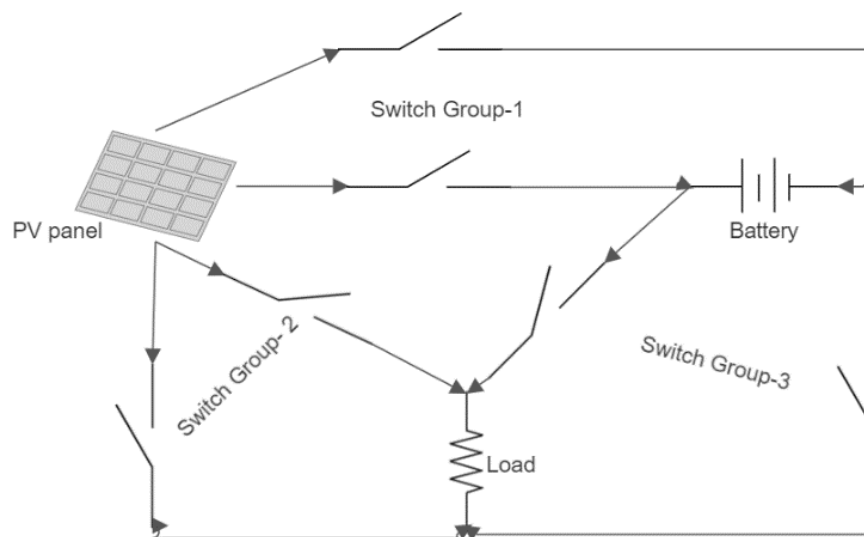


Figure 3.14. Circuit schematics.

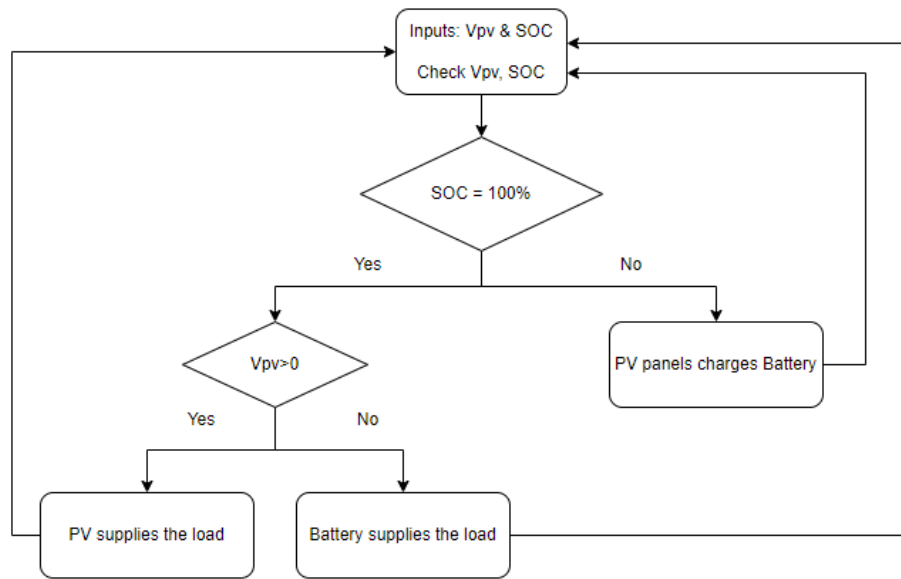


Figure 3.15. Proposed flow chart.

Table 3.1. Function conditions and actions.

Function-1	Charging
Condition	if SOC<100% & Vpv>0
Action	close switch group-1, open switch group-2&3.
Function-2	PV supplies the load
Condition	if SOC=100% & Vpv>0
Action	close switch group-2, open switch group-1&3.
Function-3	Discharging
Condition	If SOC=100% & Vpv=0
Action	close switch group-3, open switch group-1&2.

3.3.2. Control System in Simulink

Recalling the PV system in Chapter 2, additional components in blue rectangular were added. Figure 3.16 shows the overall system. A single battery, switch groups, and charge control block were added. Also, the new PV array consists of 15 parallel and 2 series per parallel strings PV panels. 12V, 10 Ah single battery is used.

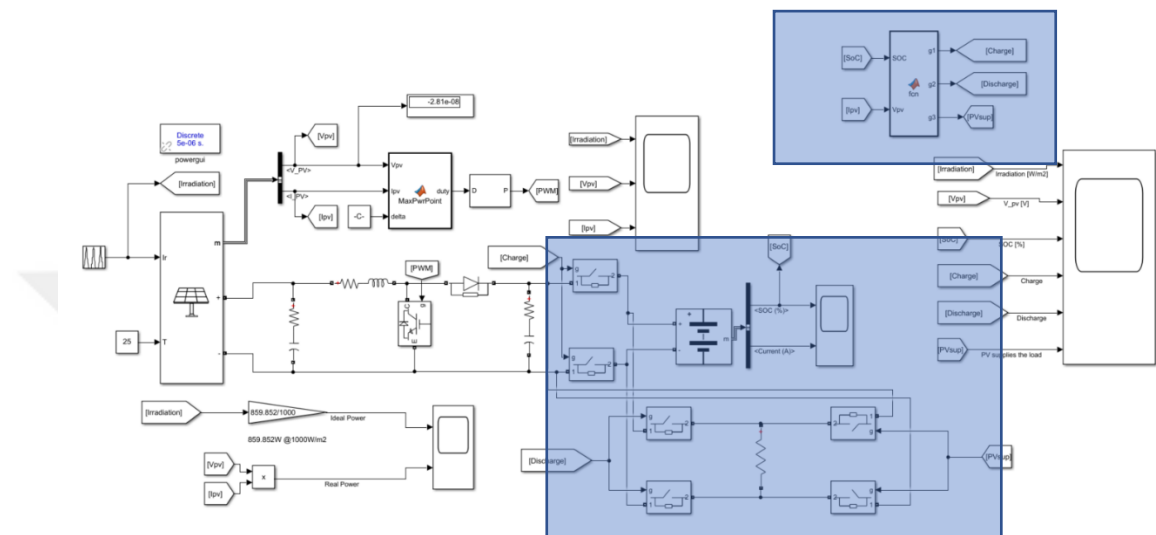


Figure 3.16. Proposed system for PV & battery control.

The charge control block can be seen in the upper blue rectangular area in Figure 3.16. Another blue rectangular block at the downside is the charge & discharge circuits (See Chapter-2).

3.3.3. Results

40 seconds of the simulation was made. Results can be seen in Figure 3.17. Although there are some transient regions, it can be seen that absence of irradiance, switches for the discharge state are closed. If irradiance exists, the system checks for SOC. If the battery is full switches for the PV supplies load state are closed and if not, the battery starts supplying the load.

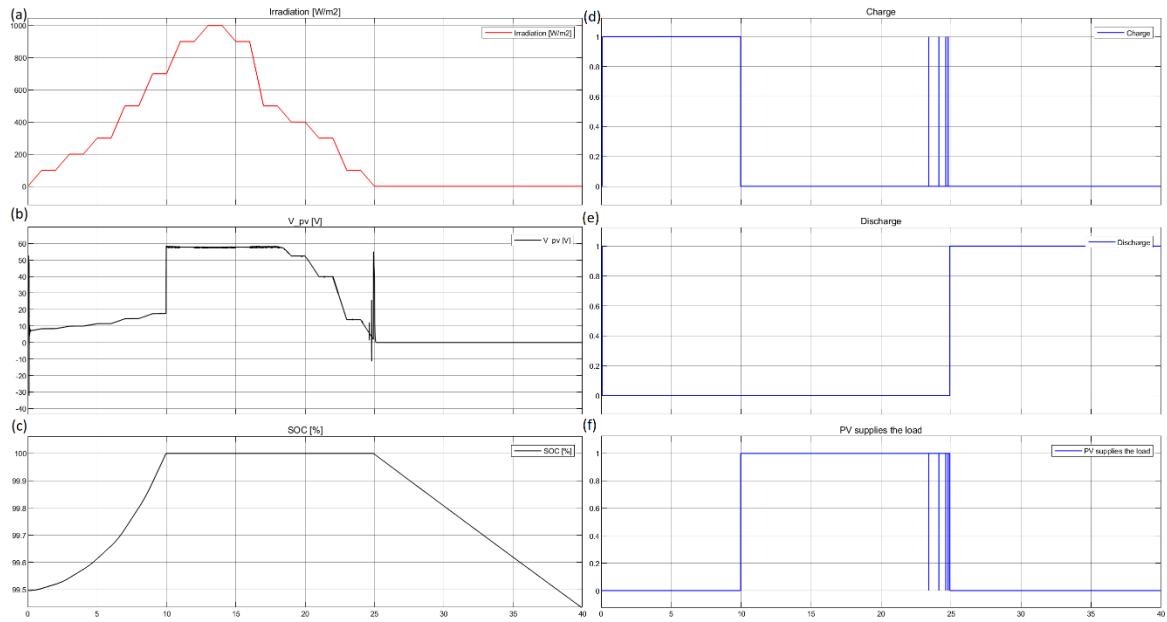


Figure 3.17. (a) Irradiances (b) V_{pv} , (c) SOC of battery, (d) Charge state, (e) Discharge state, (f) PV supplies the load state.

3.5. Electrolyzer Power Control

As mentioned in the 2.4 MathWorks Electrolyzer model is used. However, the limitations of this model were not given. In order to find the maximum power that can be delivered through the model a ramp function is used for the input power of the electrolyzer. It is seen that this model cannot exceed 150kW of electrical power due to the high temperature and pressure values inside it.

In the overall model (See Chapter 4), a control algorithm is written in order to limit (and decide) to power delivered to the electrolyzer. All supplied power (PV, wind, and battery) was checked, and set limit values to electrolyzer power. The MATLAB code for this system can be seen in Appendix II. There are several options given to the user depending on the different sizing of the overall system.

- 1- Electrolyzer power at maximum 150 kW: If the input power is higher than 150 kW, the grid will be supplied with excess power. If less, the electrolyzer will be supplied by all input powers.
- 2- Electrolyzer power at maximum 50kW: If the input power is higher than 50kW, the grid will be supplied with excess power. If less, the electrolyzer will be supplied by all input powers.
- 3- Electrolyzer power at maximum user-defined value: The user can select the maximum power that can be supplied to the electrolyzer, and excess power will be supplied to the grid.
- 4- Only hydrogen production: All power will be supplied to the electrolyzer, and the grid will not be supplied.
- 5- Only grid supply: All power will be supplied to the grid and there will be no hydrogen production.

CHAPTER 4

OVERALL SYSTEM

4.1. System Configuration

In the literature, there are several configurations of hybrid renewable energy systems. Nehrir et al discussed different approaches in their paper (Nehrir et al. 2011). Most similar systems are combined in a DC bus (Akarsu and Serdar Genç 2022; Akhtari and Baneshi 2019; Dursun, Acarkan, and Kilic 2012; Gajewski 2021; Kosmadakis and Elmasides 2019; Shaqour et al. 2020). Because all components of the system rely on DC power except the wind energy system. The output power of the wind turbine is combined through a rectifier.

Figure 4.1 shows the proposed configuration of this work. Instead of combining the battery with a DC bus, the battery is combined with PV panels. The wind turbine directly supplies the DC bus by a rectifier. The input power of the electrolyzer comes from the DC bus and the grid is supplied by an inverter which is connected to the DC bus.

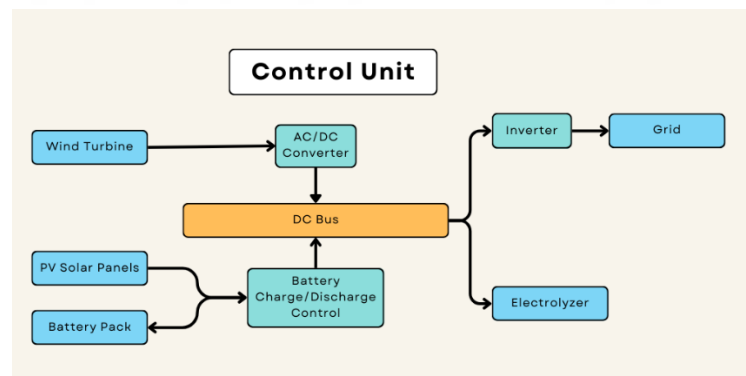


Figure 4.1. Proposed configuration of the system.

4.2. Overall System Simulink Model

The overall proposed system can be seen in Figure 4.2. There are six subsystems in the overall system: wind turbine, PV Array, Battery Energy Storage System, Electrolyzer, and Control subsystem. Also, there are 4 measurement scopes for different purposes. A MATLAB m-file is working before the simulation for initializing the system

parameters such as wind speed, temperature, solar irradiation, and electrolyzer parameters.

4.3. Subsystems

4.3.1. Wind Turbine

The subsystem takes wind speed as input and gives wind turbine power in kW as output. Figure 4.3 shows the overall subsystem and inside the subsystem. Users can decide which turbine is going to be used. Three turbines can be selected through the masked subsystem. All systems supply a DC bus, and because of that, the user can define a rectifier's efficiency. Three look-up tables are inside the system which represents the power curves of wind turbines. Also, the system allows the user to initialize an additional wind turbine. Figure 4.2 shows the power curves of wind turbines that can be selected and Figure 4.4 shows the user interface of the wind energy subsystem.

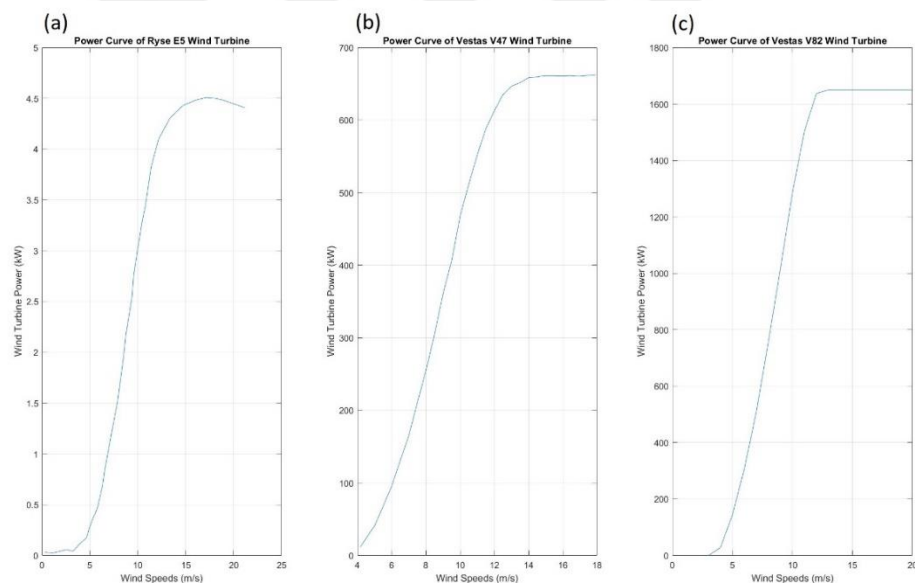


Figure 4.2. Power curves of wind turbines; (a) Ryse E5, (b) Vestas V47, (c) VestasV87

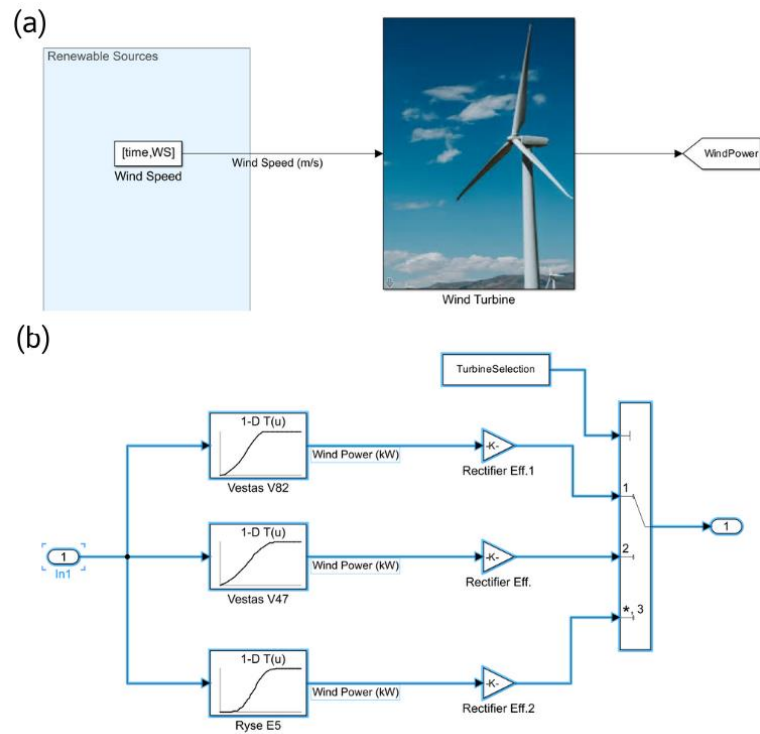


Figure 4.3. (a) Subsystem, (b) inside of the subsystem.

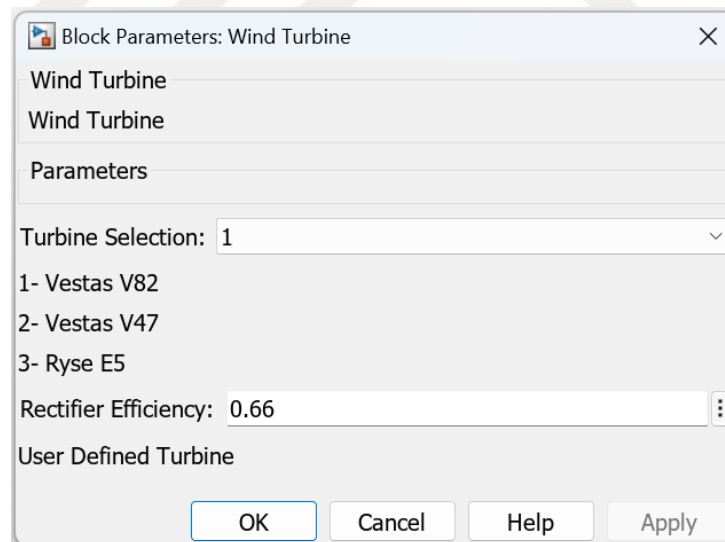


Figure 4.4. User interface for wind energy subsystem.

4.3.2. PV Array

As mentioned in Chapter-3, the PV array can follow Maximum Power Point for different irradiancies. The subsystem takes irradiation and temperature as input and gives

solar power as output. Users can define any panel parameters such as the number of panels, maximum efficiency and area of the panel, and power coefficient of temperature. Figure 4.5 shows the subsystem and inside of the subsystem and Figure 4.6 shows the user interface of the subsystem.

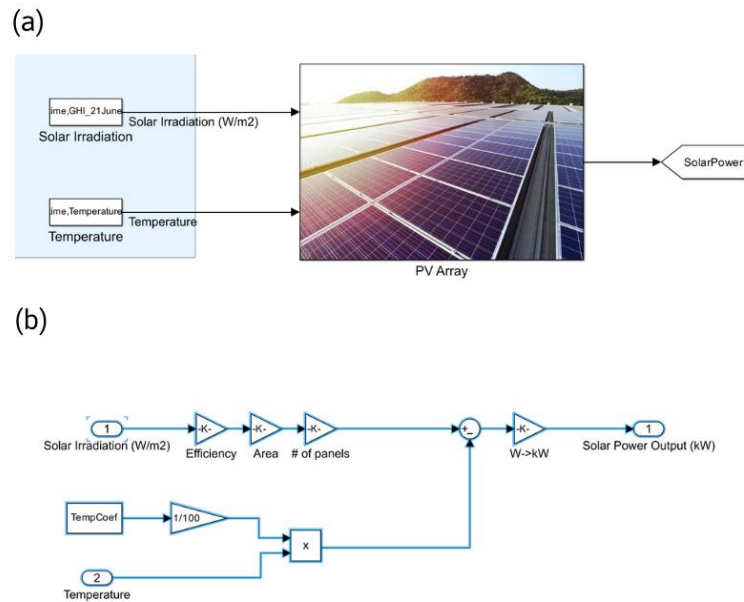


Figure 4.5. (a) Overall PV Solar system, (b) inside of the subsystem.

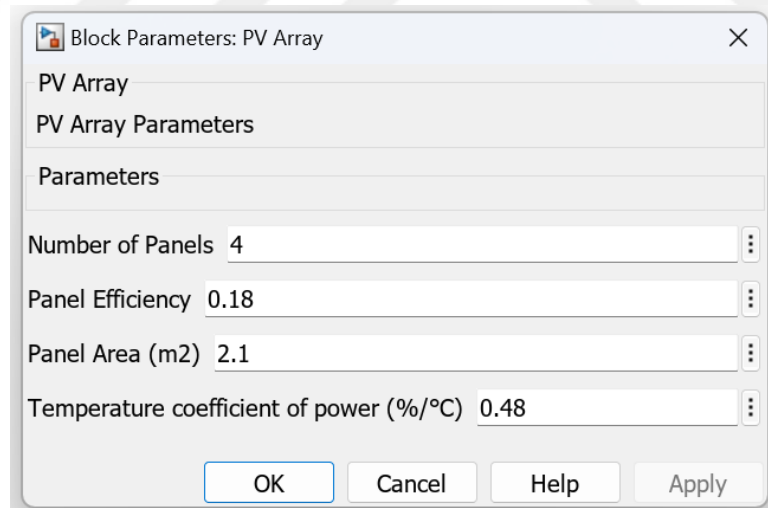


Figure 4.6. User interface for PV array subsystem.

Inside the subsystem solar power is calculated as follows:

$$P_{solar} = n \times \eta \times A \times G$$

Where n is the number of PV panels, η is the maximum efficiency, A is the area of one panel, and G is the irradiation value. However, there is also temperature power correction inside the subsystem which can be expressed as follows:

$$P_{solar,real} = P_{solar} - P_{correction}$$

Where $P_{correction} = \lambda \times P_{solar}$ It reduces the total output power with respect to the temperature coefficient of $P_{maximum}(\lambda)$.

4.3.3. Battery Energy Storage

Battery energy storage system takes charging/discharging control signals and charge power as input and gives the battery power and State of the Charge (SOC) as output. Figure 4.7 shows the subsystem and the inside of the subsystem. There are power control blocks, charge, and discharge circuits, and a battery inside the subsystem. The system charges, discharges, or remains constant SOC by signals coming from the control block. Charge power is divided by the battery voltage which gives the charging current. Then a controlled current source is connected through a charging switch. (See Chapter-3)

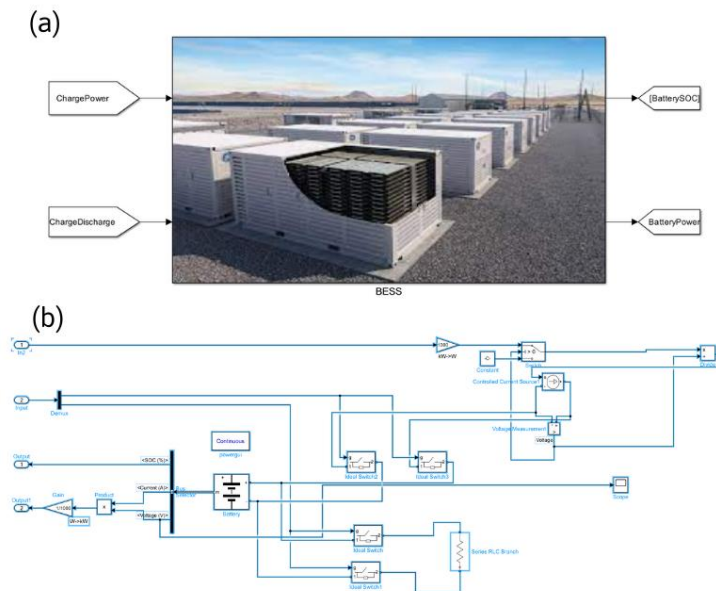


Figure 4.7. (a) BES subsystem, (b) inside of the subsystem.

Users can define the output voltage, current capacity, and initial SOC of the battery since it is also masked. The user interface of the subsystem can be seen in Figure 4.8.

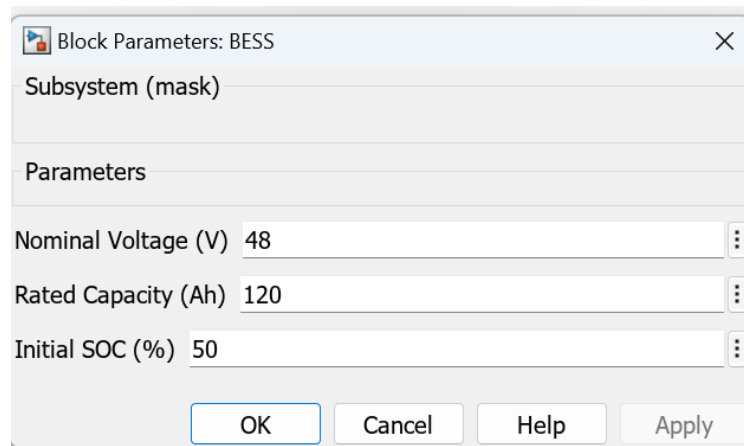


Figure 4.8. User interface of BESS



4.3.4. Electrolyzer

This subsystem takes the electrolyzer power which comes from the control block as input. It consists of an electrolyzer system and a controlled current source connected to a system that divides the input power to the voltage of the electrolyzer. Figure 4.9 shows the subsystem and the inside of the subsystem. All changes in the electrolyzer (dimensions of heat exchangers, number of cells, diameters of water and gas pipes, etc.) can be made in the initialization m-file. (See Chapter – 2)

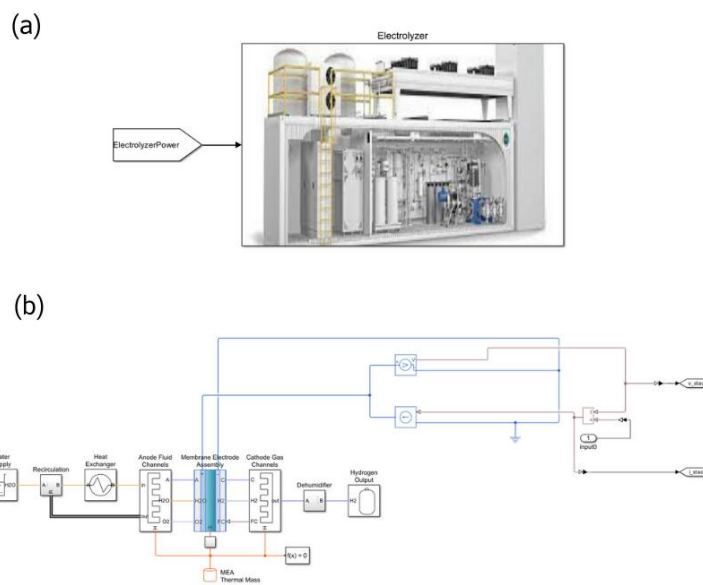


Figure 4.9. (a) electrolyzer subsystem and (b) inside of the subsystem.

4.3.5. Control Block

There are two control algorithms in the Control subsystem: charge and discharge control, and electrolyzer power control. The battery is directly connected to the solar array and charges through it. When there is no solar power, it starts to discharge. This control block takes the SOC of the battery and PV power as input and gives charging power and two control signals for charging/discharging circuits as output. Electrolyzer power cannot exceed 150kW because of high temperature and pressure levels inside the system. Because of it, electrolyzer power must be checked. Figure 4.10 shows the control subsystem and the inside of the subsystem.

It takes the SOC of the battery and all power (PV array, wind turbine, battery) as inputs and gives the charge/discharge signals, charge power, electrolyzer, and grid power as output.

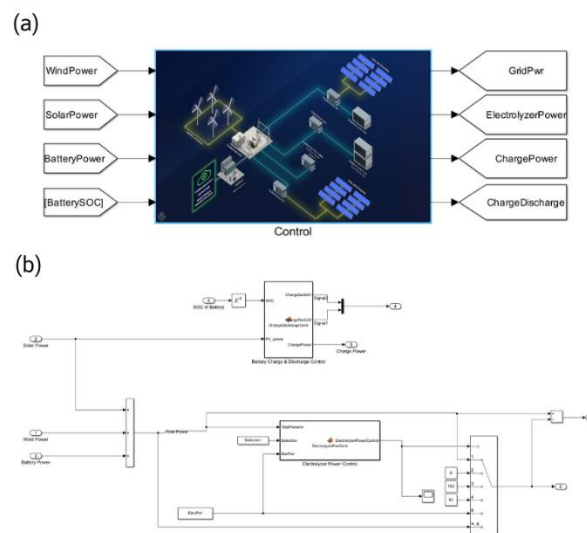


Figure 4.10. (a) Control subsystem, (b) inside of the subsystem.

This subsystem is also masked. Users can define the type of hybrid operation (See Figure 4.11). There are 5 options:

1. Only hydrogen production: All power of the hybrid plant supplies the electrolyzer.
2. Only grid supply: All power of the hybrid plant supplies the grid.
3. Hybrid (Electrolyzer at max. 150kW): Electrolyzer supplied by 150 kW power and remaining power supplies the grid.
4. Hybrid (Electrolyzer at max. 50kW): Electrolyzer supplied by 50 kW power and remaining power supplies the grid.
5. Hybrid (Electrolyzer at max. desired power): Electrolyzer supplied by user-defined power and remaining power supplies the grid.

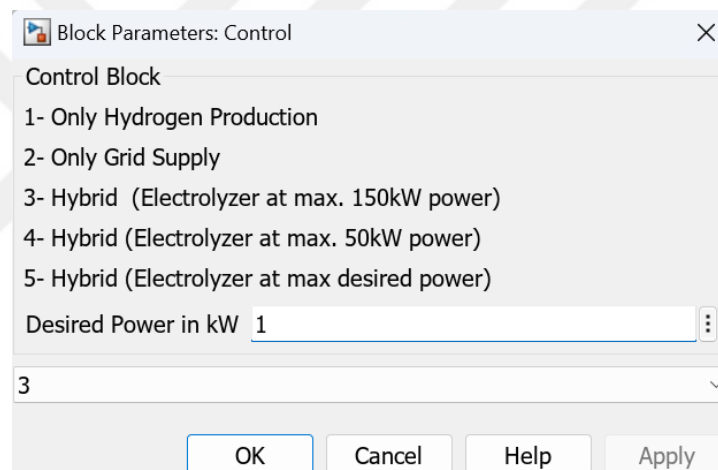


Figure 4.11. User interface of control subsystem.

4.3.6. Measurement

Four different measurements are made in this overall system: all power inputs (PV array, wind turbine, battery), output powers (electrolyzer, grid), electrolyzer measurements, and battery measurements.

Electrolyzer measurements consist of hydrogen production (g/s), the total amount of hydrogen produced (kg), stack voltage, stack current, stack temperature, and power of the electrolyzer. SOC, power of the battery, and charge/discharge signals are measured in

battery measurements. Figure 4.12 shows the measurement block and subsystem that is used for electrolyzer measurements.

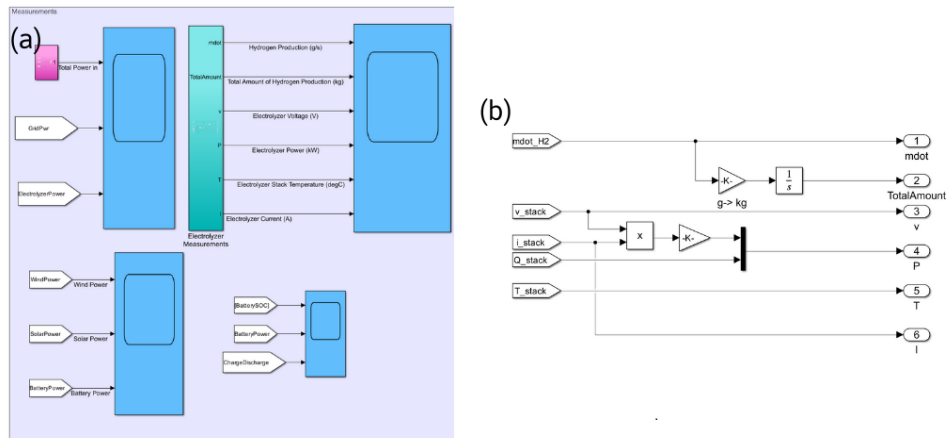


Figure 4.12. (a) Measurement scopes, (b) Subsystem for electrolyzer measurements.

4.4. Results

Many simulations are made representing different cases regarding battery SOC, different turbines, different PV array sizes, and different power controls. Wind speed and solar irradiation values remained constant for all the simulations. Figure 4.13 shows the wind speed and irradiation values for the simulations. Table 1.1 shows the different cases.

Table 4.1. Different cases investigated.

Case	Turbine	# of panels	Initial Battery SOC (%)	Battery Capacity (kWh)	Control Decision
I-a	Ryse E-5	4	100%	5.76	Hybrid - Electrolyzer power at 1kW
I-b	Ryse E-5	4	100%	5.76	Only hydrogen production
I-c	Ryse E-5	4	100%	5.76	Only grid supply
II-a	Ryse E-5	4	50%	5.76	Hybrid - Electrolyzer power at 1kW
II-b	Ryse E-5	4	50%	5.76	Only hydrogen production
II-c	Ryse E-5	4	50%	5.76	Only grid supply
III-a	Ryse E-5	4	0%	5.76	Hybrid - Electrolyzer power at 1kW
III-b	Ryse E-5	4	0%	5.76	Only hydrogen production
III-c	Ryse E-5	4	0%	5.76	Only grid supply
IV	Vestas V82	50	50%	57.6	Hybrid – Electrolyzer power at max 150kW
V	Vestas V47	25	50%	28.8	Hybrid – Electrolyzer power at max 50 kW

Results for Case IV and Case V can be seen in Appendix - II

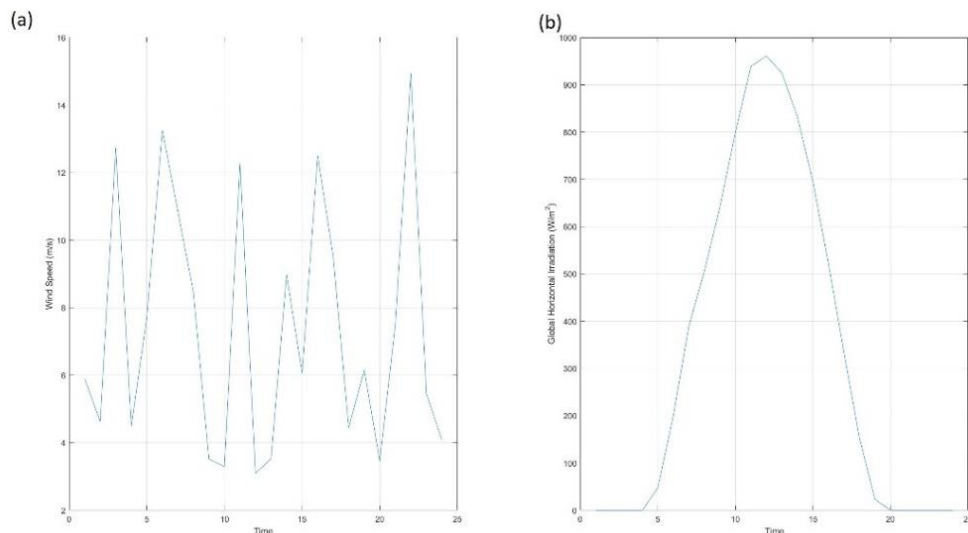


Figure 4.13. (a) Wind speed and (b) GHI

Case I:

In this case, overall system was checked for capability of battery that is fully charged. So that, the initial SOC of the battery is taken as 100%. The input power for this case is the same for all the same for each sub-cases. Figure 4.14 shows the input powers.

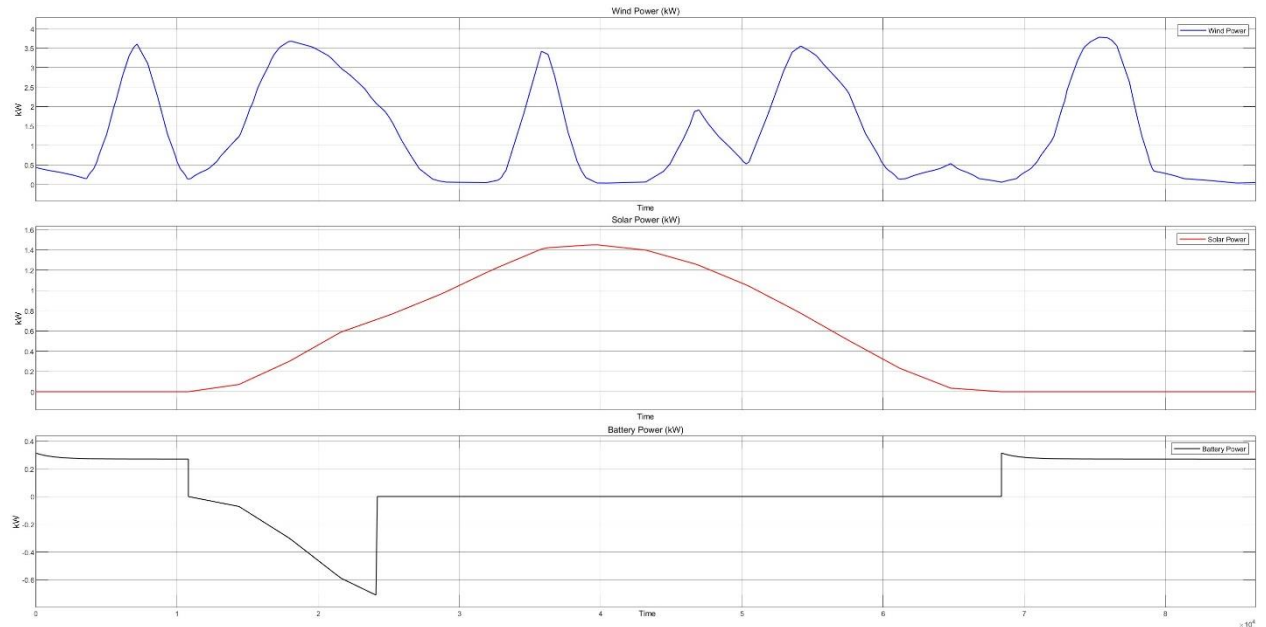


Figure 4.14. Input powers for Case-I

Case I-a:

In this case, electrolyzer power is taken as 1kW. It can be seen that if there is enough power system tries to operate the electrolyzer at 1kW power. Figure 4.15 shows the input and output powers, Figure 4.16 shows the electrolyzer measurements, and Figure 4.17 shows the battery measurements. Grid supplied by 88kWh of energy, and electrolyzer consumed 79kWh of energy resulting 0.5237kg hydrogen production.

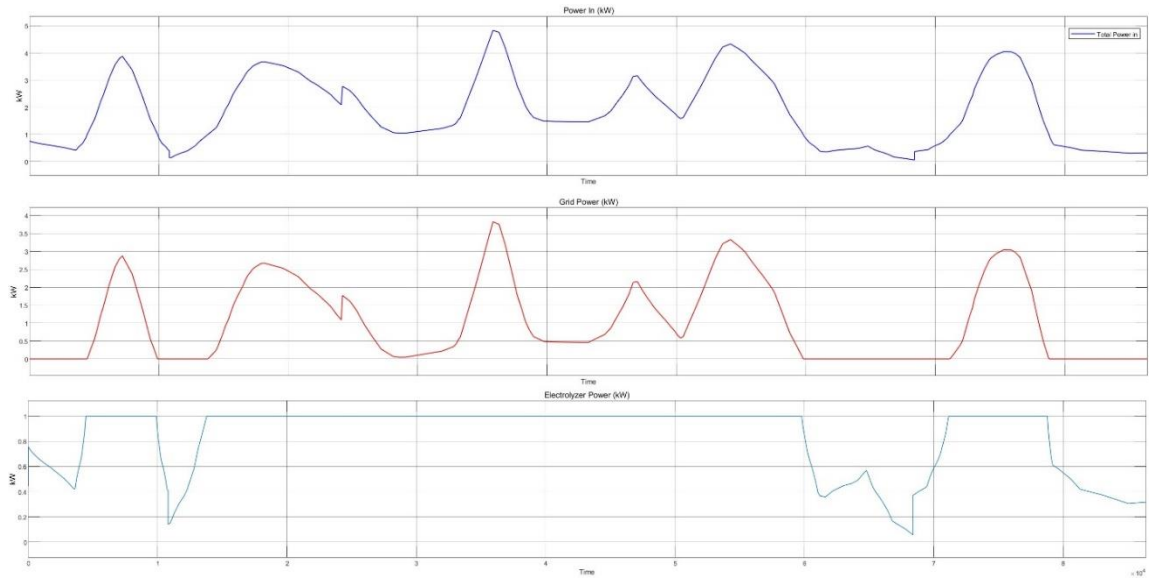


Figure 4.15. Input and output powers for Case 1-a.

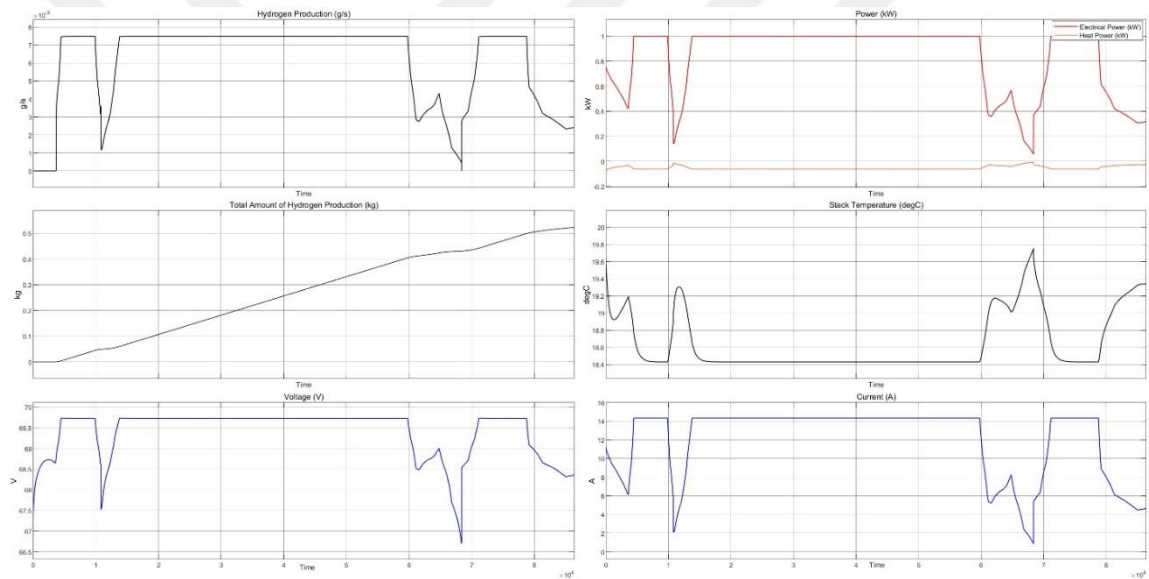


Figure 4.16. Electrolyzer measurements for Case I-a.

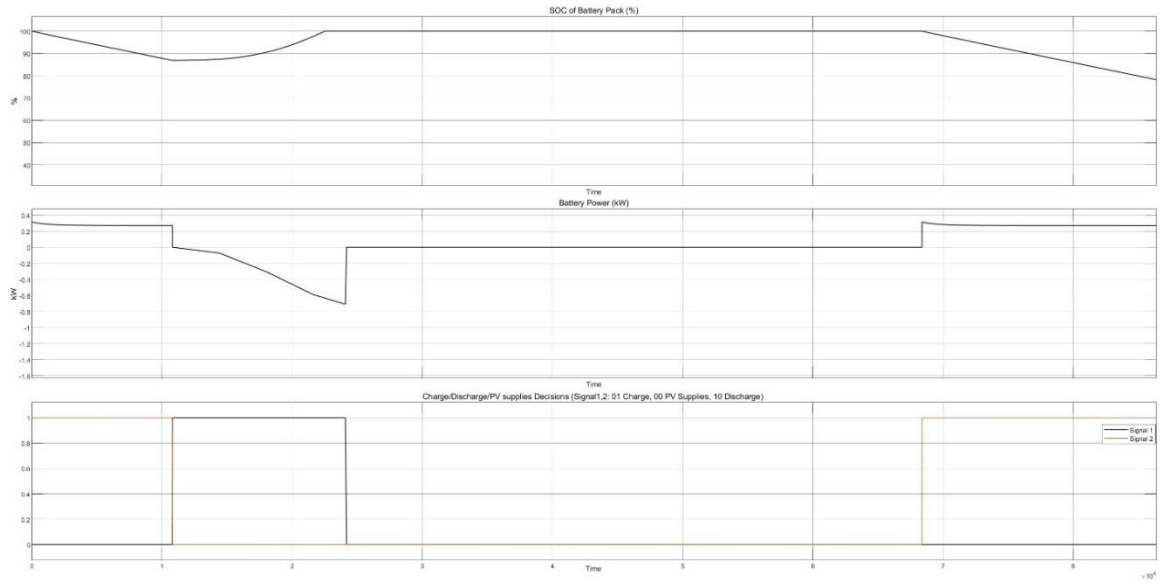


Figure 4.17. Battery measurements for Case I-a.

Case I-b:

In this case, there is no grid supply but only hydrogen is produced. Figure 4.18 shows the input and output powers, Figure 4.19 shows the electrolyzer measurements, and Figure 4.20 shows the battery measurements. Electrolyzer consumed 160kWh of energy resulting in 1.1532kg of hydrogen production.

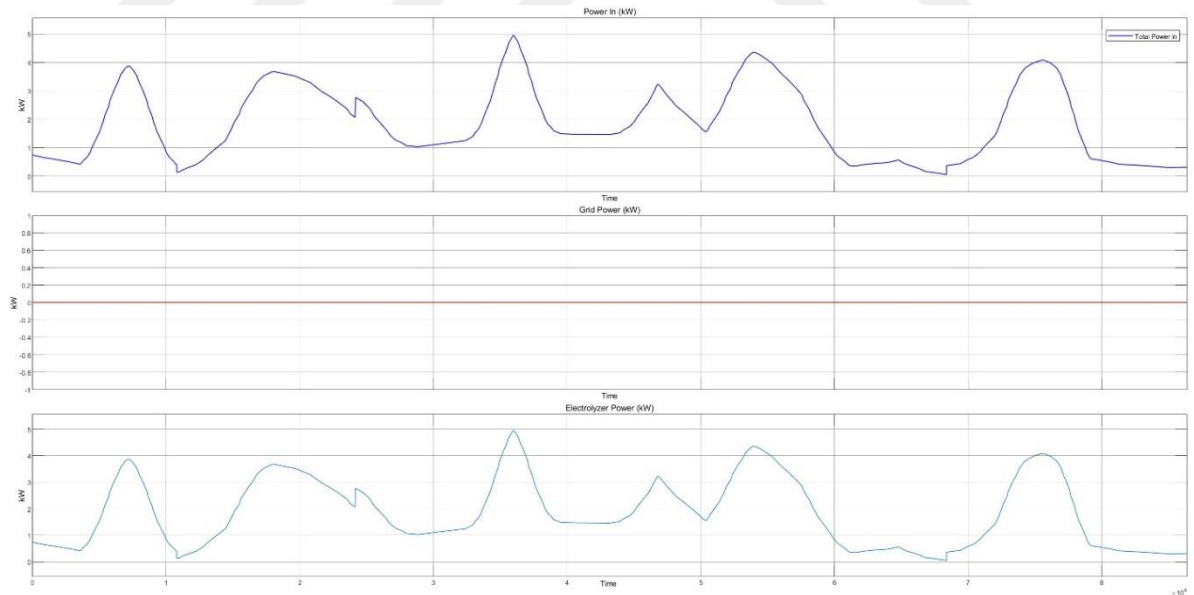


Figure 4.18. Input and output powers for Case I-b.

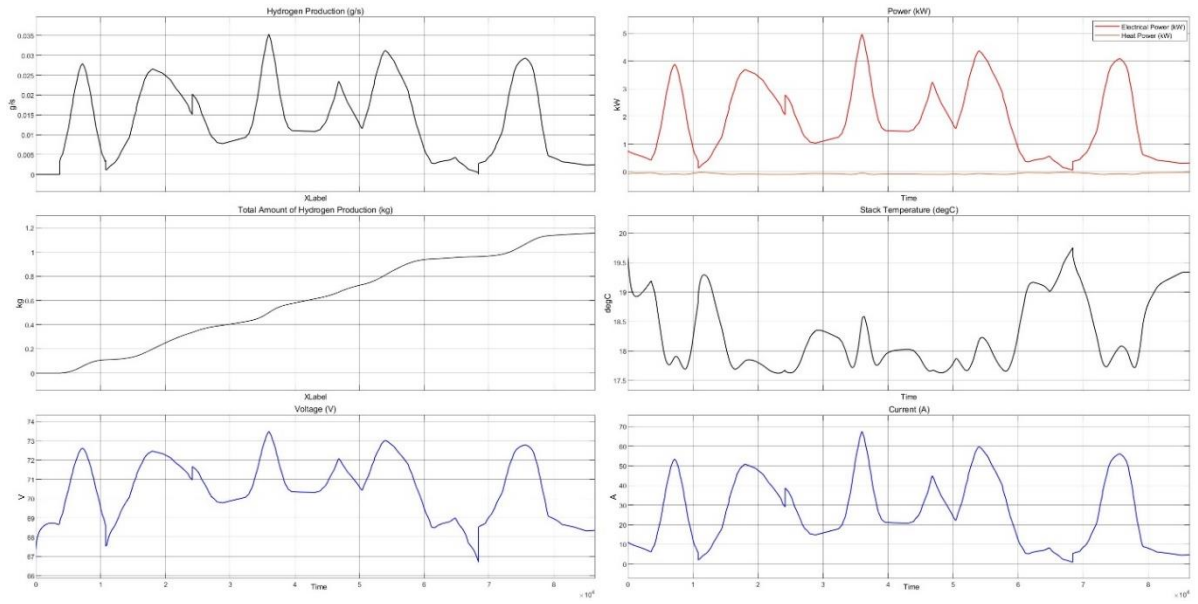


Figure 4.19. Electrolyzer measurements for Case I-b.

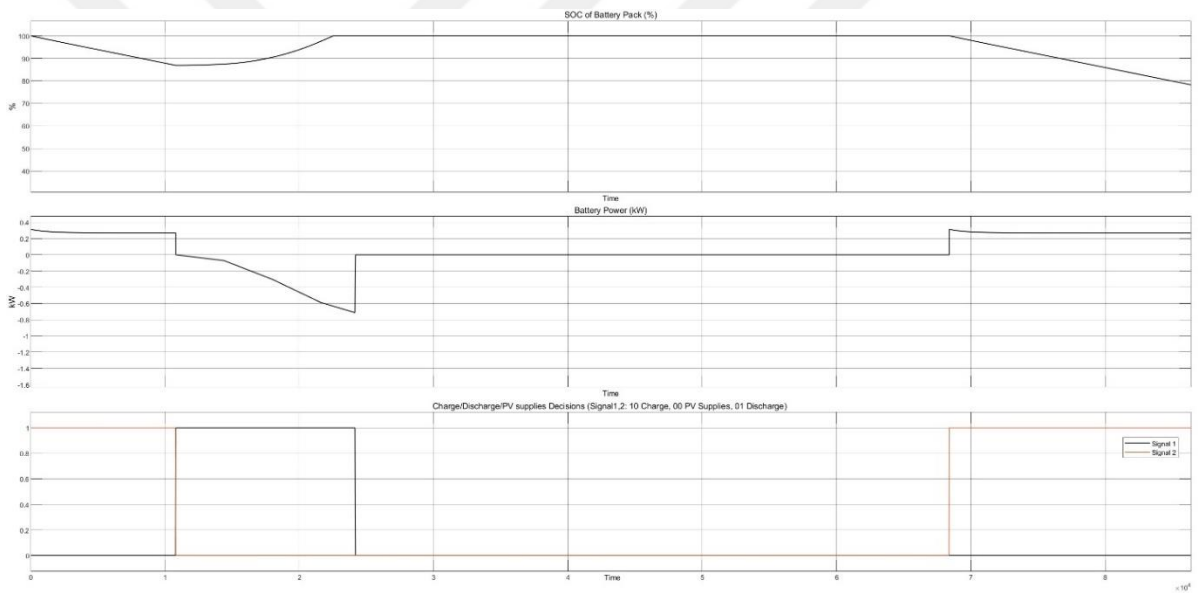


Figure 4.20. Battery measurements for Case I-b.

Case I-c:

In this case, there is no hydrogen production but only the grid is supplied. Figure 4.21 shows the input and output powers, and Figure 4.22 shows the battery measurements. The Grid is supplied with 159kWh of energy.

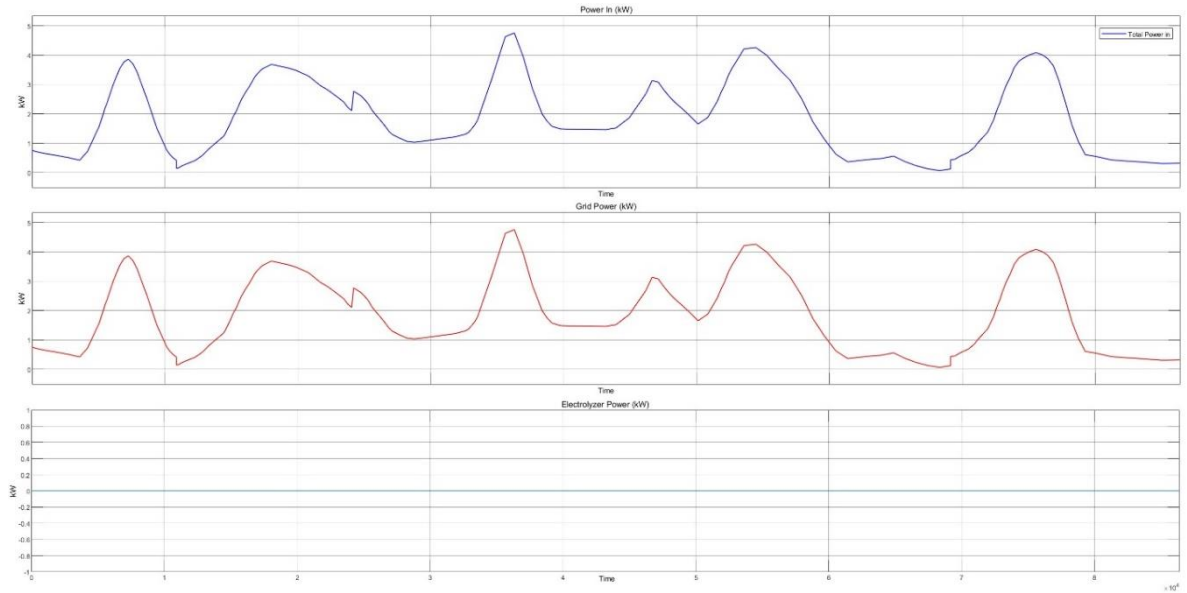


Figure 4.21. Input and output powers for Case I-c.

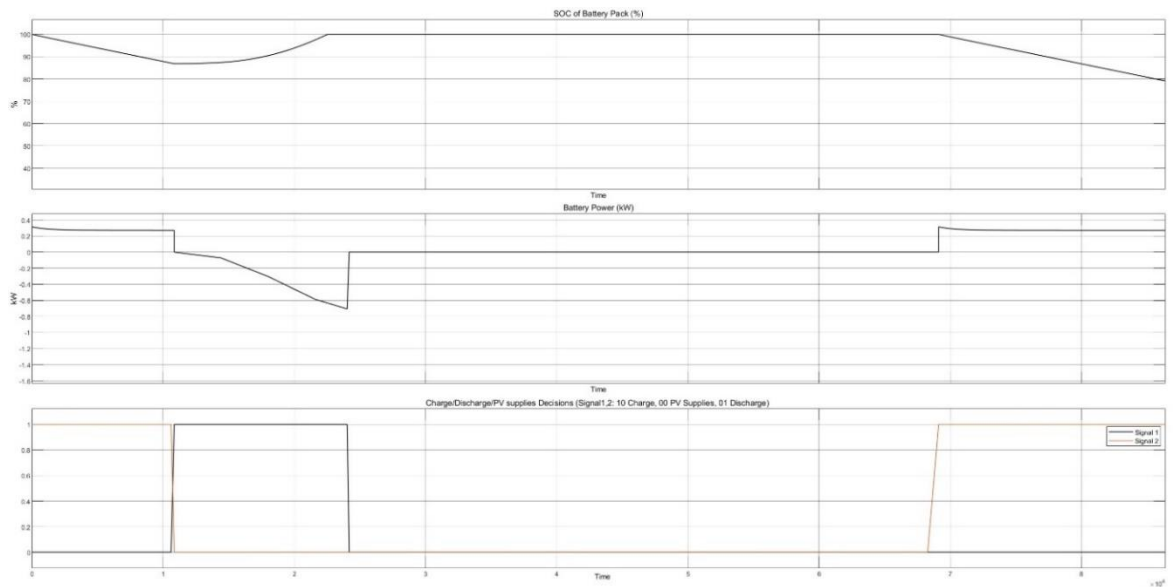


Figure 4.22. Battery measurements Case I-c.

Case II:

This case is considered in order to see the battery charges until it is SOC becomes 100%. So that, the initial SOC of the battery is taken as 50%. Input power for this case is the same for all the same for each sub-cases. Figure 4.23 shows the input powers.

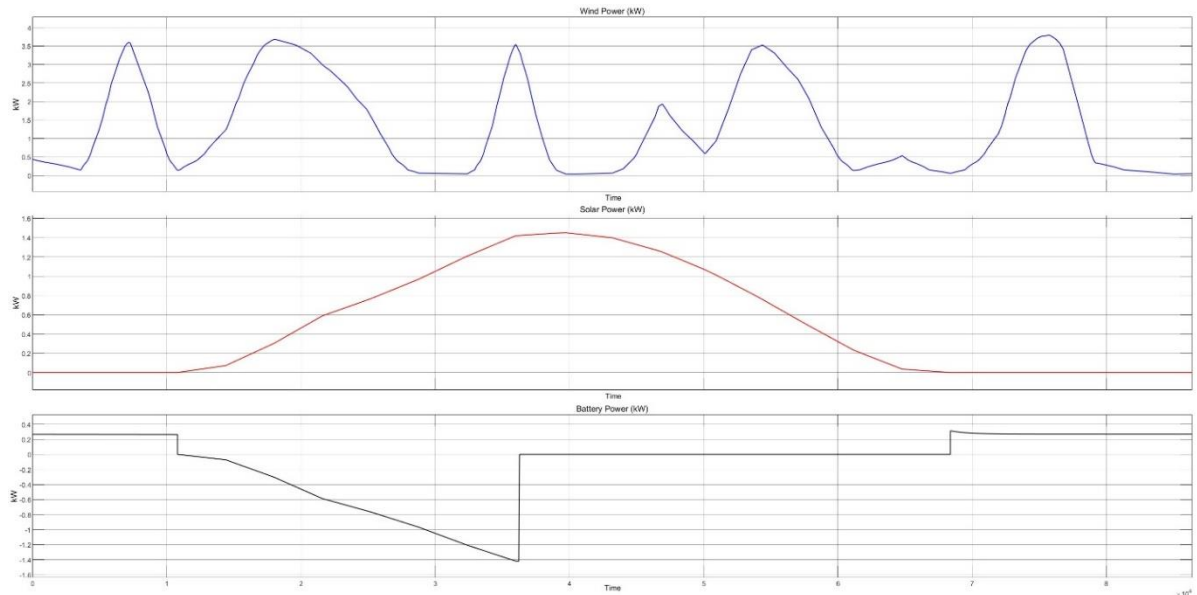


Figure 4.23. Input powers for Case II

Case II-a:

In this case, electrolyzer power is taken as 1kW. It can be seen that if there is enough power system tries to operate the electrolyzer at 1kW power. Figure 4.24 shows the input and output powers, Figure 4.25 shows the electrolyzer measurements, and Figure 4.26 shows the battery measurements. The grid was supplied with 80 kWh of energy, and the electrolyzer consumed 65 kWh, resulting in 0.478 kg of hydrogen production.

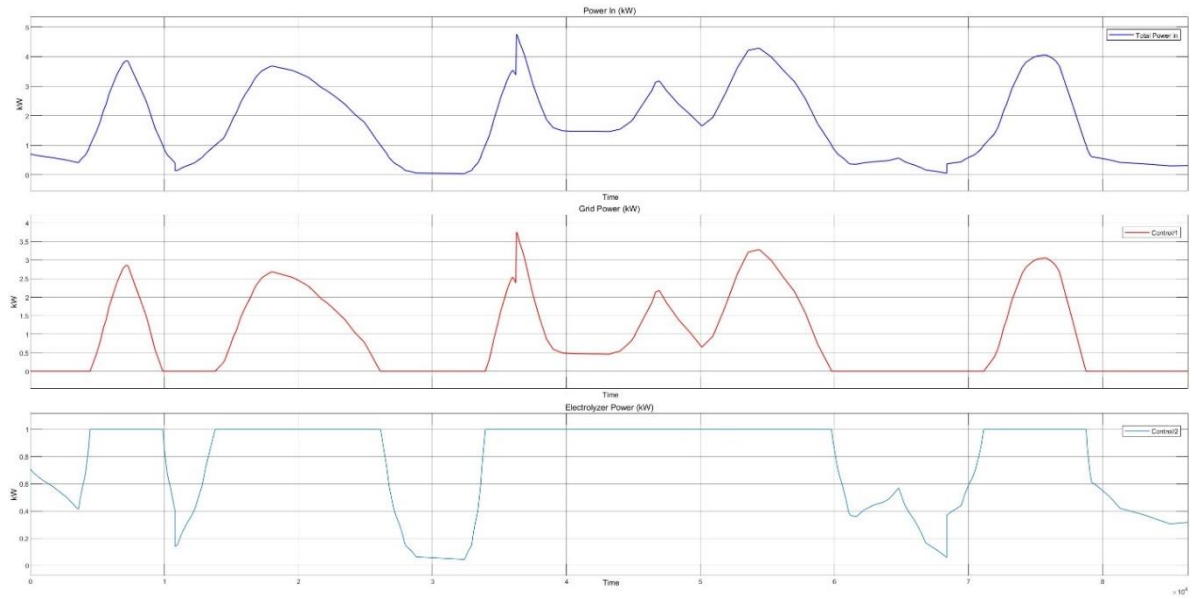


Figure 4.24. Input and output powers for Case II-a.

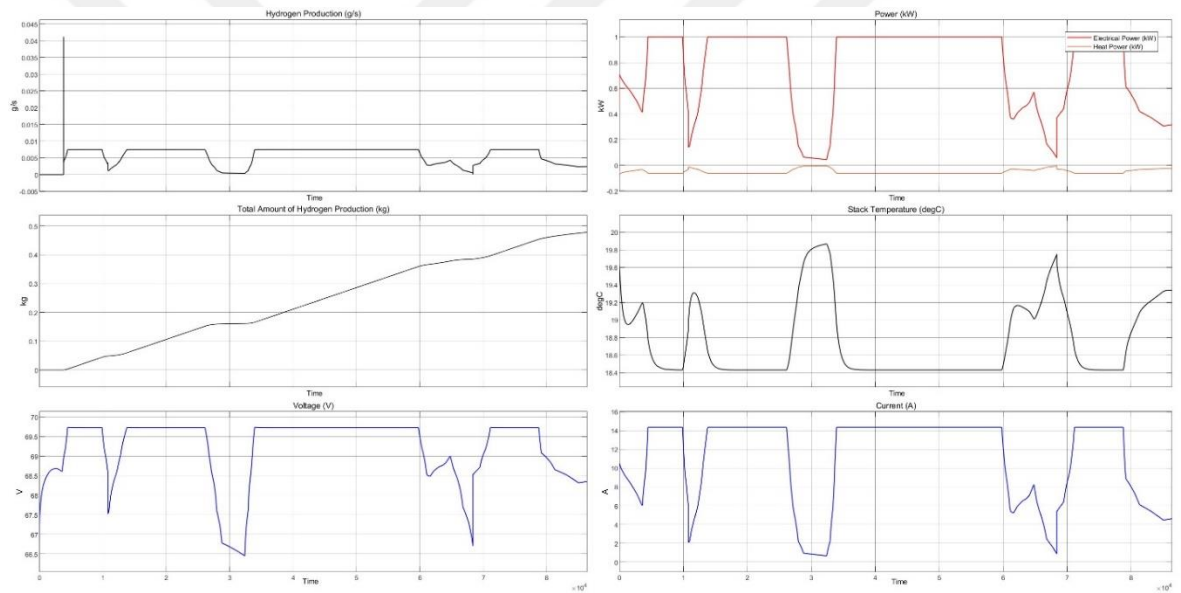


Figure 4.25. Electrolyzer measurements for Case II-a.

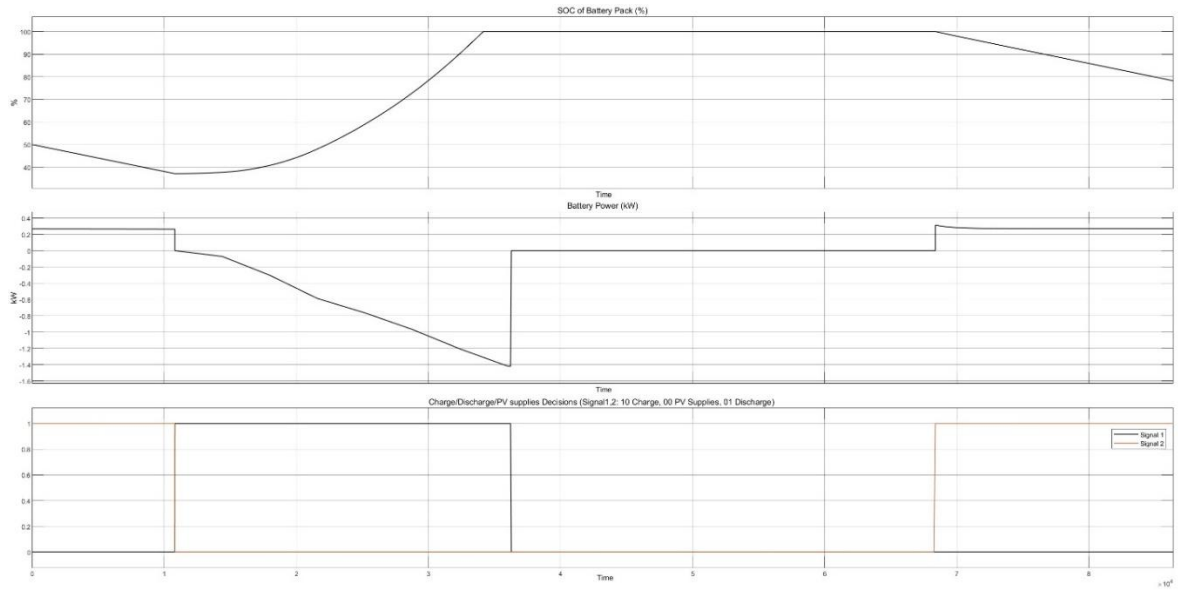


Figure 4.26. Battery measurements for Case II-a.

Case II-b:

In this case, there is no grid supply but only hydrogen is produced. Figure 4.27 shows the input and output powers, Figure 4.28 shows the electrolyzer measurements, and Figure 4.29 shows the battery measurements. Electrolyzer consumed 147 kWh of energy resulting in 1.06kg of hydrogen production.

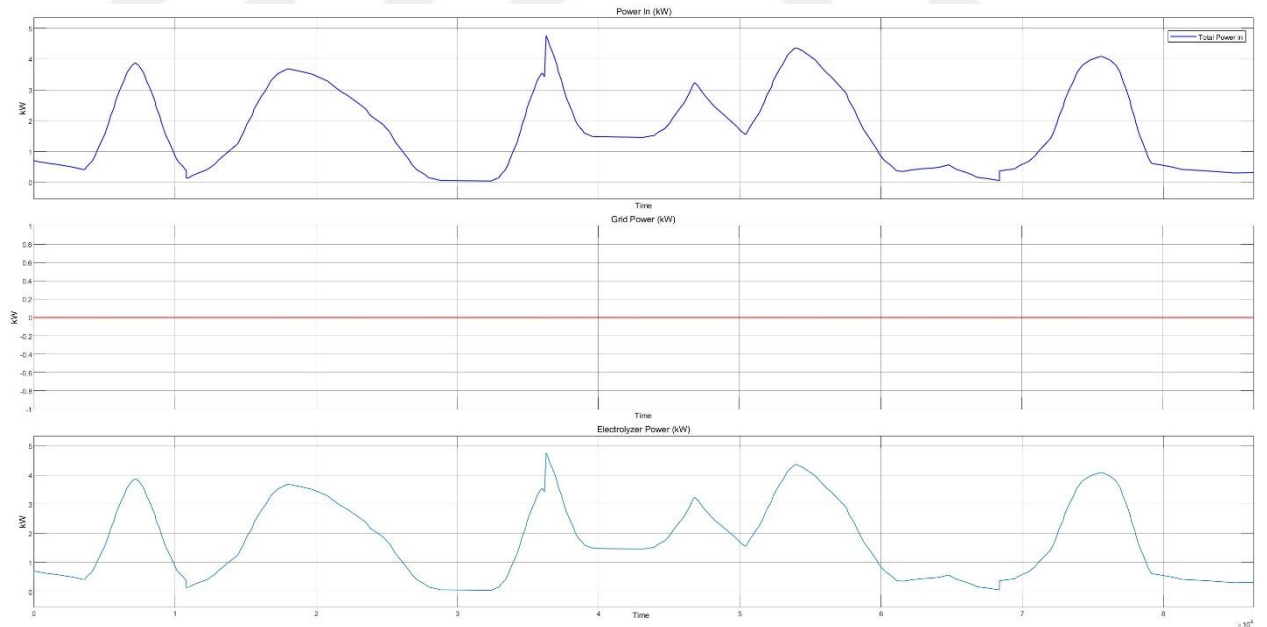


Figure 4.27. Input and output powers for Case II-b.

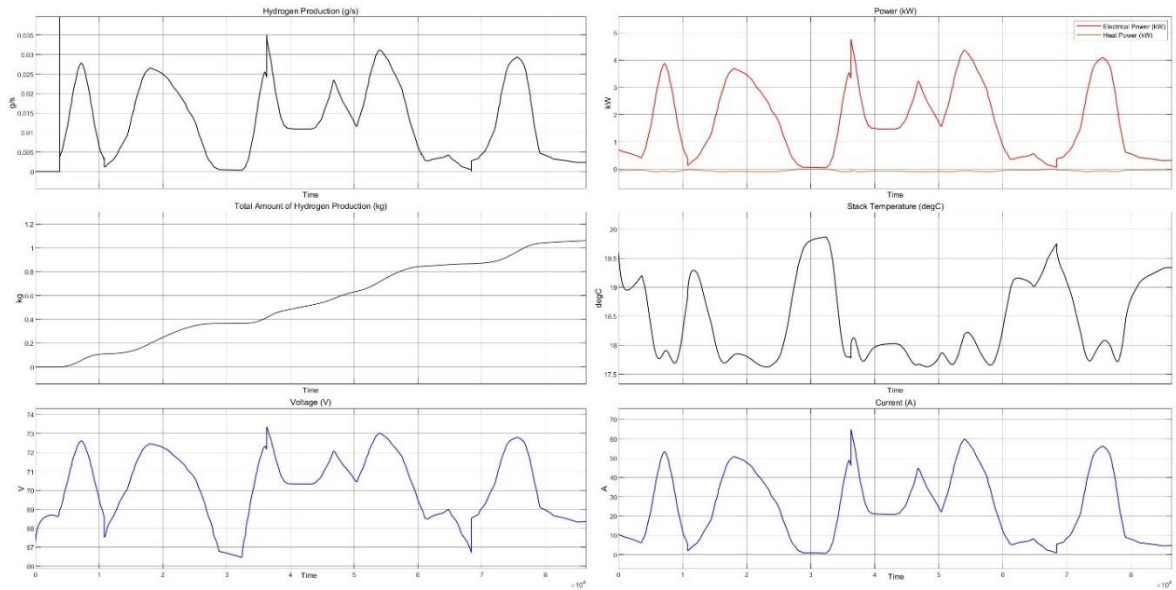


Figure 4.28. Electrolyzer measurements for Case II-b.

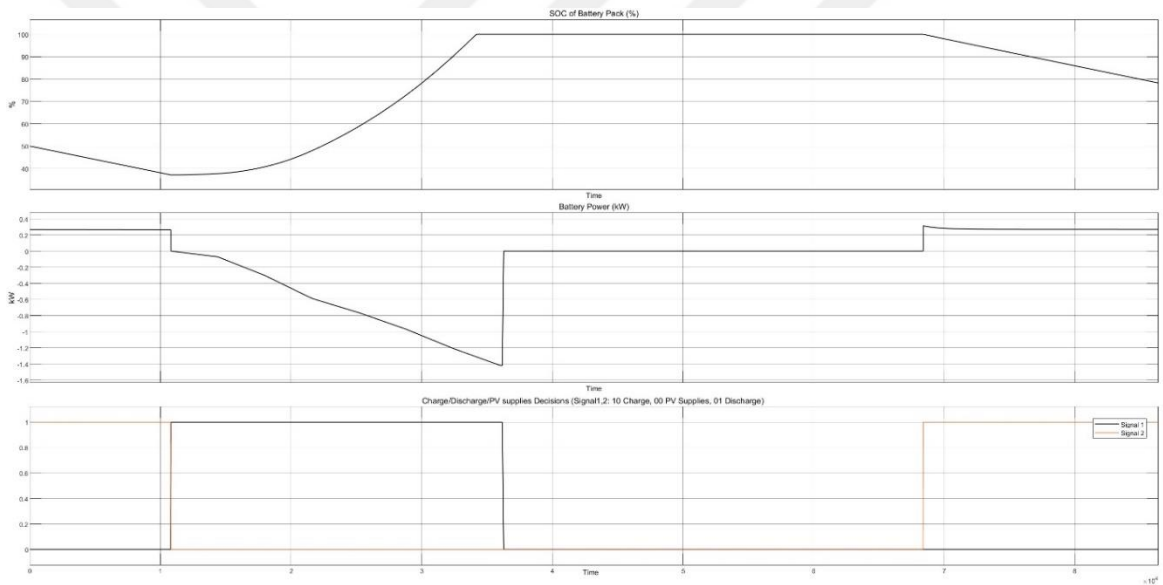


Figure 4.29. Battery measurements for Case II-b.

Case II-c:

In this case, there is no hydrogen production but only the grid is supplied. Figure 4.30 shows the input and output powers, and Figure 4.31 shows the battery measurements. Grid supplied by 147 kWh of energy.

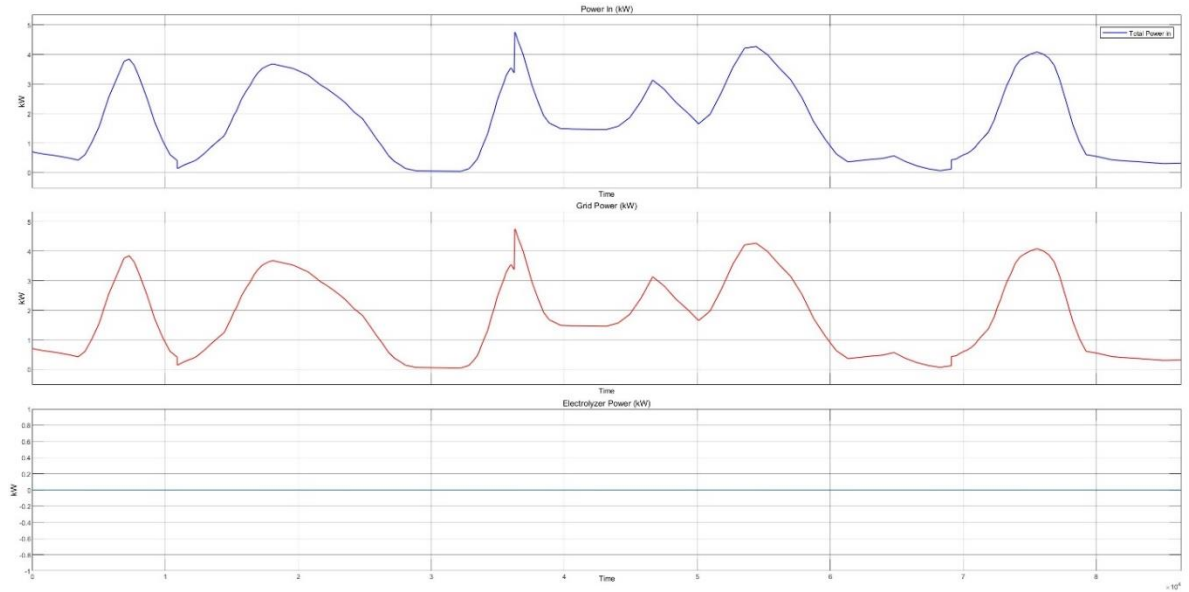


Figure 4.30. Input and output powers for Case II-c.

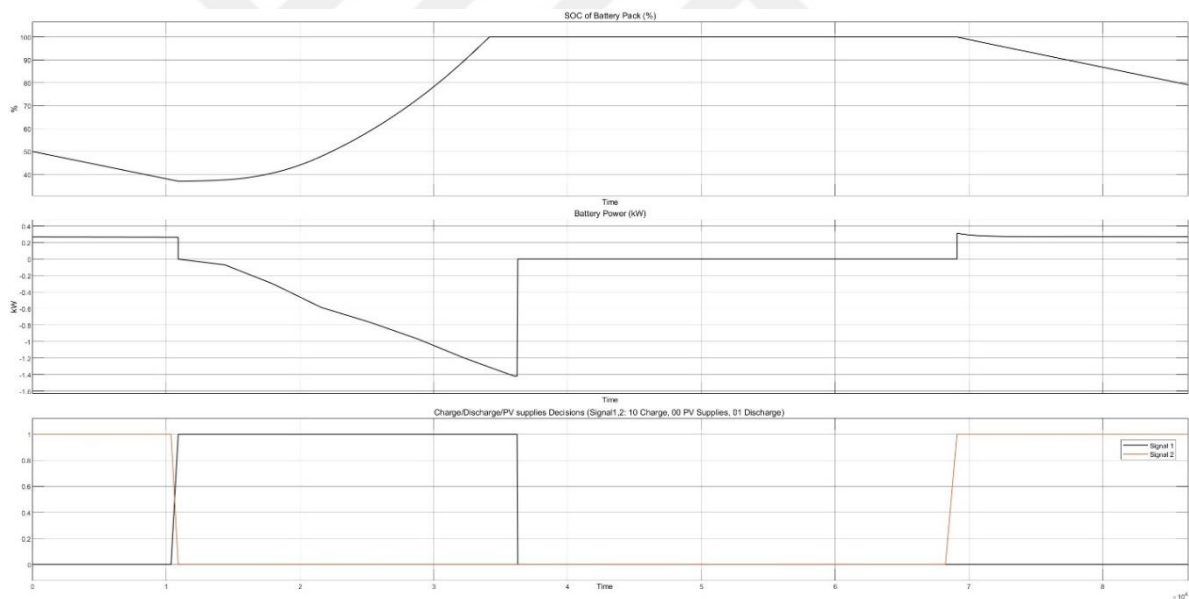


Figure 4.31. Battery measurements for Case II-c.

Case III:

In order to see if the battery's ability to get fully charged if only there is PV power, this case is considered. So that, the initial SOC of the battery is taken as 0%. Input power for this case is the same for all the same for each sub-cases. Figure 4.32 shows the input powers.

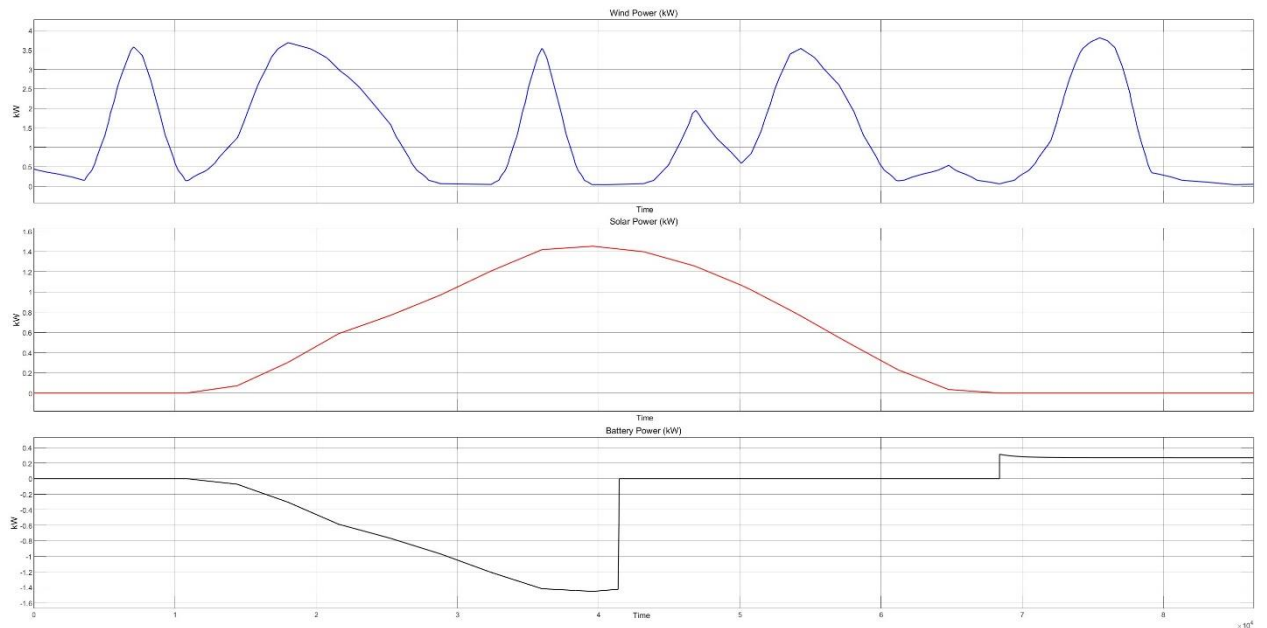


Figure 4.32. Input powers for Case III.

Case III-a:

In this case, electrolyzer power is taken as 1kW. It can be seen that if there is enough power system tries to operate the electrolyzer at 1kW power. Figure 4.33 shows the input and output powers, Figure 4.34 shows the electrolyzer measurements, and Figure 4.35 shows the battery measurements. The grid was supplied with 75.2 kWh of energy, and the electrolyzer consumed 61 kWh, resulting in 0.4471 kg of hydrogen production.

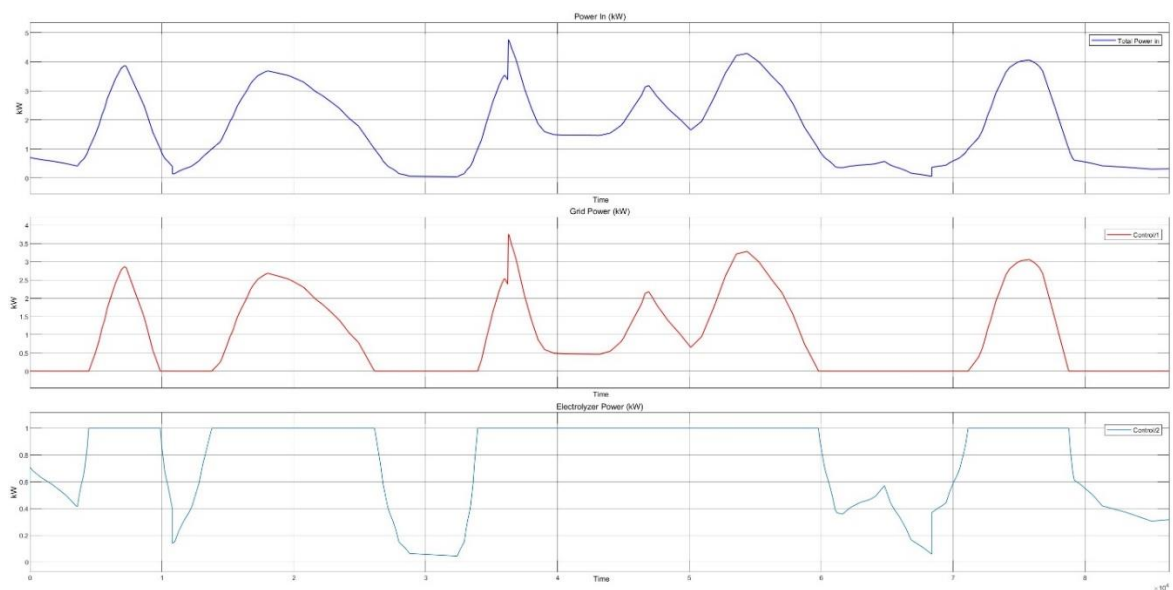


Figure 4.33. Input and output powers for Case III-a.

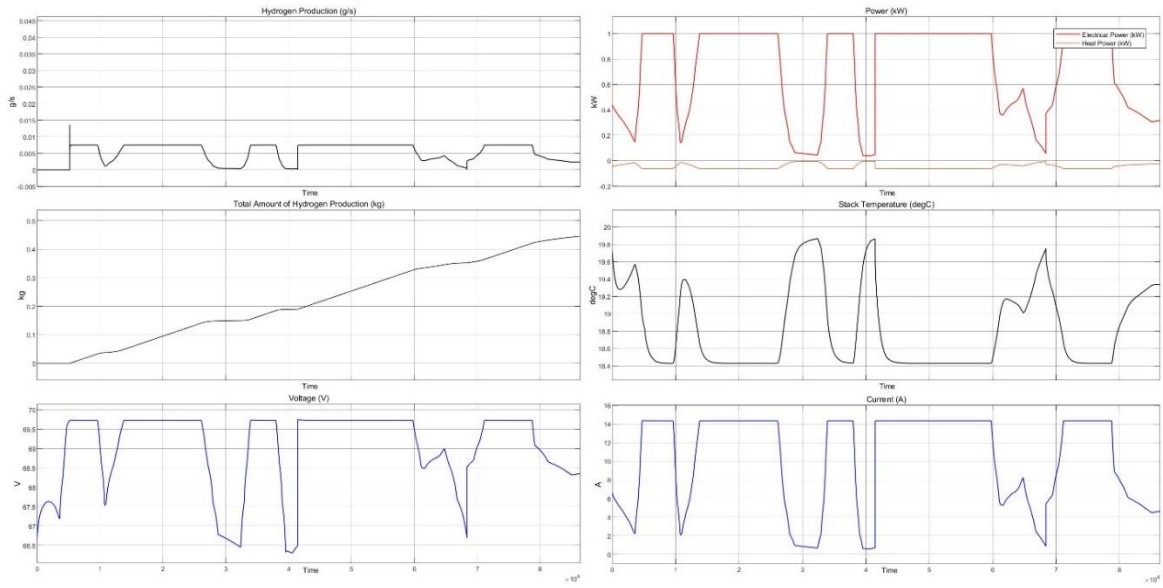


Figure 4.34. Electrolyzer measurements for Case III-a.

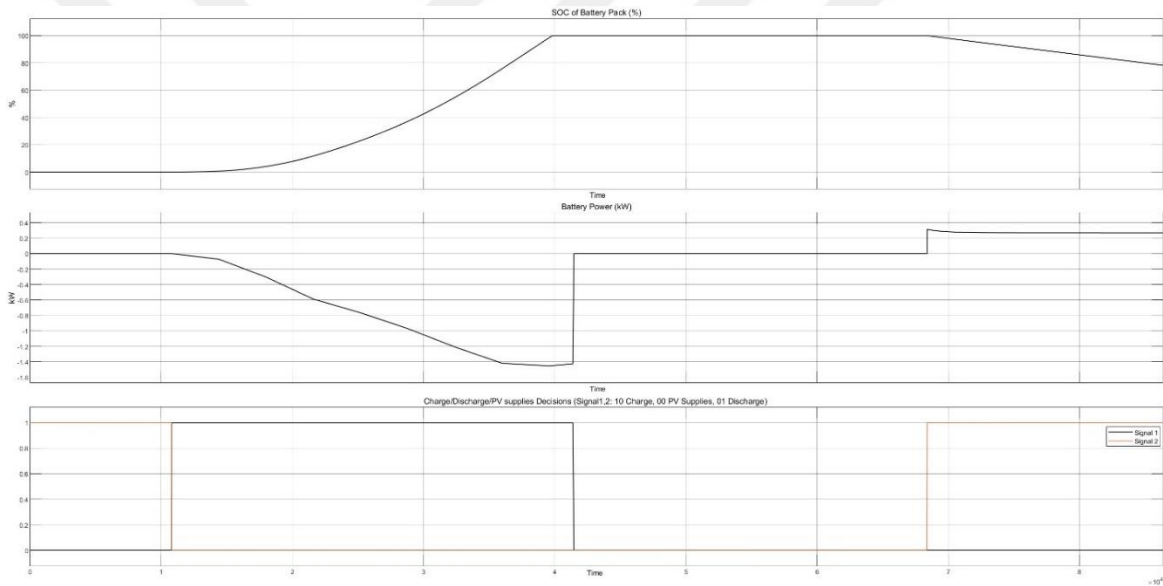


Figure 4.35. Battery measurements for Case III-a.

Case III-b:

In this case, there is no grid supply but only hydrogen is produced. Figure 4.36 shows the input and output powers, Figure 4.37 shows the electrolyzer measurements, and Figure 4.38 shows the battery measurements. Electrolyzer consumed 137 kWh of energy resulting in 0.9875 kg of hydrogen production.

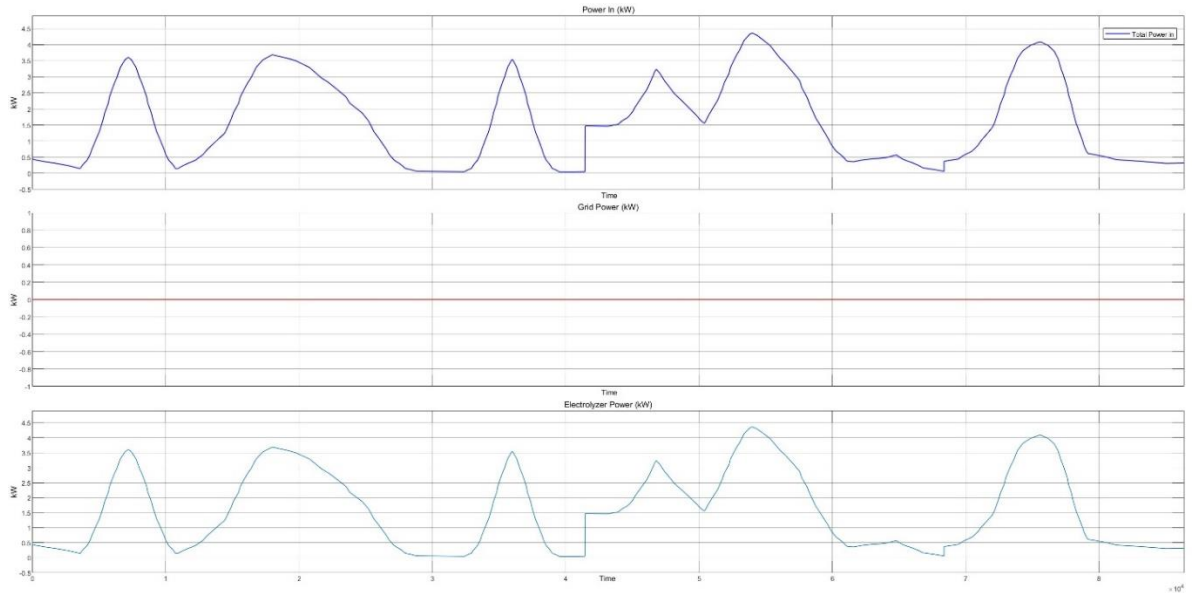


Figure 4.36. Input and output powers for Case III-b.

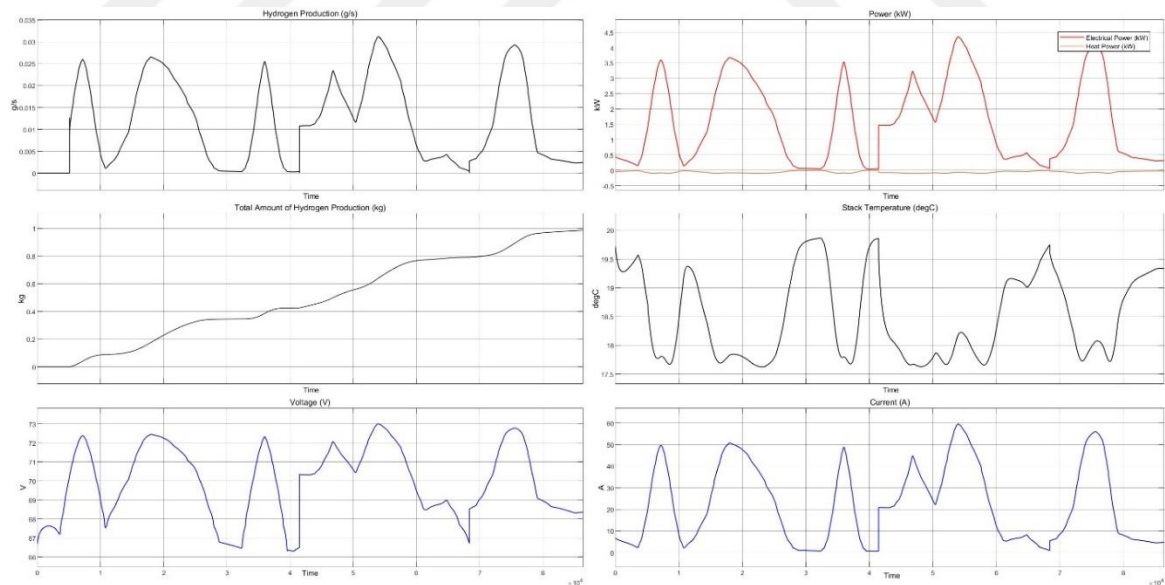


Figure 4.37. Electrolyzer measurements for Case III-b.

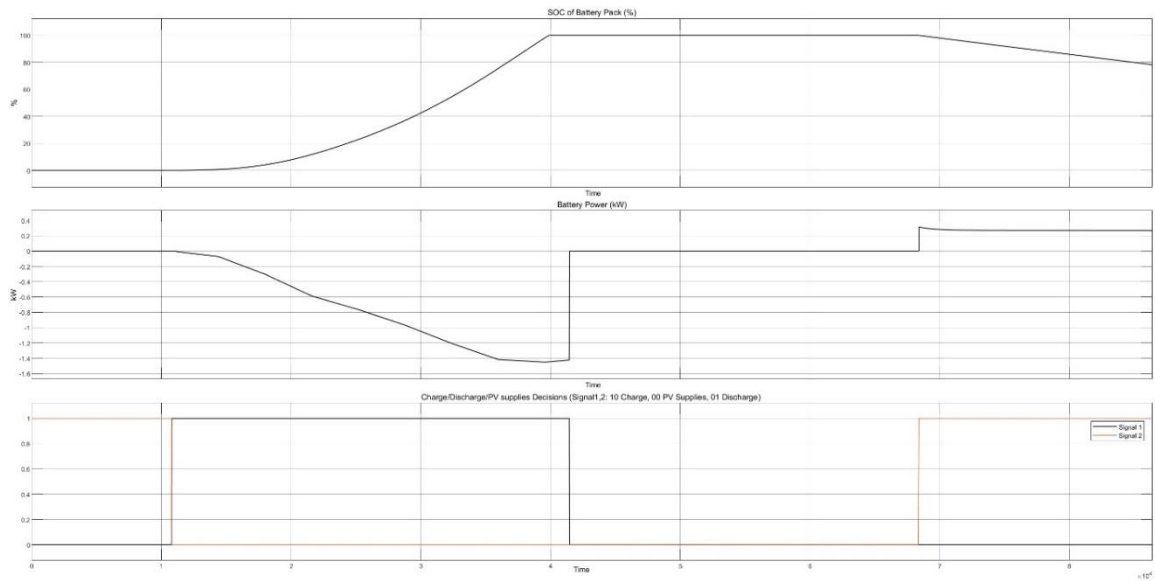


Figure 4.38. Battery measurements for Case III-b.

Case III-c:

In this case, there is no hydrogen production but only the grid is supplied. Figure 4.39 shows the input and output powers, and Figure 4.39 shows the battery measurements. Grid supplied by 137 kWh of energy.

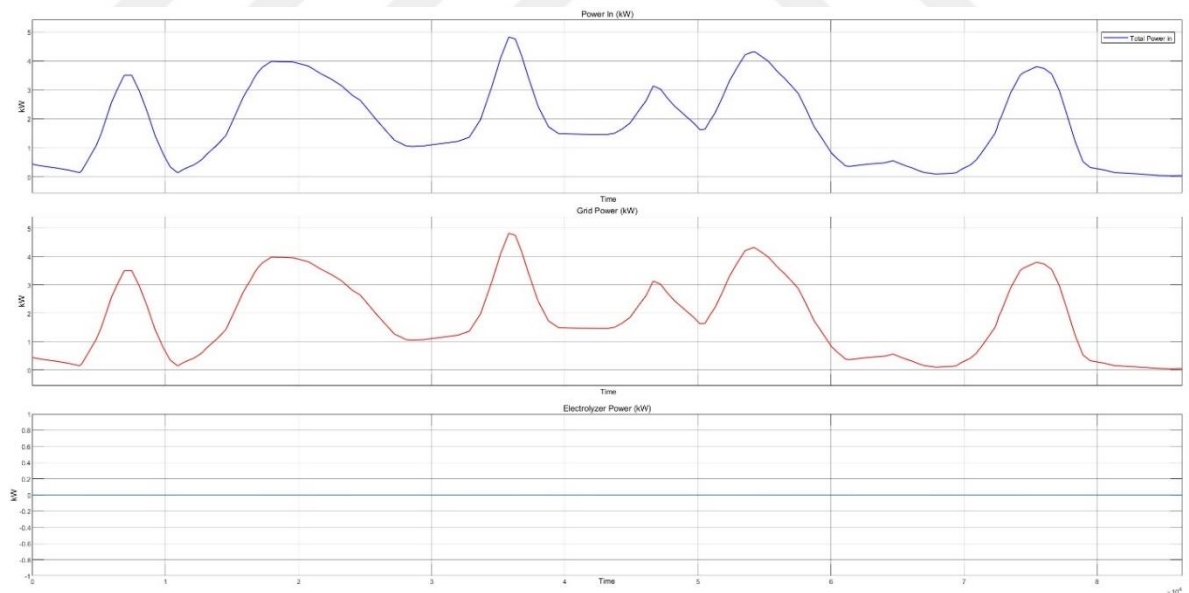


Figure 4.39 Input and output powers for Case III-c

CHAPTER 5

CONCLUSIONS

This thesis aimed to model a hybrid renewable energy plant based on the models in the literature. Control strategies for every individual component are also modeled. HRES in the thesis consists of Wind Energy Conversion System (WECS), a PV array, Battery Energy Storage System (BESS), and an electrolyzer. The system is also grid-connected.

Direct-drive Permanent Magnet Synchronous Generator (PMSG) wind turbine was selected for this research. The reason behind it is that it is a very common type for small-scale wind turbines and has no requirement for a drivetrain. All individual components of a WECS are modeled; mechanical model of the wind turbine, PMSG, universal bridge, boost converter, MPPT control, inverter, and filter. Perturbation and Observe (P&O) algorithm is selected for MPPT control. The PV array system consists of PV modules, MPPT control, and a boost converter. Same with the WECS, the P&O algorithm is used. BESS includes a battery pack with battery cells inside it and charge and discharge circuits. MathWorks's Electrolyzer model is used because it enables the user to monitor every important parameter of an electrolyzer such as stack voltage and temperature, heat and electrical power consumption, and hydrogen generation. For every model 20 to 30 seconds of simulations were made in order to see transient regions in the system.

Different control strategies were investigated. MPPT control was managed by the P&O algorithm for the PV array and WECS. In addition to that, the PV array and battery storage are combined in the same DC bus, and the necessary algorithm is made, and discharge and charge circuits were designed. The Electrolyzer model cannot exceed a power of 150kW. Because of that, electrolyzer power control was necessary. This same control also allows the user to make decisions between only grid supply and only hydrogen production. Hybrid operation is also possible.

An overall model including WECS, PV array, BESS, and electrolyzer was designed. The system also has two different controls: electrolyzer power control and

battery charge and discharge control. All individual systems can be user-defined meaning the user can decide which wind turbine to use, the size of the PV array and battery, and also the operation. One-day simulations were made for 11 different cases. Cases are decided for different sizes of the systems, operations, and initial SOC of the battery.

As a conclusion, every component of a simple HRES was modeled and simulated for a short time. Different control strategies were investigated. An overall model for one-day simulations was made. For future prospects, any energy-related technology (Supercapacitors, EV charging stations, etc.) can be added to the overall system.



REFERENCES

- Abdin, Z., C.J. Webbn, and E.MacA. Gray. 2018. "Retraction Notice to 'Solar Hydrogen Hybrid Energy Systems for off-Grid Electricity Supply: A Critical Review.'" *Renewable and Sustainable Energy Reviews* 83: 175.
<https://doi.org/10.1016/j.rser.2017.12.004>.
- Abdullah, M. A., A. H.M. Yatim, C. W. Tan, and R. Saidur. 2012. "A Review of Maximum Power Point Tracking Algorithms for Wind Energy Systems." *Renewable and Sustainable Energy Reviews* 16 (5): 3220–27.
<https://doi.org/10.1016/j.rser.2012.02.016>.
- Ahmed, Jubaer, and Zainal Salam. 2015. "An Improved Method to Predict the Position of Maximum Power Point during Partial Shading for PV Arrays." *IEEE Transactions on Industrial Informatics* 11 (6): 1378–87.
<https://doi.org/10.1109/TII.2015.2489579>.
- Ahmed, Sajib, Saad Mekhilef, Marizan Binti, and Kok Soon. 2022. "Performances of the Adaptive Conventional Maximum Power Point Tracking Algorithms for Solar Photovoltaic System." *Sustainable Energy Technologies and Assessments* 53 (PA): 102390. <https://doi.org/10.1016/j.seta.2022.102390>.
- Akarsu, Beyhan, and Mustafa Serdar Genç. 2022. "Optimization of Electricity and Hydrogen Production with Hybrid Renewable Energy Systems." *Fuel* 324 (PA): 124465. <https://doi.org/10.1016/j.fuel.2022.124465>.
- Akhtari, Mohammad Reza, and Mehdi Baneshi. 2019. "Techno-Economic Assessment and Optimization of a Hybrid Renewable Co-Supply of Electricity, Heat and Hydrogen System to Enhance Performance by Recovering Excess Electricity for a Large Energy Consumer." *Energy Conversion and Management* 188 (January): 131–41. <https://doi.org/10.1016/j.enconman.2019.03.067>.
- Akrofi, M.M., and M. Okitasari. 2022. "Integrating Solar Energy Considerations into Urban Planning for Low Carbon Cities: A Systematic Review of the State-of-the-Art." *Urban Governance* 2 (1): 157–72. <https://doi.org/10.1016/j.ugj.2022.04.002>.
- Ali, Ahmed Ismail M., and Hassanien Ramadan A. Mohamed. 2022. "Improved P&O MPPT Algorithm with Efficient Open-Circuit Voltage Estimation for Two-Stage Grid-Integrated PV System under Realistic Solar Radiation." *International Journal of Electrical Power and Energy Systems* 137 (May 2021): 107805.
<https://doi.org/10.1016/j.ijepes.2021.107805>.
- Alik, Rozana, and Awang Jusoh. 2018. "An Enhanced P&O Checking Algorithm MPPT for High Tracking Efficiency of Partially Shaded PV Module." *Solar Energy* 163 (March): 570–80. <https://doi.org/10.1016/j.solener.2017.12.050>.
- Apata, O., and D. T.O. Oyedokun. 2020a. "An Overview of Control Techniques for Wind Turbine Systems." *Scientific African* 10: e00566.
<https://doi.org/10.1016/j.sciaf.2020.e00566>.

- 2020b. "An Overview of Control Techniques for Wind Turbine Systems." *Scientific African* 10: e00566. <https://doi.org/10.1016/j.sciaf.2020.e00566>.
- Atlam, Ozcan, and Mohan Kolhe. 2011. "Equivalent Electrical Model for a Proton Exchange Membrane (PEM) Electrolyser." *Energy Conversion and Management* 52 (8–9): 2952–57. <https://doi.org/10.1016/j.enconman.2011.04.007>.
- Baba, Ali Omar, Guangyu Liu, and Xiaohui Chen. 2020. "Classification and Evaluation Review of Maximum Power Point Tracking Methods." *Sustainable Futures* 2 (April): 100020. <https://doi.org/10.1016/j.sftr.2020.100020>.
- Babaei, Reza, David S.K. Ting, and Rupp Carriveau. 2022. "Optimization of Hydrogen-Producing Sustainable Island Microgrids." *International Journal of Hydrogen Energy* 47 (32): 14375–92. <https://doi.org/10.1016/j.ijhydene.2022.02.187>.
- Baker, John. 2008. "New Technology and Possible Advances in Energy Storage." *Energy Policy* 36 (12): 4368–73. <https://doi.org/10.1016/j.enpol.2008.09.040>.
- Basu, Srijit, Alfred John, Akshay, and Anil Kumar. 2021. "Design and Feasibility Analysis of Hydrogen Based Hybrid Energy System: A Case Study." *International Journal of Hydrogen Energy* 46 (70): 34574–86. <https://doi.org/10.1016/j.ijhydene.2021.08.036>.
- Belhachat, F., and C. Larbes. 2015. "Modeling, Analysis and Comparison of Solar Photovoltaic Array Configurations under Partial Shading Conditions." *Solar Energy* 120 (October): 399–418. <https://doi.org/10.1016/j.solener.2015.07.039>.
- Bendib, Boualem, Hocine Belmili, and Fateh Krim. 2015a. "A Survey of the Most Used MPPT Methods: Conventional and Advanced Algorithms Applied for Photovoltaic Systems." *Renewable and Sustainable Energy Reviews* 45: 637–48. <https://doi.org/10.1016/j.rser.2015.02.009>.
- 2015b. "A Survey of the Most Used MPPT Methods: Conventional and Advanced Algorithms Applied for Photovoltaic Systems." *Renewable and Sustainable Energy Reviews*. Elsevier Ltd. <https://doi.org/10.1016/j.rser.2015.02.009>.
- Benghanem, Mohamed, Adel Mellit, Hamad Almohamadi, Sofiane Haddad, Nedjwa Chettibi, Abdulaziz M. Alanazi, Drigos Dasalla, and Ahmed Alzahrani. 2023. "Hydrogen Production Methods Based on Solar and Wind Energy: A Review." *Energies*. MDPI. <https://doi.org/10.3390/en16020757>.
- Castano, S., L. Gauchia, E. Voncila, and J. Sanz. 2015. "Dynamical Modeling Procedure of a Li-Ion Battery Pack Suitable for Real-Time Applications." *Energy Conversion and Management*. Elsevier Ltd. <https://doi.org/10.1016/j.enconman.2014.12.076>.
- Chen, Min, and Gabriel A. Rincón-Mora. 2006. "Accurate Electrical Battery Model Capable of Predicting Runtime and I-V Performance." *IEEE Transactions on Energy Conversion* 21 (2): 504–11. <https://doi.org/10.1109/TEC.2006.874229>.
- Cheng, Ming, and Ying Zhu. 2014. "The State of the Art of Wind Energy Conversion Systems and Technologies: A Review." *Energy Conversion and Management*. Elsevier Ltd. <https://doi.org/10.1016/j.enconman.2014.08.037>.

- Christiana Honsberg, and Stuart Bowden. n.d. “Solar Cell Structure.” Accessed June 5, 2023. <https://www.pveducation.org/pvcdrom/solar-cell-operation/solar-cell-structure>.
- Cox, Sadie, Laura Beshilas, and Eliza Hotchkiss. n.d. “Www.Resilient-Energy.Org | Www.Nrel.Gov/Usaid-Partnership.” www.resilient-energy.org.
- Cros, Sylvain, Jordi Badosa, André Szantaï, and Martial Haeffelin. 2020. “Reliability Predictors for Solar Irradiance Satellite-Based Forecast.” *Energies* 13 (21). <https://doi.org/10.3390/en13215566>.
- Díaz-González, Francisco, Andreas Sumper, Oriol Gomis-Bellmunt, and Fernando D. Bianchi. 2013. “Energy Management of Flywheel-Based Energy Storage Device for Wind Power Smoothing.” *Applied Energy* 110: 207–19. <https://doi.org/10.1016/j.apenergy.2013.04.029>.
- Diouf, Boucar, and Ramchandra Pode. 2015. “Potential of Lithium-Ion Batteries in Renewable Energy.” *Renewable Energy*. Elsevier Ltd. <https://doi.org/10.1016/j.renene.2014.11.058>.
- Dursun, Erkan, Bora Acarkan, and Osman Kilic. 2012. “Modeling of Hydrogen Production with a Stand-Alone Renewable Hybrid Power System.” *International Journal of Hydrogen Energy* 37 (4): 3098–3107. <https://doi.org/10.1016/j.ijhydene.2011.11.029>.
- Edenhofer, Ottmar., Ramón Pichs Madruga, Y. Sokona, United Nations Environment Programme., World Meteorological Organization., Intergovernmental Panel on Climate Change. Working Group III., and Potsdam-Institut für Klimafolgenforschung. 2012. *Renewable Energy Sources and Climate Change Mitigation : Special Report of the Intergovernmental Panel on Climate Change*. Cambridge University Press.
- Evans, Annette, Vladimir Strezov, and Tim J. Evans. 2012. “Assessment of Utility Energy Storage Options for Increased Renewable Energy Penetration.” *Renewable and Sustainable Energy Reviews* 16 (6): 4141–47. <https://doi.org/10.1016/j.rser.2012.03.048>.
- Faye, Omar, Jerzy Szpunar, and Ubong Eduok. 2022. “A Critical Review on the Current Technologies for the Generation, Storage, and Transportation of Hydrogen.” *International Journal of Hydrogen Energy*. Elsevier Ltd. <https://doi.org/10.1016/j.ijhydene.2022.02.112>.
- Foss, Matthew. 2022. “The Impact of Renewables on Energy Security.” *Canadian Foreign Policy Journal* 28 (3): 234–48. <https://doi.org/10.1080/11926422.2022.2118138>.
- G. Konstantinou, B. Hredzak. 2021. “Power Electronics for Hybrid Energy Systems.” In *Hybrid Renewable Energy Systems and Microgrids*, edited by Ersan Kabalci, Hybrid Renewable Energy Systems and Microgrids. Academic Press.
- Gajewski, Piotr. 2021. “Turbine , Photovoltaic Panels and Battery Energy Storage.”

- “Global Hydrogen Review 2021.” 2021. *Global Hydrogen Review 2021*.
<https://doi.org/10.1787/39351842-en>.
- Goodenough, John B., and Youngsik Kim. 2010. “Challenges for Rechargeable Li Batteries.” *Chemistry of Materials*. <https://doi.org/10.1021/cm901452z>.
- GWEC. n.d. “Annual Wind Report 2022.”
- Hamdi, Hichem, Chiheb Ben Regaya, and Abderrahmen Zaafouri. 2019. “Real-Time Study of a Photovoltaic System with Boost Converter Using the PSO-RBF Neural Network Algorithms in a MyRio Controller.” *Solar Energy* 183 (May): 1–16.
<https://doi.org/10.1016/j.solener.2019.02.064>.
- HCI Energy. 2023. “Leveraging Lithium-Ion Batteries for Renewable Energy Storage,” May 25, 2023. <https://www.hcienergy.com/blog/leveraging-lithium-ion-batteries-for-renewable-energy-storage>.
- Hoarca, Ioan Cristian. 2021. “Mathematical Modeling and Simulation of PV Systems Part I: Mathematical Modeling and Simulink Implementation.” In *2021 International Conference on Applied and Theoretical Electricity, ICATE 2021 - Proceedings*. Institute of Electrical and Electronics Engineers Inc.
<https://doi.org/10.1109/ICATE49685.2021.9465047>.
- Hua, Chihchiang, Jongrong Lin, and Chihming Shen. 1998. “Implementation of a DSP-Controlled Photovoltaic System with Peak Power Tracking.” *IEEE TRANSACTIONS ON INDUSTRIAL ELECTRONICS*. Vol. 45.
- International Energy Agency (IEA). 2019. “Renewables 2019.”
- International Renewable Energy Agency, and Abu Dhabi and International Labour Organization Geneva. n.d. *Renewable Energy and Jobs: Annual Review 2022*.
- Johansson, Bengt. 2013. “Security Aspects of Future Renewable Energy Systems-A Short Overview.” *Energy* 61 (November): 598–605.
<https://doi.org/10.1016/j.energy.2013.09.023>.
- Jose Zayas. 2014. “Wind Turbine Scaling Enables Projects to Reach New Heights.” 2014. <https://www.energy.gov/eere/wind/articles/wind-turbine-scaling-enables-projects-reach-new-heights>.
- Kar, Subhasri, Sumit Banerjee, and C. K. Chanda. 2021. “Stepwise Modelling and Analysis of A PV Module in Matlab Simulink.” In *2021 International Conference on Intelligent Technologies, CONIT 2021*. Institute of Electrical and Electronics Engineers Inc. <https://doi.org/10.1109/CONIT51480.2021.9498343>.
- Kesraoui, M., N. Korichi, and A. Belkadi. 2011. “Maximum Power Point Tracker of Wind Energy Conversion System.” *Renewable Energy* 36 (10): 2655–62.
<https://doi.org/10.1016/j.renene.2010.04.028>.
- Kosmadakis, I., and C. Elmasides. 2019. “Towards Performance Enhancement of Hybrid Power Supply Systems Based on Renewable Energy Sources.” *Energy Procedia* 157 (2018): 977–91. <https://doi.org/10.1016/j.egypro.2018.11.265>.

- Kota, Venkata Reddy, and Muralidhar Nayak Bhukya. 2017. "A Novel Linear Tangents Based P&O Scheme for MPPT of a PV System." *Renewable and Sustainable Energy Reviews* 71 (November 2016): 257–67. <https://doi.org/10.1016/j.rser.2016.12.054>.
- Koutroulis, Eftichios, and Kostas Kalaitzakis. 2006. "Design of a Maximum Power Tracking System for Wind-Energy-Conversion Applications." *IEEE Transactions on Industrial Electronics* 53 (2): 486–94. <https://doi.org/10.1109/TIE.2006.870658>.
- Krupke, Christopher, Jihong Wang, Jonathan Clarke, and Xing Luo. 2017. "Modeling and Experimental Study of a Wind Turbine System in Hybrid Connection with Compressed Air Energy Storage." *IEEE Transactions on Energy Conversion* 32 (1): 137–45. <https://doi.org/10.1109/TEC.2016.2594285>.
- Kumar, Dipesh, and Kalyan Chatterjee. 2016. "A Review of Conventional and Advanced MPPT Algorithms for Wind Energy Systems." *Renewable and Sustainable Energy Reviews* 55: 957–70. <https://doi.org/10.1016/j.rser.2015.11.013>.
- Lasheen, Mohamed, Ali Kamel Abdel Rahman, Mazen Abdel-Salam, and Shinichi Ookawara. 2017. "Adaptive Reference Voltage-Based MPPT Technique for PV Applications." *IET Renewable Power Generation* 11 (5): 715–22. <https://doi.org/10.1049/iet-rpg.2016.0749>.
- Leidy Tatiana Contreras Montoya, Santiago Lain, Mohamad Issa, Adrian Ilinca. 2021. "Renewable Energy Systems." In *Hybrid Renewable Energy Systems and Microgrid*, edited by Ersan Kabalci, 103–77. Academic Press.
- Li, Hong, Duo Yang, Wenzhe Su, Jinhu Lu, and Xinghuo Yu. 2019. "An Overall Distribution Particle Swarm Optimization MPPT Algorithm for Photovoltaic System under Partial Shading." *IEEE Transactions on Industrial Electronics* 66 (1): 265–75. <https://doi.org/10.1109/TIE.2018.2829668>.
- Lottie Limb. 2022. "The Race for Renewable Batteries: What's the Future of Solar and Wind Storage?," July 22, 2022. <https://www.euronews.com/green/2022/07/21/the-race-for-renewable-batteries-whats-the-future-of-solar-and-wind-storage>.
- Luta, Doudou N., and Atanda K. Raji. 2018. "Decision-Making between a Grid Extension and a Rural Renewable off-Grid System with Hydrogen Generation." *International Journal of Hydrogen Energy* 43 (20): 9535–48. <https://doi.org/10.1016/j.ijhydene.2018.04.032>.
- Ma, Qian, Xiang Huang, Feng Wang, Chao Xu, Reza Babaei, and Hossein Ahmadian. 2022. "Optimal Sizing and Feasibility Analysis of Grid-Isolated Renewable Hybrid Microgrids: Effects of Energy Management Controllers." *Energy* 240: 122503. <https://doi.org/10.1016/j.energy.2021.122503>.
- Macedo, Sabrina Fernandes, and Drielli Peyerl. 2022. "Prospects and Economic Feasibility Analysis of Wind and Solar Photovoltaic Hybrid Systems for Hydrogen Production and Storage: A Case Study of the Brazilian Electric Power Sector."

- International Journal of Hydrogen Energy* 47 (19): 10460–73.
<https://doi.org/10.1016/j.ijhydene.2022.01.133>.
- Mahela, Om Prakash, and Abdul Gafoor Shaik. 2016. “Comprehensive Overview of Grid Interfaced Wind Energy Generation Systems.” *Renewable and Sustainable Energy Reviews*. Elsevier Ltd. <https://doi.org/10.1016/j.rser.2015.12.048>.
- Majumdar, Abhigyan, Meridian Haas, Isabella Elliot, and Shima Nazari. 2023. “Control and Control-Oriented Modeling of PEM Water Electrolyzers: A Review.” *International Journal of Hydrogen Energy*. Elsevier Ltd. <https://doi.org/10.1016/j.ijhydene.2023.04.204>.
- Manickam, Chakkarapani, Guru Praanesh Raman, Guru Raghav Raman, Saravana Ilango Ganesan, and Nagamani Chilakapati. 2017. “Fireworks Enriched P&O Algorithm for GMPPT and Detection of Partial Shading in PV Systems.” *IEEE Transactions on Power Electronics* 32 (6): 4432–43.
<https://doi.org/10.1109/TPEL.2016.2604279>.
- Mao, Mingxuan, Lichuang Cui, Qianjin Zhang, Ke Guo, Lin Zhou, and Han Huang. 2020a. “Classification and Summarization of Solar Photovoltaic MPPT Techniques: A Review Based on Traditional and Intelligent Control Strategies.” *Energy Reports* 6 (174): 1312–27. <https://doi.org/10.1016/j.egy.2020.05.013>.
- 2020b. “Classification and Summarization of Solar Photovoltaic MPPT Techniques: A Review Based on Traditional and Intelligent Control Strategies.” *Energy Reports*. Elsevier Ltd. <https://doi.org/10.1016/j.egy.2020.05.013>.
- Matam, Manjunath, and Venugopal Reddy Barry. 2018. “Improved Performance of Dynamic Photovoltaic Array under Repeating Shade Conditions.” *Energy Conversion and Management* 168 (July): 639–50.
<https://doi.org/10.1016/j.enconman.2018.05.008>.
- MathWorks. n.d. “Choose a Solver.” Accessed June 5, 2023.
<https://www.mathworks.com/help/simulink/ug/choose-a-solver.html>.
- Miranda, D., C. M. Costa, and S. Lanceros-Mendez. 2015. “Lithium Ion Rechargeable Batteries: State of the Art and Future Needs of Microscopic Theoretical Models and Simulations.” *Journal of Electroanalytical Chemistry*. Elsevier B.V. <https://doi.org/10.1016/j.jelechem.2014.12.010>.
- Mohamed, Ahmed A.S., Hamid Metwally, Ahmed El-Sayed, and S. I. Selem. 2019. “Predictive Neural Network Based Adaptive Controller for Grid-Connected PV Systems Supplying Pulse-Load.” *Solar Energy* 193 (November): 139–47.
<https://doi.org/10.1016/j.solener.2019.09.018>.
- Mohanty, Parimita, G. Bhuvaneswari, R. Balasubramanian, and Navdeep Kaur Dhaliwal. 2014. “MATLAB Based Modeling to Study the Performance of Different MPPT Techniques Used for Solar PV System under Various Operating Conditions.” *Renewable and Sustainable Energy Reviews*. Elsevier Ltd. <https://doi.org/10.1016/j.rser.2014.06.001>.

- Moor, G. D., and H. J. Beukes. 2004. "Maximum Power Point Trackers for Wind Turbines." *PESC Record - IEEE Annual Power Electronics Specialists Conference* 3: 2044–49. <https://doi.org/10.1109/PESC.2004.1355432>.
- Motahhir, Saad, Abdelaziz El Ghzizal, Souad Sebti, and Aziz Derouich. 2018. "Modeling of Photovoltaic System with Modified Incremental Conductance Algorithm for Fast Changes of Irradiance." *International Journal of Photoenergy* 2018. <https://doi.org/10.1155/2018/3286479>.
- Mousa, Hossam H.H., Abdel Raheem Youssef, and Essam E.M. Mohamed. 2019. "Variable Step Size P&O MPPT Algorithm for Optimal Power Extraction of Multi-Phase PMSG Based Wind Generation System." *International Journal of Electrical Power and Energy Systems* 108 (January): 218–31. <https://doi.org/10.1016/j.ijepes.2018.12.044>.
2021. "State of the Art Perturb and Observe MPPT Algorithms Based Wind Energy Conversion Systems: A Technology Review." *International Journal of Electrical Power and Energy Systems* 126 (PA): 106598. <https://doi.org/10.1016/j.ijepes.2020.106598>.
- Mousavi G., S. M., and M. Nikdel. 2014. "Various Battery Models for Various Simulation Studies and Applications." *Renewable and Sustainable Energy Reviews*. <https://doi.org/10.1016/j.rser.2014.01.048>.
- Nasiri, M., J. Milimonfared, and S. H. Fathi. 2014. "Modeling, Analysis and Comparison of TSR and OTC Methods for MPPT and Power Smoothing in Permanent Magnet Synchronous Generator-Based Wind Turbines." *Energy Conversion and Management* 86: 892–900. <https://doi.org/10.1016/j.enconman.2014.06.055>.
- Nasirudeen, Salami Alaba, M. S. Haruna, Maruf A. Aminu, and Opeyemi Osanaiye. 2021. "Mathematical Modelling, Simulation and Analysis of Solar PV Module in Simulink." In *2021 1st International Conference on Multidisciplinary Engineering and Applied Science, ICMEAS 2021*. Institute of Electrical and Electronics Engineers Inc. <https://doi.org/10.1109/ICMEAS52683.2021.9692395>.
- Nasser, Mohamed, Tamer F Megahed, Shinichi Ookawara, and Hamdy Hassan. 2022a. "Performance Evaluation of PV Panels / Wind Turbines Hybrid System for Green Hydrogen Generation and Storage : Energy , Exergy , Economic , and Enviroeconomic." *Energy Conversion and Management* 267 (June): 115870. <https://doi.org/10.1016/j.enconman.2022.115870>.
- Nasser, Mohamed, Tamer F. Megahed, Shinichi Ookawara, and Hamdy Hassan. 2022b. "Techno-Economic Assessment of Clean Hydrogen Production and Storage Using Hybrid Renewable Energy System of PV/Wind under Different Climatic Conditions." *Sustainable Energy Technologies and Assessments* 52 (PB): 102195. <https://doi.org/10.1016/j.seta.2022.102195>.
- Naveen Sharma. n.d. "Renewable Wind Power Generation for Promoting Energy Security." Accessed June 8, 2023.

- <https://www.goldstandard.org/projects/renewable-wind-power-generation-promoting-energy-security>.
- Neammanee, B, S Sirisumranukul, and S Chatratana. n.d. “Control Performance Analysis of Feedforward and Maximum Peak Power Tracking for Small-and Medium-Sized Fixed Pitch Wind Turbines.”
- Nehrir, M. H., C. Wang, K. Strunz, H. Aki, R. Ramakumar, J. Bing, Z. Miao, and Z. Salameh. 2011. “A Review of Hybrid Renewable/Alternative Energy Systems for Electric Power Generation: Configurations, Control, and Applications.” *IEEE Transactions on Sustainable Energy* 2 (4): 392–403.
<https://doi.org/10.1109/TSTE.2011.2157540>.
- Nikolaïdis, Pavlos, and Andreas Poullikkas. 2017. “A Comparative Overview of Hydrogen Production Processes.” *Renewable and Sustainable Energy Reviews*. Elsevier Ltd. <https://doi.org/10.1016/j.rser.2016.09.044>.
- Noguchi, Toshihiko, Shigenori Togashi, and Ryo Nakamoto. 2002. “Short-Current Pulse-Based Maximum-Power-Point Tracking Method for Multiple Photovoltaic-and-Converter Module System.” *IEEE TRANSACTIONS ON INDUSTRIAL ELECTRONICS*. Vol. 49.
- Novaes Menezes, Eduardo José, Alex Maurício Araújo, and Nadège Sophie Bouchonneau da Silva. 2018. “A Review on Wind Turbine Control and Its Associated Methods.” *Journal of Cleaner Production* 174: 945–53.
<https://doi.org/10.1016/j.jclepro.2017.10.297>.
- Olz, Samantha, and Nicolai Kirchner. 2007. “CONTRIBUTION OF RENEWABLES TO ENERGY SECURITY.”
- Pahari, Om Prakash, and Bidyadhar Subudhi. 2018. “Integral Sliding Mode-Improved Adaptive MPPT Control Scheme for Suppressing Grid Current Harmonics for PV System.” *IET Renewable Power Generation* 12 (16): 1904–14.
<https://doi.org/10.1049/iet-rpg.2018.5215>.
- Pongratananukul, N, and T Kasparis. n.d. “Tool for Automated Simulation of Solar Arrays Using General-Purpose Simulators.”
- Qolipour, Mojtaba, Ali Mostafaeipour, and Omid Mohseni Tousi. 2017. “Techno-Economic Feasibility of a Photovoltaic-Wind Power Plant Construction for Electric and Hydrogen Production: A Case Study.” *Renewable and Sustainable Energy Reviews* 78 (May): 113–23. <https://doi.org/10.1016/j.rser.2017.04.088>.
- Rehman, Shafiqur, Luai M. Al-Hadhrami, and Md Mahbub Alam. 2015. “Pumped Hydro Energy Storage System: A Technological Review.” *Renewable and Sustainable Energy Reviews* 44: 586–98.
<https://doi.org/10.1016/j.rser.2014.12.040>.
- REN21 Renewables Now. 2022. “Renewables 2022 - Global Status Report.” Paris.
- Rezk, Hegazy, Enas Taha Sayed, Mujahed Al-Dhaifallah, M. Obaid, Abou Hashema M. El-Sayed, Mohammad Ali Abdelkareem, and A. G. Olabi. 2019. “Fuel Cell as an

- Effective Energy Storage in Reverse Osmosis Desalination Plant Powered by Photovoltaic System.” *Energy* 175: 423–33.
<https://doi.org/10.1016/j.energy.2019.02.167>.
- Salameh, Ziyad M., and Fouad Dagher. 1990. “The Effect of Electrical Array Reconfiguration on the Performance of a PV-Powered Volumetric Water Pump.” *IEEE Transactions of Energy Conversion* 5: 653–58.
- Samy, M. M., S. Barakat, and H. S. Ramadan. 2019. “A Flower Pollination Optimization Algorithm for an Off-Grid PV-Fuel Cell Hybrid Renewable System.” *International Journal of Hydrogen Energy* 44 (4): 2141–52.
<https://doi.org/10.1016/j.ijhydene.2018.05.127>.
- Sánchez-Pantoja, Núria, Rosario Vidal, and M. Carmen Pastor. 2018. “Aesthetic Impact of Solar Energy Systems.” *Renewable and Sustainable Energy Reviews*. Elsevier Ltd. <https://doi.org/10.1016/j.rser.2018.09.021>.
- Saygın, Değer, Gencer Emre, and Barış Sanlı. 2021. *Türkiye'nin Ulusal Hidrojen Stratejisi İçin Öncelik Alanları*.
- Shaqour, Ayas, Hooman Farzaneh, Yuichiro Yoshida, and Tatsuya Hinokuma. 2020. “Power Control and Simulation of a Building Integrated Stand-Alone Hybrid PV-Wind-Battery System in Kasuga City, Japan.” *Energy Reports* 6: 1528–44.
<https://doi.org/10.1016/j.egy.2020.06.003>.
- Sher, Hadeed Ahmed, Arslan Abbas Rizvi, Khaled E. Addoweesh, and Kamal Al-Haddad. 2017. “A Single-Stage Stand-Alone Photovoltaic Energy System With High Tracking Efficiency.” *IEEE Transactions on Sustainable Energy* 8 (2): 755–62. <https://doi.org/10.1109/TSTE.2016.2616443>.
- Simon, Patrice, Yury Gogotsi, Patrice Simon, Yury Gogotsi, and Nature Materials. 2019. “Materials for Electrochemical Capacitors To Cite This Version : HAL Id : Hal-02417326” 7 (11): 845–54.
- Soetedjo, Aryunto, Abraham Lomi, Widodo Puji Mulayanto, and Jalan Raya Karanglo Km. 2011. *Modeling of Wind Energy System with MPPT Control. International Conference on Electrical Engineering and Informatics*. Vol. 17.
- SolarPower Europe. 2022. “EU Market Outlook For Solar Power 2022-2026.”
- Sonia Veerapen, Huiqing Wen, and Yang Du. 2017. *Design of a Novel MPPT Algorithm Based on the Two Searching Method for PV Systems under Partial*. IEEE.
- Sood, Sumit, Om Prakash, Mahdi Boukerdja, Jean Yves Dieulot, Belkacem Ould-Bouamama, Mathieu Bressel, and Anne Lise Gehin. 2020. “Generic Dynamical Model of PEM Electrolyser under Intermittent Sources.” *Energies* 13 (24).
<https://doi.org/10.3390/en13246556>.
- Taskin Jamal, Sayedus Salehin. 2021. “Hybrid Renewable Energy Sources Power Systems.” In *Hybrid Renewable Energy Systems and Microgrids*, edited by Ersan Kabalci, 179–214. Academic Press.

- Tey, Kok Soon, Saad Mekhilef, Mehdi Seyedmahmoudian, Ben Horan, Amanullah Than Oo, and Alex Stojcevski. 2018. "Improved Differential Evolution-Based MPPT Algorithm Using SEPIC for PV Systems Under Partial Shading Conditions and Load Variation." *IEEE Transactions on Industrial Informatics* 14 (10): 4322–33. <https://doi.org/10.1109/TII.2018.2793210>.
- Tiang, Tow Leong, and Dahaman Ishak. 2012. "Novel MPPT Control in Permanent Magnet Synchronous Generator System for Battery Energy Storage." In *Applied Mechanics and Materials*, 110–116:5179–83. <https://doi.org/10.4028/www.scientific.net/AMM.110-116.5179>.
- Wang, Quincy, and Liuchen Chang. 2004. "An Intelligent Maximum Power Extraction Algorithm for Inverter-Based Variable Speed Wind Turbine Systems." *IEEE Transactions on Power Electronics* 19 (5): 1242–49. <https://doi.org/10.1109/TPEL.2004.833459>.
- Wei Cheng. 2013. "Incremental Conductance Algorithm For Maximum Wind Power Extraction Using Permanent Magnet Synchronous Generator."
- Wind Energy Technologies Office. 2023. "2022 Elevated Wind Energy to New Heights." 2023. <https://www.energy.gov/eere/wind/articles/2022-elevated-wind-energy-new-heights>.
- Wu, Tsung-Hi, Wei-Chen Liu, Chin-Sien Moo, Hung-Liang Cheng, and Yong-Nong Chang. n.d. "An Electric Circuit Model of Photovoltaic with Power Electronic Converter." In .
- Zsiborács, Henrik, Gábor Pintér, András Vincze, Nóra Hegedűsné Baranyai, and Martin János Mayer. 2022. "The Reliability of Photovoltaic Power Generation Scheduling in Seventeen European Countries." *Energy Conversion and Management* 260 (May). <https://doi.org/10.1016/j.enconman.2022.115641>.

APPENDIX I – MATLAB code of P&O Algorithm

```
function duty = MaxPwrPoint(Vpv, Ipv, delta)
duty_init=0.1; duty_min=0; duty_max=0.85;

persistent Vold Pold duty_old;

if isempty(Vold)
    Vold=0;
    Pold=0;
    duty_old=0;
end
P=Vpv*Ipv; dV=Vpv-Vold; dP=P-Pold;

if dP~= 0 && Vpv>30
    if dP<0
        if dV<0
            duty= duty_old-delta;
        else
            duty= duty_old+delta;
        end
    else
        if dV<0
            duty= duty_old+delta;
        else
            duty= duty_old-delta;
        end
    end
else
    duty=duty_old;
end

if duty >= duty_max
    duty=duty_max;
elseif duty<duty_min
    duty=duty_min;
end

duty_old=duty; Vold=Vpv; Pold=P;
```

APPENDIX II – MATLAB code for Electrolyzer Power Control

```
function ElectrolyzerPowerControl = ElectrolyzerPwrCont(TotalPowerIn,  
Selection,DesPwr)  
  
if Selection ==1 % Only Hydrogen ElectrolyzerPower=Total Power  
ElectrolyzerPowerControl=1;  
else if Selection ==2 % Only Grid ElectrolyzerPower=0  
    ElectrolyzerPowerControl=2;  
  
else  
    if Selection == 3 && TotalPowerIn>150  
        ElectrolyzerPowerControl=3;  
    elseif Selection == 4 && TotalPowerIn>50  
        ElectrolyzerPowerControl=4;  
    elseif Selection == 5 && TotalPowerIn>DesPwr  
        ElectrolyzerPowerControl=5;  
    else  
        ElectrolyzerPowerControl=6;  
    end  
end  
end  
end
```

APPENDIX III – Simulation Results of Case IV and Case V

Case IV:

This case was studied because of checking model's availability for bigger scale. To see the control of the battery charging and discharging block, the initial SOC of the battery is taken as 50%. Vestas V82 Turbine and 50 PV panels were used. Figure 6.1 shows the input powers for case IV.

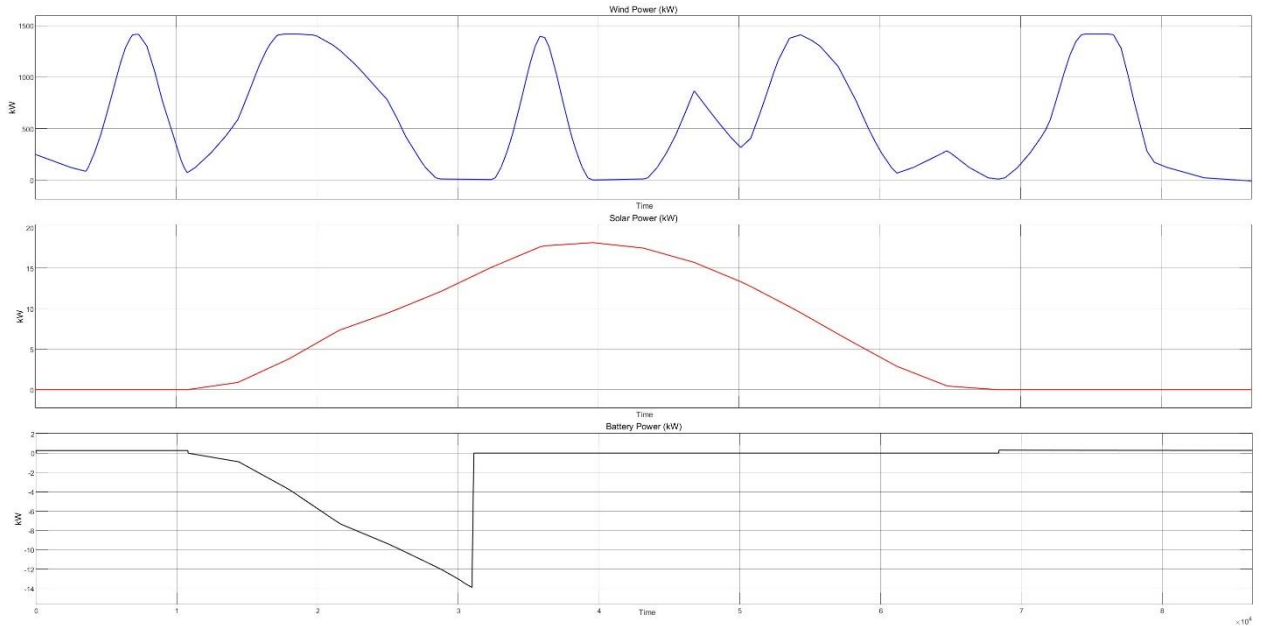


Figure 6.1. Input powers for Case IV.

In this case, electrolyzer power is taken as 150kW. It can be seen that, if there is enough power, the system tries to operate the electrolyzer at 150kW power. Figure 6.2 shows the input and output powers, Figure 6.3 shows the electrolyzer measurements, and Figure 6.4 shows the battery measurements.

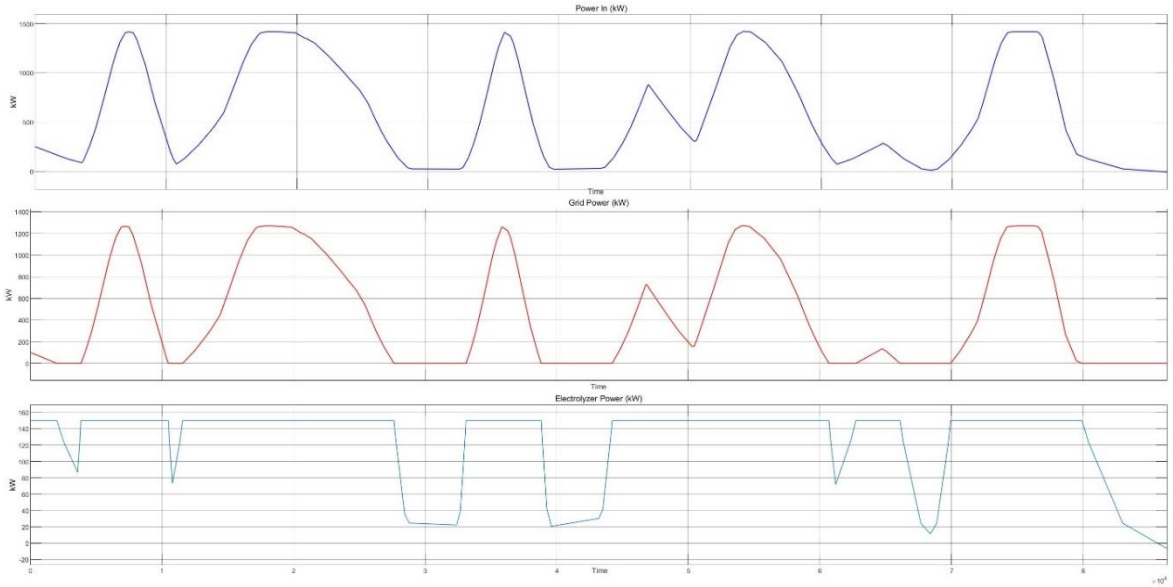


Figure 6.2. Input and output powers for Case IV.

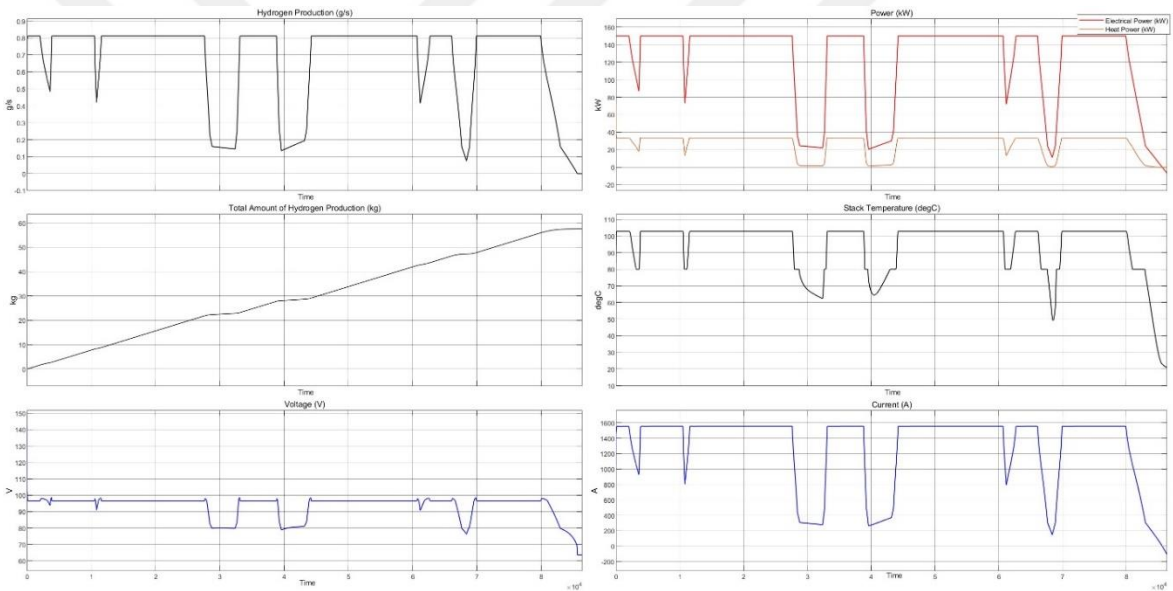


Figure 6.3. Electrolyzer Measurements for Case IV.

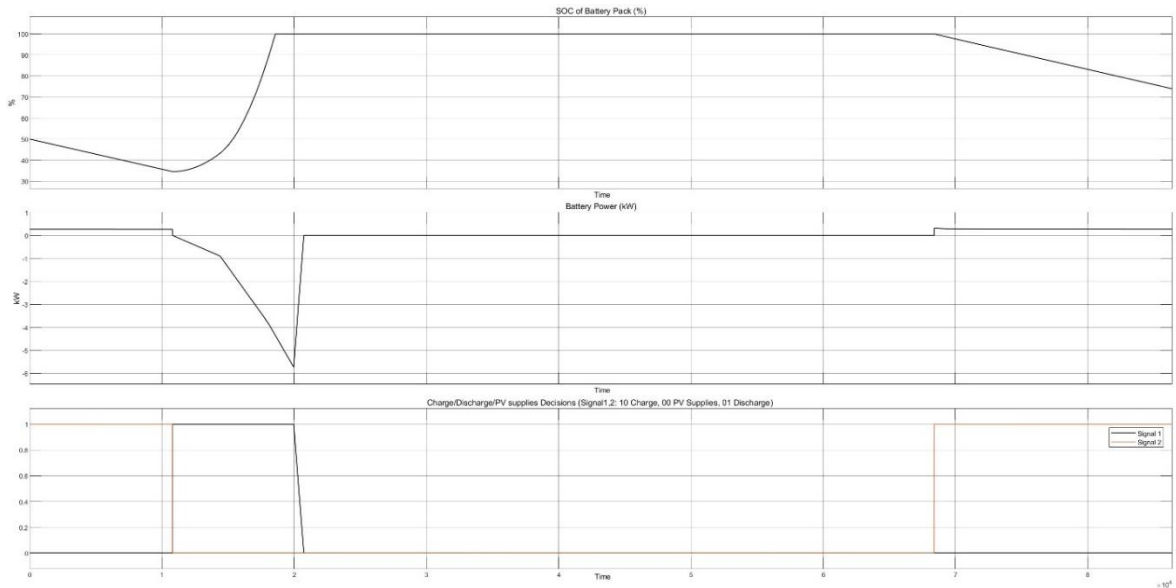


Figure 6.4. Battery measurements for Case IV.

Case V:

An average wind turbine was investigated for this case. In able to see the battery control, the initial SOC of the battery is taken as 50%. Vestas V47 wind turbine and 25 PV panels are used. Figure 6.5 shows the input powers for case IV.

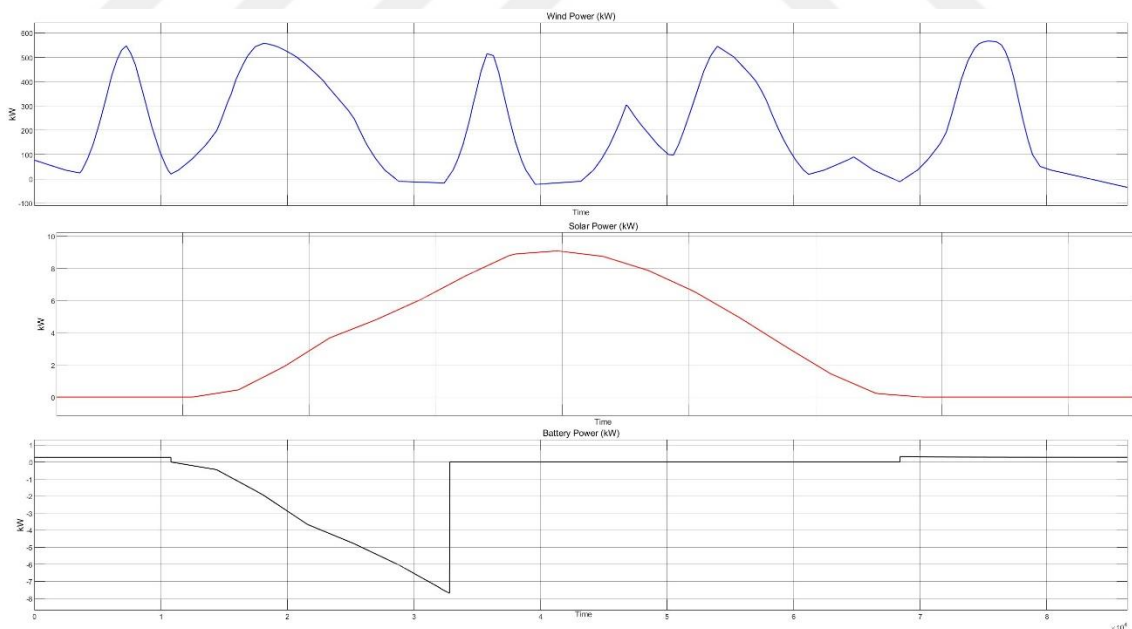


Figure 6.5. Input powers for Case V.

In this case, electrolyzer power is taken as 50kW. It can be seen that if there is enough power system tries to operate the electrolyzer at 50kW power. Figure 6.6 shows the electrolyzer measurements, and Figure 6.7 shows the battery measurements.

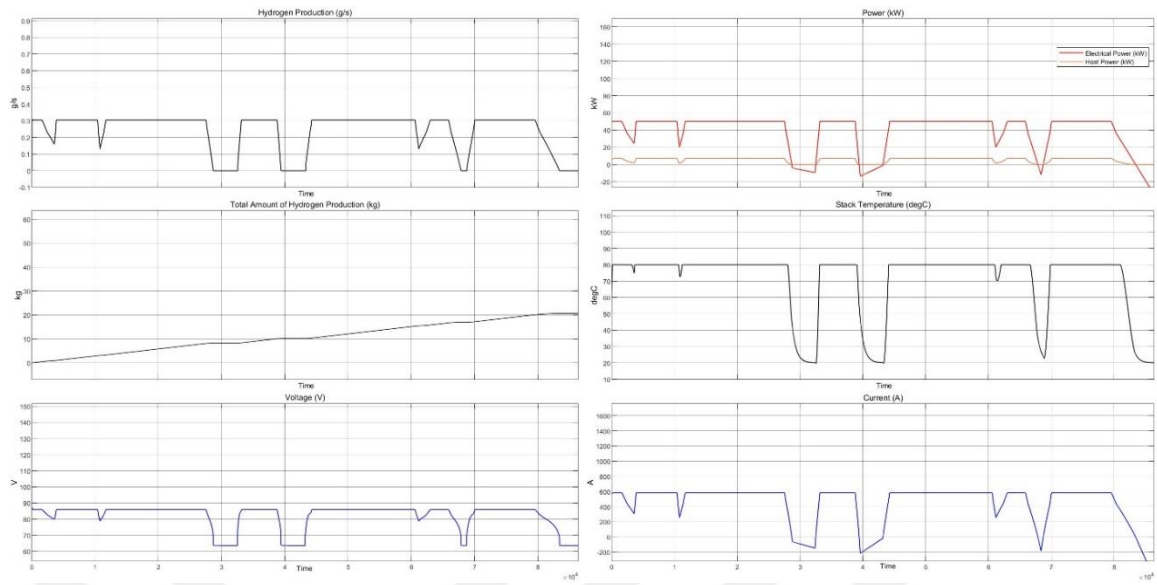


Figure 6.6. Electrolyzer Measurement for Case V.

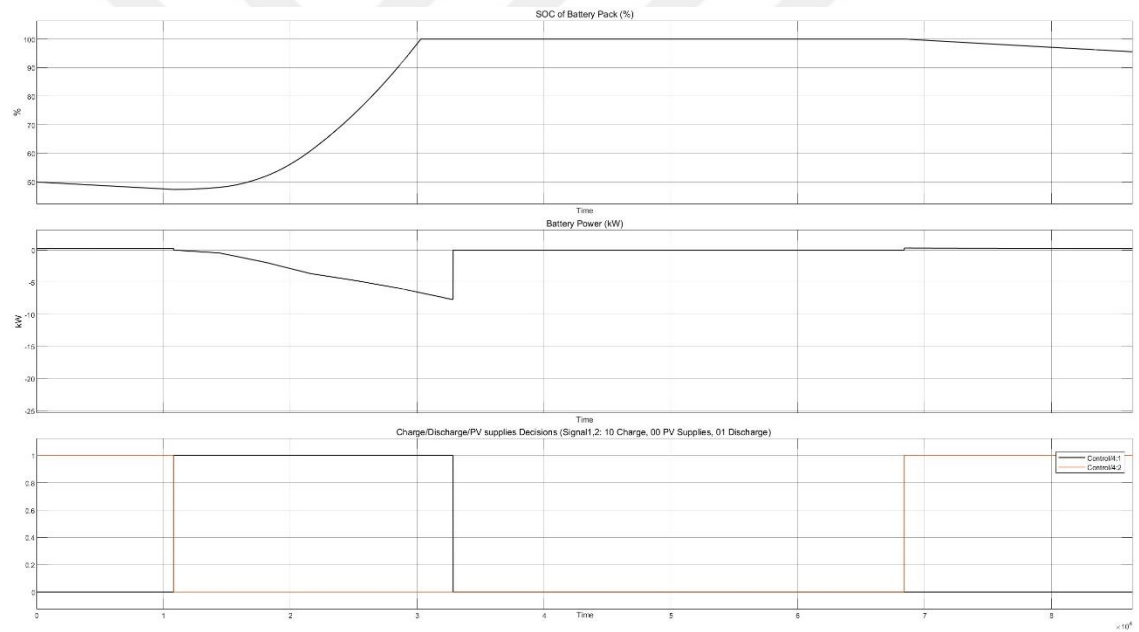


Figure 6.7. Battery measurements for Case V.